THE GREEN SYNTHESIS OF COPPER OXIDE NANOPARTICLES USING THE MORINGA OLEIFERA PLANT AND ITS SUBSEQUENT CHARACTERIZATION FOR USE IN ENERGY STORAGE APPLICATIONS†

Imosobomeh L. Ikhioya[a]*, Edwin U. Onoh[a], Agnes C. Nkele[a,e], Bonaventure C. Abor[a], B.C.N. Obitte[a], M. Maaza[b,c,d], Fabian I. Ezema[a,b,c,d]

[a]*Department of Physics and Astronomy, University of Nigeria, Nsukka, 410001, Enugu State, Nigeria*
[b]*Nanosciences African Network (NANOAFNET) iThemba LABS-National Research Foundation, 1 Old Faure Road, Somerset West 7129, P.O. Box 722, Somerset West, Western Cape Province, South Africa*
[c]*UNESCO-UNISA Africa Chair in Nanosciences/Nanotechnology, College of Graduate Studies, University of South Africa (UNISA), Muckleneuk Ridge, P.O. Box 392, Pretoria, South Africa*
[d]*Africa Centre of Excellence for Sustainable Power and Energy Development (ACE-SPED), University of Nigeria, Nsukka, Nigeria*
[e]*Department of Physics, Colorado State University, Fort Collins, U.S.A.*
Corresponding Author e-mail: imosobomeh.ikhioya@unn.edu.ng

Research Highlights:
- Successful synthesis of CuO NPs using extracts from dried, finely ground Moringa Oleifera as the reducing/capping agent
- The green synthesize CuO NPs displayed supercapacitive behavior.
- The reflection spectra demonstrate that the material exhibits low reflectance properties in the medium ultraviolet region.
- Good absorbance and low band gap energy values (E_g = 2.5 eV).
- Potential application to supercapacitor and other energy storage

In this study, we describe the environmentally friendly synthesis of copper oxide (CuO) and its subsequent characterization for use in supercapacitors. Using extracts from dried, finely ground Moringa Oleifera as the reducing/capping agent, we created the CuO NP. The produced NPs were then examined using X-ray Diffractometer (XRD), Ultraviolet-Visible spectroscopy, energy dispersive spectroscopy (EDS), and scanning electron microscopy (SEM). Electrochemical analysis techniques like cyclic voltammetry (CV) and electrochemical impedance spectroscopy (EIS) review were utilized to look at the electrochemical behavior of CuO-based electrodes. The analysis that followed determined that the green synthesize CuO NPs displayed supercapacitive behavior. This suggests that the synthesized CuO NPs will naturally encourage application as supercapacitive electrodes because it has been found that NPs absorbance varies linearly with NPs concentration, the 0.6 moles of CuO NPs produced the highest absorbance reading of 0.35 at 398 nm. The reflection spectra demonstrate that the material exhibits low reflectance properties in the medium ultraviolet region. However, as the spectra move toward the visible light region, the reflectance rises to its maximum value of 16 percent in the short ultraviolet region. The calculated crystallite sizes are as follows: 0.2 mols CuO NP, 0.3 mols CuO NP, 0.4 mols CuO NP, 0.5 mols CuO NP, and 0.6 mols CuO NP at 43.14 nm, 43.68 nm, 24.23 nm, 5.70 nm, and 12.87 nm, respectively, where Average D = 25.93 nm is the average crystalline size across all samples. the emergence of cubic grains that resemble nanorods with tube-like holes, SEM images demonstrate that CuO NPs can be distinguished from one another as seen in 0.2 mole CuO NPs.
Keywords: *CuO NPs; Supercapacitors; Energy storage; Moringa oleifera; Cyclic voltammetry*
PACS: 81.07.Wx, 82.47.Uv, 84.60.Ve, 43.30.Ky, 29.20.D

1. INTRODUCTION

The growing interest in electrochemical energy storage technologies, in particular fuel cells, super-capacitors, and batteries, promising to displacing the non-renewable systems of energy storage devices currently in vogue, is a direct result of the rising demand for renewable and environmentally friendly supply of energy and energy storage devices. Supercapacitors, one of the energy storage technologies currently in use, have been found to offer higher power and energy density than secondary batteries and conventional capacitors, respectively [1, 2]. These characteristics make them acceptable and advantageous for use in array of industries, from electronic consumer products to hybrid electrified vehicles [3].

Due to their rich redox chemical valences for use in pseudo-capacitive batteries, transition metals, and metallic oxides have drawn significant attention in the search for materials with good potential for electrochemical energy storage devices. Copper oxides have been regarded as the most alluring among these metallic oxides over time because of their numerous, established uses, such as in the fields of catalysis, gas sensors, anti-fungal/anti-microbial research, and batteries [4]. Overall, it is favorable and preferable due to its enticingly high capacitance, brilliant electrochemical performance, environmentally friendly nature, and affordable raw material costs [5-7].

According to its two valences, copper exists naturally in two oxide forms: cupric or copper II oxide (CuO) and cuprous or copper (II) oxide (CuO). Several methods have reportedly been used to prepare CuO and Cu_2O electrodes for supercapacitors [8–12]. Various CuO nanostructures, including nanorods, nanoflakes, nanowires, nanospheres,

nanoplatelets, nanoribbons, nanoflowers, micro-roses, micro-wool, flowers, willow-leaves, and dandelion-like CuO microspheres, have also been prepared using these various techniques [13–25].These nanostructures, as well as other properties like particle/grain size, superficial zone, aperture volume, and lucidity, which are governed by the strategy of deposition and specifications in particular pH, concentration of precursor materials, temperature etc., are extremely important for the electrochemical functioning of CuO-based electrodes as well as other electrode materials [26–28].

In this study, we present findings regarding the structure and characteristics of CuO NPs produced from Moringa oleifera using a green synthesis method. CuO NPs are produced using conventional methods as well, but studies have shown that green synthesis techniques are more effective at producing NPs that are low cost, adept at being characterized, and less likely to fail [29]. The use of plant extracts, fungi, bacteria, and yeast as reductants, capping, and reinforcing agents during the fabrication of the nanoparticles emphasizes the green synthesis method of producing metal oxide NPs, which ultimately strengthens biocompatibility and widespread production [30,31]. The great diversity of plants allows for the possibility of obtaining variations in nanoparticle size, shape, and morphology for a wide range of applications, production cost and time, and the presence of metabolites substances like polyphenols, phenolic acids, sugars, proteins, terpenoids and alkaloids which contribute to the bio-reduction and stabilization of the metal ions into nanoparticles make plant extracts the most promising of all these different types. [32-34]

Solvents, stabilizing or capping agents, and reducing agents are the three factors that are typically taken into account and studied when thinking about green synthesis methods. [35]. The green synthesis method is primarily regarded as environmentally friendly because it uses water or ethanol to dissolve the metal-ion precursors instead of organic solvents that might leave toxic residues behind after the synthesis process. Furthermore, since research has demonstrated that biomolecules can function as capping and reducing agents, the use of some complex chemicals that were previously employed to convert metallic salts to pure metals has been eliminated. [36]

The Moringa oleifera, is a very quickly growing, drought-resistant tree that is indigenous to India [37]. It is a member of the moringacea family. Researchers have become interested in moringa Oleifera primarily because it is a rich source of striking, potent phytochemicals. The Moringa Oleifera has demonstrated great potential in several applications, including medicine, biodiesel production, water purification, and food production, due to the presence of these phytochemicals, which include vitamins, natural sugars, alkaloids, minerals, organic acids, phenolic acids, phytosterols and flavonoids [38].

Even though few studies are already reported on the use of extracts from Moringa oleifera leaf acting as efficient reducing as well as capping agents for the biosynthesis of copper nanoparticles, for this study we investigated for the first time the uses of these nanoparticles produced using this method in supercapacitors and electrochemical energy storage devices.

CuO nanoparticles were produced and examined using a novel sol-gel process by Aparna Y, et al. They found that these particles could be used as superconductors, monitors, storage devices, and solar power transmission. Due to their cleanliness, lack of impurities, and well-organized shape, copper oxide nanoparticles make excellent catalysts for chemical reactions [45].

Due to the fascinating dimension-dependent chemical and physical properties of CuO in comparison to micrometer-sized particles, nanostructured materials provide a versatile range that can be used in a variety of situations [46]. Researchers have used bacteria like Streptococcus pyogenes, Pseudomonas aeruginosa, E. coli, and Staphylococcus aureus to examine the antibacterial properties of copper nanoparticles. The highest inhibition zone was discovered when they used the disk diffusion tests of nanoparticles dispersed in mycelial growth to investigate the bactericidal effects of copper nanoparticles. Escherichia coli and Staphylococcus aureus were both inhibited by copper nanoparticles, with inhibitory activities of 14 mm and 10 mm, respectively, in E. coli and Staphylococcus aureus. It was found that the type of nanoparticle can affect how susceptible bacteria are to it.

Gold and silver nanoparticles are now used in the printing of responsive global frameworks, according to Deng D, et al [47]. Copper nanoparticles are a substitute as a result of their modest cost and excellent electro conductivity. Notwithstanding, a significant obstacle in their use as conductive inks is the spontaneous oxidation of copper nanoparticles. According to the paper, the antioxidative copper composites were simply mixed with a lactonic acid ethanol solution before being deposited on glass slides. It has been proven that lactonic acid can react with nearby copper oxides so as to give rise to copper carboxylate, and eventually reduced by heating with nitrogen at a temperature of 200°C to copper. Due to CuO's intriguing characteristics, SF Shaffiey and his colleagues synthesized it and assessed its bactericidal abilities. CuO, a transition metal oxide, is among the most crucial. It is used in many different technological applications, including photosensitive devices, gas sensors, and critical temperature superconductors, to name a few. It has recently been looked into as an antibacterial agent for various bacteria. The process depends on the straightforward interaction of copper sulfate and de-ionized water, which is devoid of dangerous solvents, organics, and amines. Its bactericidal activity was evaluated against Aeromonas hydrophila ATCC 7966T bacteria. CuO nanoparticles have a great deal of potential as an antibacterial agent against A. hydrophila, claims this study [48].

The supercapacitive properties of CuO-based electrodes were explored via electrochemical impedance spectroscopy (EIS), cyclic voltammetry (CV) and galvanostatic charge-discharge (GCD).

2. EXPERIMENTAL DETAILS

50 g of ground air-dried Moringa oleifera leaves were immersed in 500 ml of distilled water and heated between 60 and 700°C. After allowing the extracts to cool at room temperature, they were filtered twice with filter paper (Whatman No.1 filter paper).

30 ml of the extracts were added to the $CuSO_4 \cdot 5H_2O$ solution after 1.59 g of $CuSO_4 \cdot 5H_2O$ was added to 50 ml of water and vigorously stirred until a solution was formed. When extracts are added, the solution's color abruptly changes from the copper salt solution's pale blue to dark green precipitates, which may be an indication that nanoparticles have formed. The solution was heated until it formed a brown paste, which was then transferred to a crucible and dried at 100°C for an hour before being annealed at 400°C for two hours. The powder, which was a darkish brown color, was then kept and used in subsequent research. The process was repeated for the following amounts of CuO NPs: 2.39 g, 3.19 g, 3.99 g, and 4.78 g, which correspond to 0.3 mols, 0.4 mols, 0.5 moles, and 0.6 moles, respectively.

While structural analyses were accomplished by utilizing an X-ray diffractometer, the surface morphology of the respective formed CuO NPs was investigated using the image obtained from scanning electron microscopy (SEM) (XRD). Measurements were made using the CuO-based electrode which is the working electrode, platinum as the counter electrodes, while the Ag/AgCl electrode is the reference electrode in 1M KOH electrolyte so as to scrutinize the supercapacitor rendition of the CuO NPs.
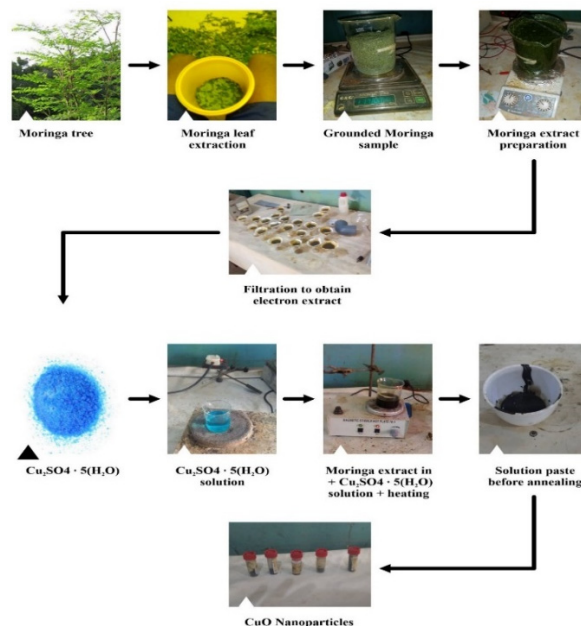

Figure 1. Pictorial diagram of the experimental Procedure

3. RESULTS AND DISCUSSIONS
3.1. XRD analysis

Figure 2 displays the copper oxide nanoparticles' XRD pattern. The pattern showed diffraction peaks at 34.9°, 43.3°, 50.5°, and 74.1°, respectively, which corresponded to reflections from planes; (222), (110), (200), and (311). The inter-atomic distance between the atoms and the crystallite size of the CuO NPs were determined through analysis.
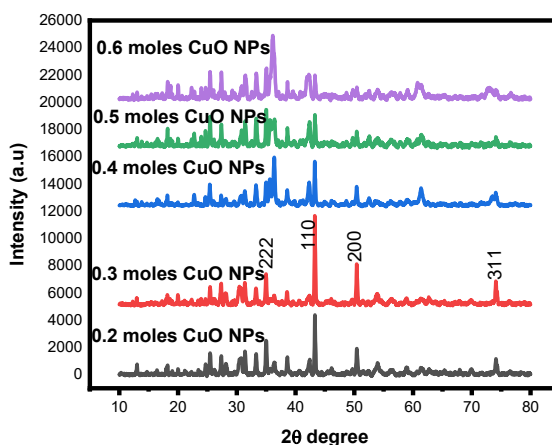

Figure 2. X-Ray Diffraction partner of the synthesized CuO NPs

The crystallite size D (nm) was calculated from the XRD data by employing the Debye Scherrer formula [39]:

$$D = \frac{K\lambda}{\beta cos(\theta)} \qquad (1)$$

where K is the Scherrer constant, which ranges from 0.68 to 2.08, and D is the crystallite size. Its value has been determined to be 0.94 for spherical crystallites with cubic symmetry. Where $CuK\alpha$= 1.5406 Å is the X-ray wavelength, β connoting line broadening about FWHM measured in radians, while θ in degrees connotes Bragg's angle.

The calculated crystallite sizes are 0.2 mols CuO NP, 0.3 mols CuO NP, 0.4 mols CuO NP, 0.5 mols CuO NP, and 0.6 mols CuO NP, respectively, at 43.14 nm, 43.68 nm, 24.23 nm, 5.70 nm, and 12.87 nm, where Average D = 25.93 nm is the average crystalline size across all the samples.The interplanar spacing was also obtained using Bragg's Law given as:

$$d_{hkl} = \frac{n\lambda}{2\theta};$$ (2)

The Scherrer's constant remains unchanged, and n stands for the number of fringes. After combining all the data for different peak values, the interatomic spacing's mean value was determined to be 3.7755 Å.

3.2. SEM analysis

The surface morphologies of the synthesized CuO NPs at various concentrations were thoroughly examined using SEM images. The initial stages in the formation of the microstructure include nucleation, a surface heterogeneous reaction, particle accumulation, followed by organizing itself to much larger particles. The development of nanorod-like grains with cubic shapes and tube-like holes, as was seen in 0.2 mole CuO NPs, distinguishes CuO NPs across the board, according to the SEM images. A strong candidate for use in supercapacitors, this morphology also suggests high porosity and offers a reactive surface that is helpful for ion transport. [40]
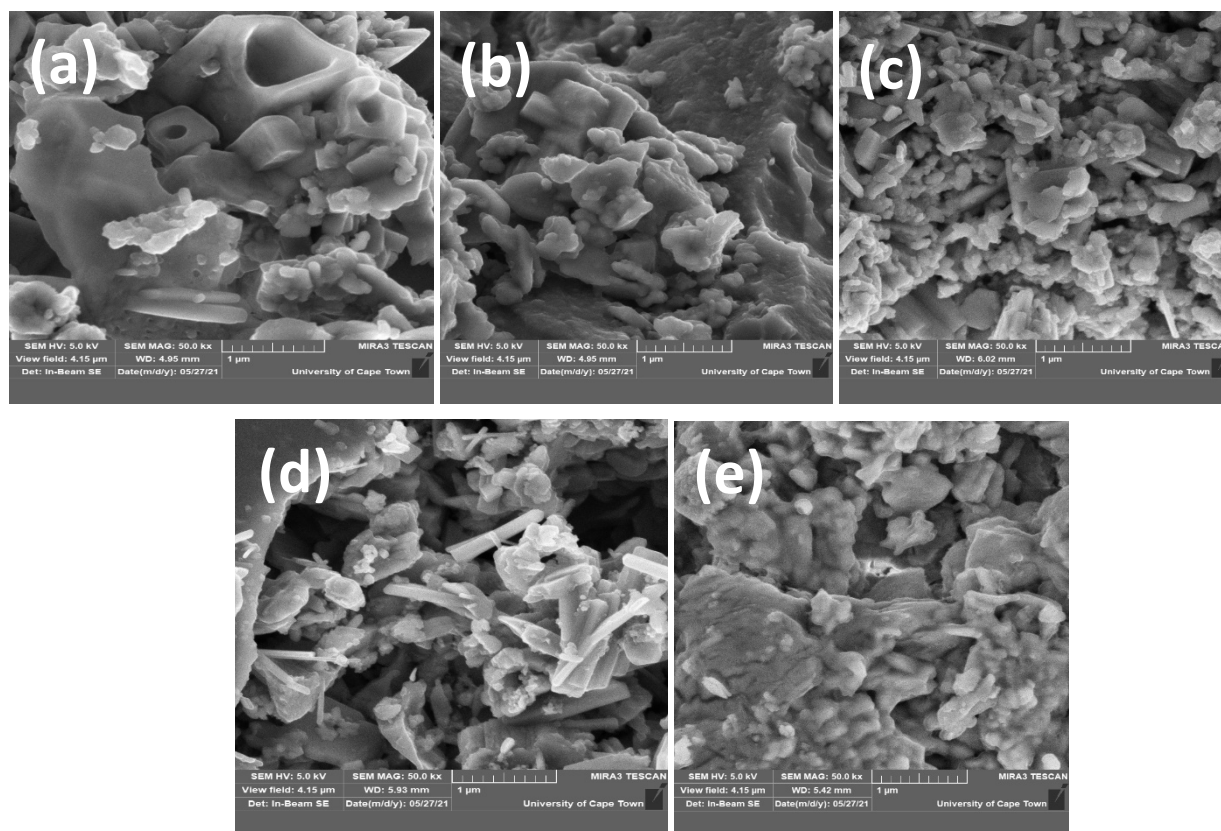
Figure 3. SEM images of the synthesized CuO NPs for 0.2 mols, 0.3 mols, 0.4 mols, 0.5 mols, and 0.6 mols corresponding to a, b, c, d, and e respectively.

3.3. EDS analysis

In order to ascertain the elemental configuration of the examined CuO NPs, an EDS method is used. EDS analysis revealed the presence of Cu and also revealed the presence of S, suggesting that the precursor was a bluestone (CuSO4)

3.4. Optical analysis of the synthesized CuO NPs

UV spectroscopy was used to obtain the optical studies of the various sample concentrations, which are listed as 0.2 mols, 0.3 mols, 0.4 mols, 0.5 mols, and 0.6 mols. These studies are discussed further below. A plot of absorbance versus wavelength in Figure 5 (a) demonstrates that the 0.2 moles of CuO NPs absorb very little in the short-wavelength ultraviolet region, with a minimum value of 0.0635 at 328 nm. Finally, the NPs' absorbance gradually increased until it reached a maximum value of 0.183 at 384 nm in the medium ultraviolet region. The 0.6 moles of CuO NPs produced the

highest absorbance reading of 0.35 at 398 nm because it is observed that NPs absorbance varies linearly with NPs concentration. However, this is in agreement with the theoretical predictions of the Beer-Lambert law, which states that the amount of absorption is proportional to the concentration of the absorber. In general, it is significant to note that this material's low absorbance properties, as compared to lithium-ion batteries, make it a good choice for use in supercapacitors as energy storage devices and in the pursuit of environmentally friendly forms of energy supply. Figure 5 (b), The transmittance spectra convey that the absorbance spectra have an inverse relationship. The NPs with the highest concentration, 0.6 mol, corresponds to the lowest percentage transmittance in Figure 5 (b), while the NPs' absorbance value is at its highest. The 0.2 mols CuO NPs, on the other hand, exhibit greater radiation transmission in the short-wavelength ultraviolet region, as shown in Figure 5 (b). Eventually getting to its maximum, of 86.5 percent at 323 nm. This percentage transmittance value slightly drops to a minimum percentage value of 66 percent at 390 nm. The samples' high transmittance characteristics in the visible light and short-wavelength ultraviolet regions demonstrate their suitability for both passive and active solar technology. Figure 5 (c), The material has low reflectance characteristics in the medium ultraviolet region, as shown by the reflection spectra. The reflectance, however, increases to its maximum value of 16 percent in the short ultraviolent region as the spectra moves toward the visible light region. In the region of visible light, a continuous spectrum is seen as the spectra slightly decreases from the maximum to about 15%.
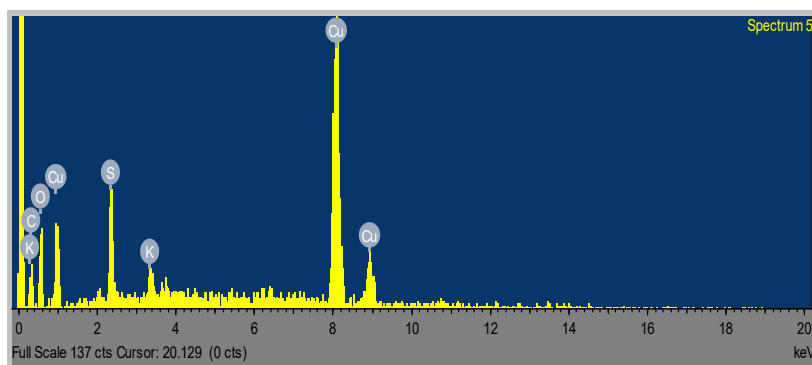

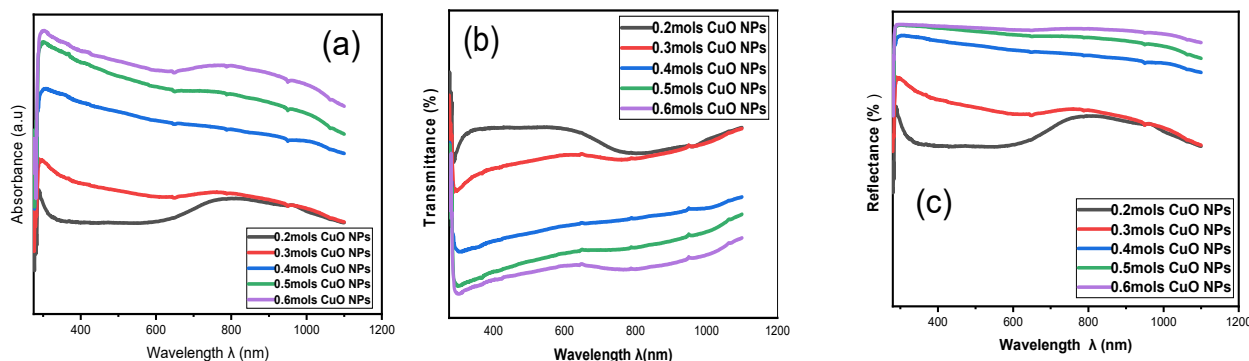**Figure 4.** EDS spectrum of the synthesized CuO NPs

Figure 5. Spectra of (a) Absorbance, (b) transmittance, and (c) reflectance of the synthesized CuO NPs

The distance between an electron's valence band and conduction band is depicted in Figure 6(a), and this distance is known as the band gap or energy gap.
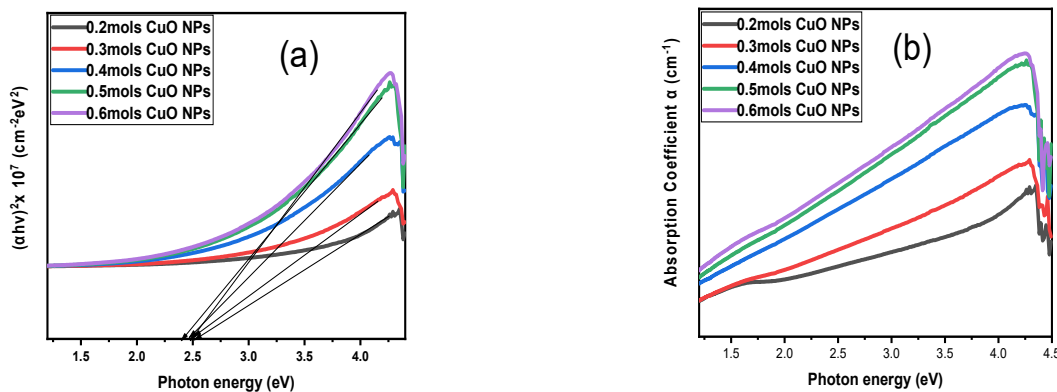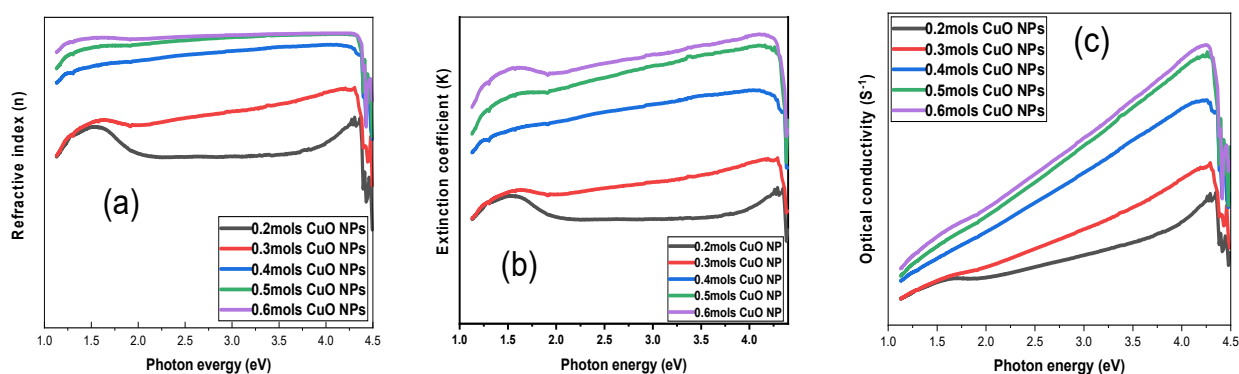

Figure 6. Spectra of (a) Absorption coefficient square and (b) absorption coefficient of the synthesized CuO NPs

An important factor in determining a material's electrical conductivity is the energy band gap, outlining an energy range where electronic state cannot exist. If the atom's valence band is filled and the conduction band is extremely empty, electrons cannot move through the material. On the contrast, if there is electron transfer from the valence to the conduction band, current can flow [19]. The average band gap of the CuO NPs across all samples, as seen in the Tauc plot in Figure 6 (a), was 2.5 eV. All of the prepared samples have a high light absorption coefficient in the ultraviolet and visible light region, indicating an increase in the likelihood of direct transitions occurring, as shown in Figure 6 (b), which is the plot of absorption coefficient against photon energy. Additionally, it was observed that the absorption coefficient gradually rises as photon energy rises, which is related to the interactions between the incident electrons and the electrons in the CuO NPs.

The atoms of the medium continuously absorb and re-emit light particles as it passes through it, slowing down the light's speed over time. Since refractive index and wavelength are inversely proportional, light moves more slowly as the refractive index increases. According to the theoretical prediction, the refractive index gradually decreases as the photon energy increases as seen in the spectra. In Figure 7 (a) the maximum refractive index for the 0.2 mol CuO NPs was reached; however, this value slightly decreased as the photon energy of the incident radiation increased toward the visible light and near-infrared regions. The extinction coefficient is a measurement of how strongly a substance absorbs light at any given fixed wavelength. It measures how electromagnetic waves are dampened when they enter a medium. The following formula relates the extinction coefficient to the absorption coefficient:

$$K = \frac{\lambda \alpha}{4\pi} \tag{3}$$

The maximum extinction coefficient for all samples of CuO NPs was found at E = 4.32 eV in the ultraviolent region according to Figure 7(b), with a proportional increase as sample concentration increased. The optical conductivity of the CuO NPs reveals that the optical conductivity of the CuO NPs increases as the photon energy increases as seen in Figure 7 (c).


Figure 7. Spectra of (a) Refractive index, (b) extinction coefficient, and (c) optical conductivity of the synthesized CuO NPs

The imaginary component of the dielectric constant describes a material's capacity to permanently absorb energy from a time-varying electric field, while the real component describes a material's capacity to interact with an electric field (store and remit energy) without doing so. This suggests that a high imaginary part dielectric constant absorbs a lot of energy.

The Dielectric constant and refractive index of the material is related via the equation;

$$\varepsilon = n^2 \tag{5}$$

The maxima and minima of the electromagnetic radiation spectrum occur in the same energy region when the real dielectric against photon energy and the imaginary dielectric constant plots are compared.
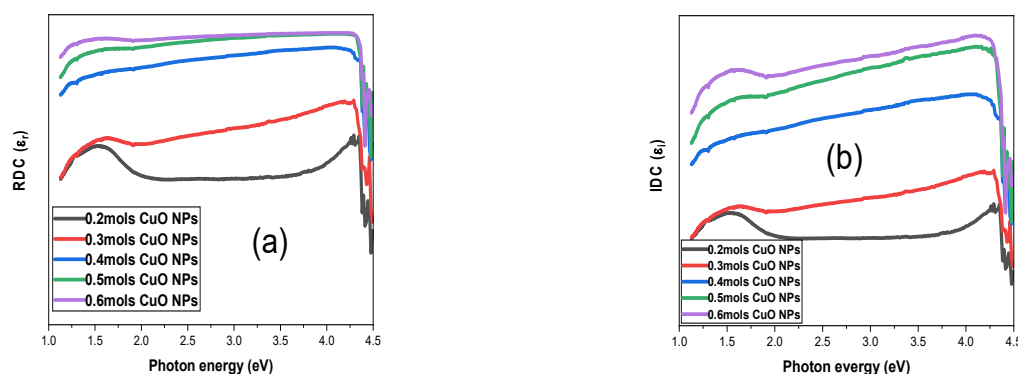
Figure 8. Spectra of (a) real dielectric constant and (b) imaginary dielectric constant of the synthesized CuO NPs

The maximum value was obtained for the 0.2 mols CuO NPs in the ultraviolet region at ε_r and ε_i equivalent to 5.58 and 0.0687, respectively, at the same value for Photo energy equal to 4.42 eV. Moving forward, it was also noted that a direct relationship existed between the two terms of the dielectric constant and the sample concentration, with the 0.6 mol CuO NPs sample providing the highest values of ε_r and ε_i of 6.98 and 0.1504 respectively at the same photon energy, which in this case decreased slightly to 4.25 eV.

3.5. Electrochemical impedance spectroscopy studies (EIS)

An EIS study was conducted to scrutinize the interrelation between the surface electronic properties of the electrolyte (1M KOH) and the CuO-based NPs electrodes, and also to verify their diverse reaction kinetics and resistances. The EIS measurements were assessed using frequency ranges from 1.0 Hz – 100.0 kHz.0.2 mols CuO-based NPs and 0.3 moles CuO-based NPs electrodes have unvarying electrolytic resistance (Re) together with working electrode's resistance (Rw) respectively as 13.0 Ω and 0.9 Ω, 0.4 mols CuO-based NPs and 0.5 moles CuO-based NPs electrodes have unvarying electrolytic resistance (Re) as the working electrode's resistance (Rw) of 12.0 Ω and 0.8 Ω, respectively, while 0.6mols of CuO NPs have its electrolytic resistance (Re) as 12.0 Ω whereas its working electrode's resistance (Rw) is 0.7Ω. This suggests that the CuO-based NPs electrodes offer great interfacial area.
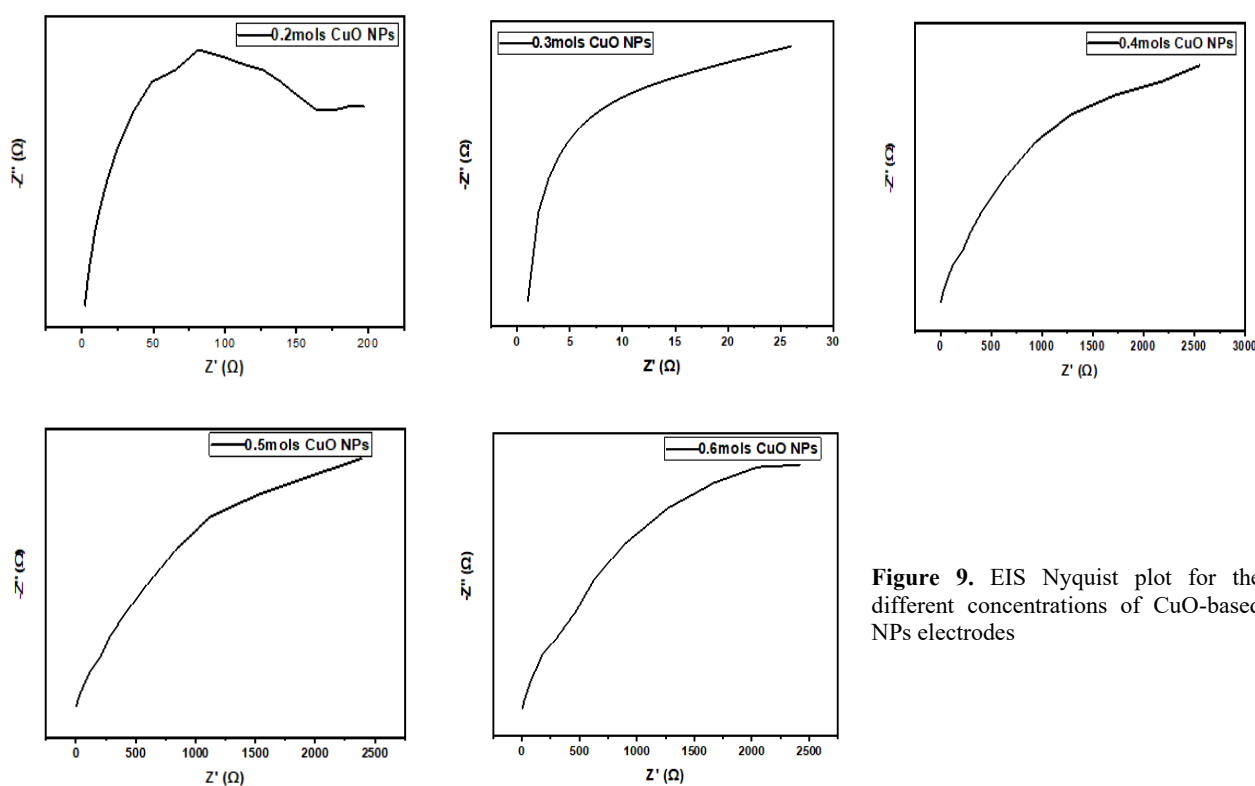

Figure 9. EIS Nyquist plot for the different concentrations of CuO-based NPs electrodes
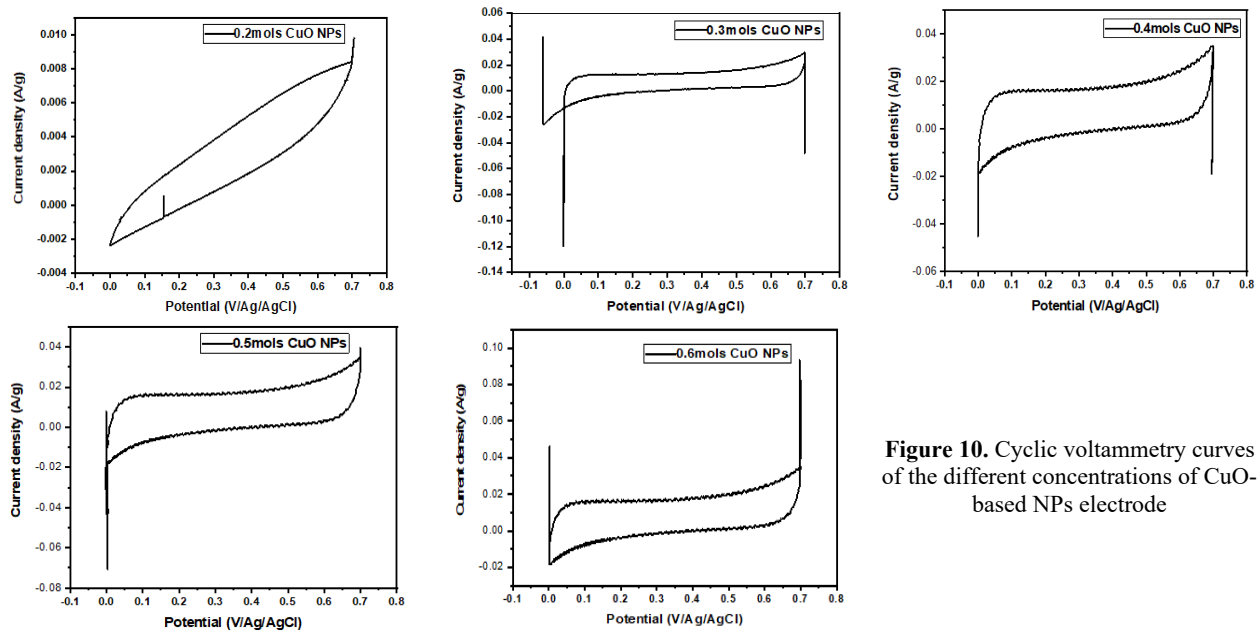
3.6. Cyclic voltammetry (CV)

The utilization of a cyclic voltammetry was to understand capacitive behavior exhibited by the electrode which is a result of the convenience of the CuO-based NPs electrode to the 1M KOH electrolyte. The different concentrations of the CuO-based NPs electrodes were recorded at the same scan rate of 10 mV/s.

From the plot, the very sharp peaks of the CV curves are due to redox reactions occurring during the process which is consistent with the Cu^{2+} to Cu^+ reduction process and Cu^+ to Cu^{2+} oxidation process [45]. From our CV curve, the specific capacitance of the different concentrations of CuO-based electrodes was all calculated using this equation [41-44];

$$C_s = \frac{\int IdV}{mS\Delta V} \tag{6}$$

Given that $\int IdV$ is gotten by incorporating the area under the CV curve, where specific capacitance is connoted as Cs, the current is given as I, voltage as V, the scan rate is given as S, and M as the active mass of the different concentrations of the CuO NPs electrode. The specific capacitance of the different CuO NPs gave 176 Fg^{-1} for 0.2 mols CuO NP, 181 Fg^{-1} for 0.3 mols, 322 Fg^{-1} for 0.4mols, 328 Fg^{-1} for 0.5mols and 212 Fg^{-1} for 0.6 mols. The high specific capacitance that is gotten could be credited to the rapid transportation of charges during intercalation between the CuO NPs electrode and the 1M KOH electrolyte.
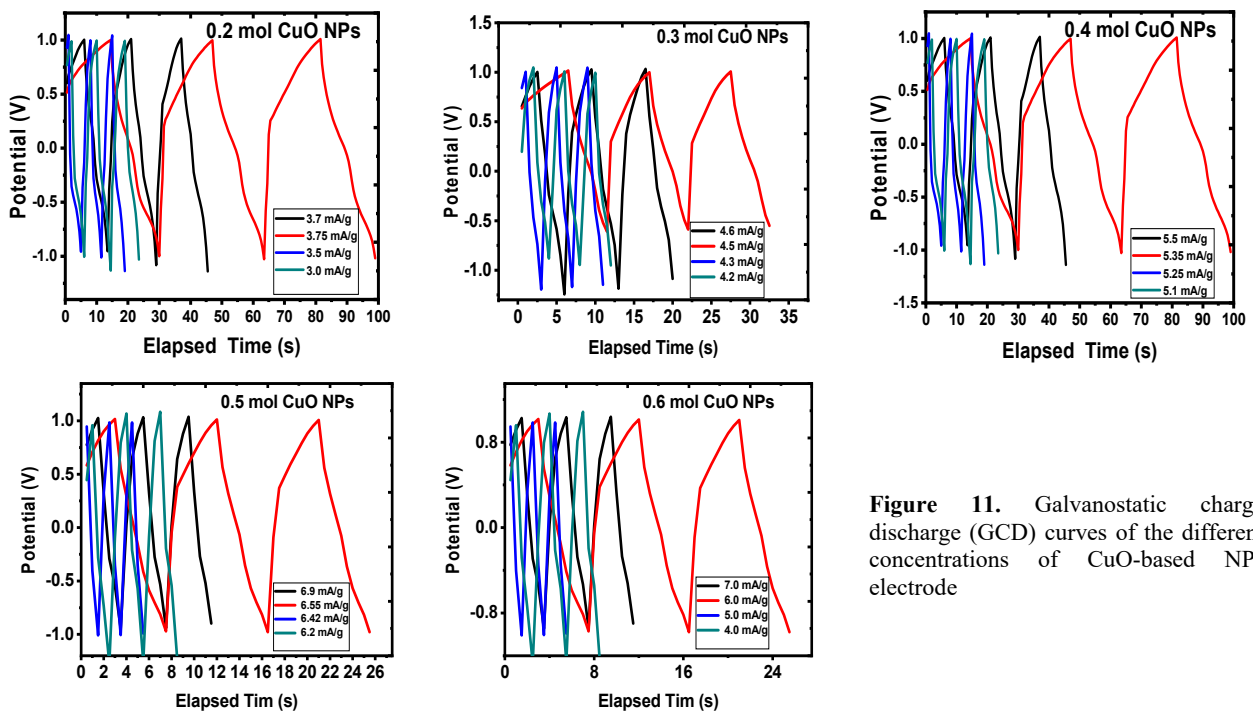
Figure 10. Cyclic voltammetry curves of the different concentrations of CuO-based NPs electrode

3.7. Galvanostatic charge discharge (GCD)

We also conducted the galvanostatic charge-discharge (GCD) estimation in an unchanged electrolyte environment with the CV. From the GCD curves, it could be observed that the material exhibits pseudo-capacitive performance. From the GCD, the specific capacitance was calculated using this equation [41-44];

$$C_s = \frac{I t_d}{m \Delta V} \tag{7}$$

Given that the specific capacitance is connoted as Cs, the current is given as I, while the time of discharge is given as td. For the denominator, m is the active mass of the CuO-based electrode given as m, while the voltage is given as V.

Figure 11. Galvanostatic charge discharge (GCD) curves of the different concentrations of CuO-based NPs electrode

4. CONCLUSION

In conclusion, due to the rising interest and demand for supercapacitors as energy storage devices when compared to lithium-ion batteries and the quest for an environmentally friendly form of energy supply, we successfully synthesized CuO NPs using an environmentally friendly, cost-effective, and simple approach; which is green synthesis as against the conventional chemical methods used. The low band gap values of 2.5 eV and the resultant electrochemical analysis test

results carried out on the different samples establish the fact that the synthesized CuO NPs exhibited supercapacitive properties, hence can be used in supercapacitor and other energy storage applications.

Conflicts of Interest. None to declare

Ethical Statement. The paper reflects the authors' research and analysis truthfully and completely.

Data Availability Statement. The data that support the findings of this study are available on request from the corresponding author.

Author contribution. The study's conceptualization, methodology, and experiments were all contributed to by all of the writers. Imosobomeh L. Ikhioya, Edwin U. Onoh, Bonaventure C. Abor, B.C.N. Obitte, and Agnes C. Nkele did the material preparation, methodology, experiment, graph plotting, and analysis. Imosobomeh L. Ikhioya and Edwin U. Onoh wrote the manuscript's first draft, with the help of Malik Maaza and Fabian I. Ezema for editing. The final manuscript was read and approved by all writers.

ORCID IDs
Imosobomeh L. Ikhioya, https://orcid.org/0000-0002-5959-4427

REFERENCES
[1] M. Heon, S. Lofland, J. Applegate, R. Nolte, E. Cortes, J.D. Hettinger, P.L. Taberna, P. Simon, P. Huang, M. Brunet, and Y. Gogotsi, "Continuous carbide-derived carbon films with high volumetric capacitance", Energy & Environmental Science, **4**(1), 135-138D (2011). https://doi.org/10.1039/c0ee00404a
[2] D. Ahn, I. Yoo, Y.M. Koo, N. Shin, J. Kim, and T.J. Shin, "Effects of cobalt-intercalation and polyaniline coating on electrochemical performance of layered manganese oxides", Journal of Materials Chemistry, **21**(14), 5282-5289 (2011). https://doi.org/10.1039/C0JM03548C
[3] G. Wee, W.F. Mak, N. Phonthammachai, A. Kiebele, M.V. Reddy, B.V.R. Chowdari, G. Gruner, M. Srinivasan, and S.G. Mhaisalkar, "Particle size effect of silver nanoparticles decorated single walled carbon nanotube electrode for supercapacitors", Journal of the Electrochemical Society, **157**(2), A179 (2009). https://doi.org/10.1149/1.3267874
[4] J. Liu, J. Wang, C. Xu, H. Jiang, C. Li, L. Zhang, J. Lin, and Z.X. Shen, "Advanced energy storage devices: basic principles, analytical methods, and rational materials design", Advanced science, **5**(1), 1700322 (2018). https://doi.org/10.1002/advs.201700322
[5] H. Zhang, and M. Zhang, "Synthesis of CuO nanocrystalline and their application as electrode materials for capacitors", Materials Chemistry and Physics, **108**(2-3), 184-187 (2008). https://doi.org/10.1016/j.matchemphys.2007.10.005
[6] V.D. Patake, S.S. Joshi, C.D. Lokhande, and O.S. Joo, "Electrodeposited porous and amorphous copper oxide film for application in supercapacitor", Materials Chemistry and Physics, **114**(1), 6-9 (2009). https://doi.org/10.1016/j.matchemphys.2008.09.031
[7] X. Zhang, W. Shi, J. Zhu, D.J. Kharistal, W. Zhao, B.S. Lalia, H.H. Hng, and Q. Yan, "High-power and high-energy-density flexible pseudocapacitor electrodes made from porous CuO nanobelts and single-walled carbon nanotubes", ACS nano, **5**(3), 2013-2019 (2011). https://doi.org/10.1021/nn1030719
[8] I.M. Tiginyanu, O. Lupan, V.V. Ursaki, L. Chow, and M. Enachi, "3-11 - Nanostructures of metal oxides", Comprehensive Semiconductor Science and Technology, **3**, 396-479 (2011). https://doi.org/10.1016/B978-0-44-453153-7.00105-X
[9] S.E. Moosavifard, M.F. El-Kady, M.S. Rahmanifar, R.B. Kaner, and M.F. Mousavi, "Designing 3D highly ordered nanoporous CuO electrodes for high-performance asymmetric supercapacitors", ACS applied materials & interfaces, **7**(8), 4851-4860 (2015). https://doi.org/10.1021/am508816t
[10] W. Xu, S. Dai, G. Liu, Y. Xi, C. Hu, and X. Wang, "CuO nanoflowers growing on carbon fiber fabric for flexible high-performance supercapacitors", Electrochimica Acta, **203**, 1-8 (2016). https://doi.org/10.1016/j.electacta.2016.03.170
[11] D.P. Dubal, G.S. Gund, R. Holze, H.S. Jadhav, C.D. Lokhande, and C.J. Park, "Surfactant-assisted morphological tuning of hierarchical CuO thin films for electrochemical supercapacitors", Dalton Transactions, **42**(18), 6459-6467 (2013). https://doi.org/10.1039/C3DT50275A
[12] S.K. Shinde, D.P. Dubal, G.S. Ghodake, D.Y. Kim, and V.J. Fulari, "Nanoflower-like CuO/Cu (OH) 2 hybrid thin films: Synthesis and electrochemical supercapacitive properties", Journal of Electroanalytical Chemistry, **732**, 80-85 (2014). https://doi.org/10.1016/j.jelechem.2014.09.004
[13] G. Fan, and F. Li, "Effect of sodium borohydride on growth process of controlled flower-like nanostructured Cu2O/CuO films and their hydrophobic property", Chemical engineering journal, **167**(1), 388-396 (2011). https://doi.org/10.1016/j.cej.2010.12.090
[14] H. Li, S. Yu, and X. Han, "Fabrication of CuO hierarchical flower-like structures with biomimetic superamphiphobic, self-cleaning and corrosion resistance properties", Chemical Engineering Journal, **283**, 1443-1454 (2016). https://doi.org/10.1016/j.cej.2015.08.112
[15] Y. Ma, H. Li, R. Wang, H. Wang, W. Lv, and S. Ji, "Ultrathin willow-like CuO nanoflakes as an efficient catalyst for electro-oxidation of hydrazine", Journal of Power Sources, **289**, 22-25 (2015). https://doi.org/10.1016/j.jpowsour.2015.04.151
[16] Y. Ma, H. Wang, J. Key, S. Ji, W. Lv, and R. Wang, "Control of CuO nanocrystal morphology from ultrathin "willow-leaf" to "flower-shaped" for increased hydrazine oxidation activity", Journal of Power Sources, **300**, 344-350 (2015). https://doi.org/10.1016/j.jpowsour.2015.09.087
[17] D.P. Dubal, G.S. Gund, R. Holze, and C.D. Lokhande, "Mild chemical strategy to grow micro-roses and micro-woolen like arranged CuO nanosheets for high performance supercapacitors", Journal of Power Sources, **242**, 687-698 (2013). https://doi.org/10.1016/j.jpowsour.2013.05.013
[18] G. Wang, J. Huang, S. Chen, Y. Gao, and D. Cao, "Preparation and supercapacitance of CuO nanosheet arrays grown on nickel foam", Journal of Power Sources, **196**(13), 5756-5760 (2011). https://doi.org/10.1016/j.jpowsour.2011.02.049

[19] A.C. Nwanya, D. Obi, K.I. Ozoemena, R.U. Osuji, C. Awada, A. Ruediger, M. Maaza, F. Rosei, and F.I. Ezema, "Facile synthesis of nanosheet-like CuO film and its potential application as a high-performance pseudocapacitor electrode", Electrochimica Acta, **198**, 220-230 (2016). https://doi.org/10.1016/j.electacta.2016.03.064

[20] W. Zhang, H. Wang, Y. Zhang, Z. Yang, Q. Wang, J. Xia, and X. Yang, "Facile microemulsion synthesis of porous CuO nanosphere film and its application in lithium-ion batteries", Electrochimica Acta, **113**, 63-68 (2013). https://doi.org/10.1016/j.electacta.2013.09.043

[21] J. Wang, and W.D. Zhang, "Fabrication of CuO nanoplatelets for highly sensitive enzyme-free determination of glucose", Electrochimica Acta, **56**(22), 7510-7516 (2011). https://doi.org/10.1016/j.electacta.2011.06.102

[22] F. Cao, X.H. Xia, G.X. Pan, J. Chen, and Y.J. Zhang, "Construction of carbon nanoflakes shell on CuO nanowires core as enhanced core/shell arrays anode of lithium ion batteries", Electrochimica Acta, **178**, 574-579 (2015). https://doi.org/10.1016/j.electacta.2015.08.055

[23] B. Heng, C. Qing, D. Sun, B. Wang, H. Wang, and Y. Tang, "Rapid synthesis of CuO nanoribbons and nanoflowers from the same reaction system, and a comparison of their supercapacitor performance", RSC advances, 3(36), 15719-15726 (2013). https://doi.org/10.1039/C3RA42869A

[24] Z. Zhang, H. Che, Y. Wang, L. Song, Z. Zhong, and F. Su, "Preparation of hierarchical dandelion-like CuO microspheres with enhanced catalytic performance for dimethyldichlorosilane synthesis", Catalysis Science & Technology, 2(9), 1953-1960 (2012). https://doi.org/10.1039/C2CY20199B

[25] M.J. Deng, C.C. Wang, P.J. Ho, C.M. Lin, J.M. Chen, and K.T. Lu, "Facile electrochemical synthesis of 3D nano-architectured CuO electrodes for high-performance supercapacitors", Journal of Materials Chemistry A, 2(32), 12857-12865 (2014). https://doi.org/10.1039/C4TA02444C

[26] A. Vlad, N. Singh, J. Rolland, S. Melinte, P.M. Ajayan, and J.F. Gohy, "Hybrid supercapacitor-battery materials for fast electrochemical charge storage", Scientific reports, **4**, 4315 (2014). https://doi.org/10.1038/srep04315

[27] G. Wang, L. Zhang, and J. Zhang, "A review of electrode materials for electrochemical supercapacitors", Chemical Society Reviews, **41**(2), 797-828 (2012). https://doi.org/10.1039/C1CS15060J

[28] X. Zhang, W. Shi, J. Zhu, D.J. Kharistal, W. Zhao, B.S. Lalia, H.H. Hng, and Q. Yan, "High-power and high-energy-density flexible pseudocapacitor electrodes made from porous CuO nanobelts and single-walled carbon nanotubes", ACS nano, 5(3), 2013-2019 (2011). https://doi.org/10.1021/nn1030719

[29] T.M. Abdelghany, A.M. Al-Rajhi, M.A. Al Abboud, M.M. Alawlaqi, A. GanashMagdah, E.A. Helmy, and A.S. Mabrouk, "Recent advances in green synthesis of silver nanoparticles and their applications: about future directions. A review", BioNanoScience, **8**(1), 5-16 (2018). https://doi.org/10.1007/S12668-017-0413-3

[30] M. Nasrollahzadeh, F. Ghorbannezhad, Z. Issaabadi, and S.M. Sajadi, "Recent developments in the biosynthesis of Cu-based recyclable nanocatalysts using plant extracts and their application in the chemical reactions", The Chemical Record, **19**(2-3), 601-643 (2019). https://doi.org/10.1002/tcr.201800069

[31] M. Nasrollahzadeh, S. Mahmoudi-GomYek, N. Motahharifar, and M.G. Gorab, "Recent developments in the plant-mediated green synthesis of Ag-based nanoparticles for environmental and catalytic applications", The Chemical Record, **19**(12), 2436-2479 (2019). https://doi.org/10.1002/tcr.201800202

[32] M. Nasrollahzadeh, M. Atarod, M. Sajjadi, S.M. Sajadi, and Z. Issaabadi, "Plant-mediated green synthesis of nanostructures: mechanisms, characterization, and applications", in: *Interface science and technology,* Vol. 28, (Elsevier, Amsterdam, 2019). pp. 199-322.

[33] M. Shah, D. Fawcett, and S. Sharma, S.K. Tripathy and G.E.J. Poinern, "Green Synthesis of Metallic Nanoparticles via Biological Entities", Materials (Basel), **8**(11), 7278–7308 (2015). https://doi.org/10.3390%2Fma8115377

[34] V.V. Gusel'nikova, and D. Korzhevskiy, "NeuN as a neuronal nuclear antigen and neuron differentiation marker", Acta Naturae, **7**(2), 42-47 (2015). https://pubmed.ncbi.nlm.nih.gov/26085943

[35] C.P. Devatha, and A.K. Thalla, "Green synthesis of nanomaterials", Synthesis of inorganic nanomaterials, 169-184 (2018). https://doi.org/10.1016/B978-0-08-101975-7.00007-5

[36] H. Duan, D. Wang, and Y. Li, "Green chemistry for nanoparticle synthesis", Chemical Society Reviews, **44**(16), 5778-5792 (2015). https://doi.org/10.1039/C4CS00363B

[37] L. Gopalakrishnan, K. Doriya, and D.S. Kumar, "Moringa oleifera: A review on nutritive importance and its medicinal application", Food science and human wellness, **5**(2), 49-56 (2016). https://doi.org/10.1016/j.fshw.2016.04.001

[38] R.K. Saini, I. Sivanesan, and Y.S. Keum, "Phytochemicals of Moringa oleifera: a review of their nutritional, therapeutic and industrial significance", Biotech, **6**(2), 1-14 (2016). https://doi.org/10.1007/s13205-016-0526-3

[39] P. Scherrer, "Bestimmungdergrosse und der innerenstruktur yon kolloiteilchenmittels", Gott. Nachr Math. Phys, **2**, 98-100 (1918).

[40] S.K. Shindea, M.B. Jalak, G.S. Ghodake, N.C. Maile, V.S. Kumbhar, D.S. Lee, V.J. Fulari, and D.-Y. Kim, "Chemically synthesized nanoflakes-like NiCo2S4 electrodes for high-performance supercapacitor application", Appl. Surf. Sci. **466**, 822-829 (2019). https://doi.org/10.1016/j.apsusc.2018.10.100

[41] H.E. Nsude, K.U. Nsude, G.M. Whyte, R.M. Obodo, C. Iroegbu, M. Maaza, and F.I. Ezema, "Green synthesis of CuFeS2 nanoparticles using mimosa leaves extract for photocatalysis and supercapacitor applications", Journal of Nanoparticle Research, **22**(11), 1-13 (2020). https://doi.org/10.1007/s11051-020-05071-7

[42] S. Najib, F. Bakan, N. Abdullayeva, R. Bahariqushchi, S. Kasap, G. Franzò, et al, "Tailoring morphology to control defect structures in ZnO electrodes for high-performance supercapacitor devices", Nanoscale, **12**(30), 16162-16172 (2020). https://doi.org/10.1039/D0NR03921G

[43] M.Ö. Alaş, A. Güngör, R. Genç, and E. Erdem, "Feeling the power: robust supercapacitors from nanostructured conductive polymers fostered with Mn 2+ and carbon dots", Nanoscale, **11**(27), 12804-12816 (2019). https://doi.org/10.1039/C9NR03544C

[44] M. Toufani, S. Kasap, A. Tufani, F. Bakan, S. Weber, and E. Erdem, "Synergy of nano-ZnO and 3D-graphene foam electrodes for asymmetric supercapacitor devices", Nanoscale, **12**(24), 12790-12800 (2020). https://doi.org/10.1039/D0NR02028A

[45] A.O. Aliyu, S. Garba, and O. Bognet, "Green Synthesis, Characterization and Antimicrobial Activity of Vanadium Nanoparticles Using Leaf Extract of Moringa Oleifera," **11**(1), 42–48 (2018). https://doi.org/10.9790/5736-1101014248

[46] A.A. Radhakrishnan, and B.B. Beena, "Structural and Optical Absorption Analysis of CuO Nanoparticles", Indian Journal of Advances in Chemical Science, **2**(2), 158–161 (2014). https://www.ijacskros.com/artcles/IJACS-M64.pdf

[47] D. Deng, T. Qi, Y. Chen, Y. Jin, and F. Xiao, "Preparation of antioxidative nano copper pastes for printed electronics application," in: *13th International Conference on Electronic Packaging Technology & High Density Packaging*, (2012). pp. 250-253. https://doi.org/10.1109/ICEPT-HDP.2012.6474611

[48] S.F. Shaffiey, M. Shapoori, A. Bozorgnia, and M. Ahmadi, "Synthesis and evaluation of bactericidal properties of CuO nanoparticles against Aeromonas hydrophila", Nanomedicine Journal, **1**(3), 198–204 (2014). https://doi.org/10.7508/nmj.2014.03.010

ЗЕЛЕНИЙ СИНТЕЗ НАНОЧАСТИНОК ОКСИДУ МІДІ З ВИКОРИСТАННЯМ РОСЛИНИ MORINGA OLEIFERA ТА ЙОГО ПОДАЛЬША ХАРАКТЕРИЗАЦІЯ ДЛЯ ВИКОРИСТАННЯ У НАКОПИЧУВАЧАХ ЕНЕРГІЇ

Імособоме Л. Іхіоя[a], Едвін У. Оно[a], Агнес К. Нкеле[a,e], Бонавентура К. Абор[a],
Б.С.Н. Обітте[a], М. Мааза[b,c,d], Фабіан І. Езема[a,b,c,d]

[a]Факультет фізики та астрономії, Університет Нігерії, Нсукка, 410001, штат Енугу, Нігерія
[b]Африканська мережа нанонаук (NANOAFNET) Національний дослідницький фонд iThemba LABS, 1 Стара Фор-роуд, Сомерсет Вест, Західна Капська провінція, Сомерсет Вест, Південна Африка
[c]Африканська кафедра нанонаук/нанотехнологій ЮНЕСКО-UNISA, Коледж післядипломних досліджень, Університет Південної Африки (UNISA, хребет Макленек, P.O. Box 392, Преторія, Південна Африка
[d]Африканський центр передового досвіду для стійкої енергетики та енергетичного розвитку (ACE-SPED), Університет Нігерії, Нсукка
[e]Факультет фізики, Університет штату Колорадо, Форт-Коллінз, США

Основні моменти дослідження:
• Успішний синтез наночастинок CuO з використанням екстрактів висушеної, дрібно подрібненої Moringa Oleifera як відновника/закриваючого агента
• Зелені синтезовані наночастинки CuO продемонстрували суперємнісну поведінку.
• Спектри відбиття демонструють, що матеріал демонструє низькі властивості відбивання в середньому ультрафіолетовому діапазоні.
• Хороша абсорбція та низькі значення енергії забороненої зони (E_g = 2,5 eB).
• Потенційне застосування для суперконденсаторів та інших накопичувачів енергії

У цьому дослідженні ми описуємо екологічно чистий синтез оксиду міді (CuO) і його подальшу характеристику для використання в суперконденсаторах. Використовуючи екстракти висушеної, дрібно подрібненої Moringa Oleifera як відновлювача/блокуючого агента, ми створили CuO наночастинки (НЧ). Отримані НЧ потім досліджували за допомогою рентгенівського дифрактометра (XRD), ультрафіолетово-видимої спектроскопії, енергодисперсійної спектроскопії (EDS) і скануючої електронної мікроскопії (SEM). Методи електрохімічного аналізу, такі як циклічна вольтамперометрія (CV) і спектроскопія електрохімічного опору (EIS), були використані для вивчення електрохімічної поведінки електродів на основі CuO. Наступний аналіз визначив, що зелені синтезовані наночастинки CuO демонструють суперємнісну поведінку. Це свідчить про те, що синтезовані наночастинки CuO природним чином заохочуватимуть застосування як суперємнісних електродів, оскільки було виявлено, що поглинання наночастинок змінюється лінійно залежно від концентрації наночастинок, 0,6 моль наночастинок CuO дало найвищий показник поглинання 0,35 при 398 нм. Спектри відбиття демонструють, що матеріал демонструє низькі властивості відбиття в середньому ультрафіолетовому діапазоні. Однак, коли спектр рухається до області видимого світла, коефіцієнт відбиття зростає до максимального значення 16% у короткому ультрафіолетовому діапазоні. Розраховані розміри кристалітів такі: 0,2 моль CuO NP, 0,3 моль CuO NP, 0,4 моль CuO NP, 0,5 моль CuO NP і 0,6 моль CuO NP при 43,14 нм, 43,68 нм, 24,23 нм, 5,70 нм і 12,87 нм, відповідно, де Average D = 25,93 нм є середнім розміром кристалів для всіх зразків. Поява кубічних зерен, які нагадують наностржні з трубчастими отворами, SEM-зображення демонструють, що НЧ CuO можна відрізнити одна від одної, як це видно у на 0,2 моль НЧ CuO.

Ключові слова: *наночастинки CuO; суперконденсатори; накопичувач енергії; Moringa oleifera; циклічна вольтамперометрія*

PREPARATION AND PROPERTIES OF ZrO₂/SiC-H₂O NANOFLUIDS TO USE FOR ENERGY STORAGE APPLICATION†

Ahmed Hashim[a]*, **Farhan Lafta Rashid**[b], **Noor Al-Huda Al-Aaraji**[c], **Bahaa H. Rabee**[a]

ᵃDepartment of Physics, College of Education for Pure Sciences, University of Babylon, Babylon, Iraq
ᵇUniversity of Kerbala, College of Engineering, Petroleum Engineering Department, Iraq
ᶜDepartment of Medical Physics, Al-Mustaqbal University College, Babylon, Iraq
*Corresponding Author e-mail: ahmed_taay@yahoo.com
Recived December 18, 2022; revised January 1, 2023; accepted January 5, 2023

More than half of the energy used in total comes in the form of heat energy. An essential environmental protection technique to increase energy efficiency is learning how to employ thermal energy storage (TES) technology to fully use intermittent and unstable heat, such as solar heat utilization and industrial waste heat. Sensible heat storage, latent heat storage, and thermochemical heat storage are all types of thermal energy storage. This work describes the creation of ZrO₂/SiC-H₂O nanofluids and their characteristics for use in energy storage applications. Results reveal that increasing the concentration of ZrO₂/SiC NPs from 0.3 gm/L to 1.2 gm/L at photon wavelength (=380nm) increased absorbance by roughly 83.7% and reduced transmittance by 81.2%. Additionally, when ZrO₂/SiC NP concentrations rise, the absorbance rises as well, indicating improved nanofluid dispersion. Additionally, when the concentration of ZrO₂/SiC NPs reached 1.2gm/L, the electrical conductivity of ZrO₂/SiC- H₂O nanofluids improved by nearly 74%, and the melting time reduced with an increase in the concentration of ZrO₂/SiC nanoparticles.
Keywords: *Energy storage; nanofluids; transmittance; absorbance; melting*
PACS: 61.25.he, 61.46.-w, 44.35.-c, 47.57.Ng, 84.60.-h

1. Introduction

As heat transfer fluids, conventional fluids like water, motor oil, and ethylene glycol are often utilized. Other conventional fluids include methanol. The poor heat transfer performance of these typical fluids impedes both the performance increase and the compactness of heat exchangers, despite the fact that a variety of methods are used to improve heat transfer. Increasing the rate of heat transmission may be accomplished by the use of a method that involves the use of solid particles as an additive that is suspended within the base fluid. To enhance the heat transfer properties of traditional fluids, the most important concept is to increase the thermal conductivity of the fluid. It is anticipated that the thermal conductivity of a base fluid may be improved by suspending metallic solid tiny particles inside the base fluid. This is due to the fact that the thermal conductivity of a solid metal is higher than that of a base fluid. For a good number of years now [1-10], people have been aware of the fact that the suspension of solid particles, such as those measuring millimeters or micrometers in size, may increase the thermal conductivity of typical fluids. [Such particles] The thermophysical parameters of a nanofluid, including its density, viscosity, thermal conductivity, and specific heat capacity, have a significant impact on the flow and heat transfer performance of the nanofluid. Enhancing or degrading the thermophysical characteristics of a nanofluid is one method that is being used in a number of different activities with the goal of improving the performance of nanofluids. For example, it is generally known that the majority of metallic nanoparticles have a much better thermal conductivity compared to traditional heat transfer fluids (HTFs) such as water and ethylene glycol. This finding has been backed up by extensive research. Organic particles, such as those manufactured from rice husk or wood, on the other hand, have a lower density and a lower heat conductivity than traditional HTFs. Therefore, the concept of attempting to improve the thermal conductivity of nanofluids by adding metallic particles and reducing the viscosity of traditional HTFs by adding organic particles is an innovative one [11-16].

Rocha et al. [17] studied water-based nanofluids of Al₂O₃ and ZrO₂ with relation to their potentially useful uses in heat transfer. Dispersed solutions of mentioned nanofluids were created with three distinct concentrations (0.01% vol., 0.05% vol., and 0.1% vol.) using commercial nanofluids. These concentrations were 0.01% vol., 0.05% vol., and 0.1% vol. Experiments conducted by Shajahan et al. [18] evaluated the thermal hydraulic performance of ZrO₂, a water-based nanofluid with varying volume concentrations of 0.1%, 0.25%, and 0.5%, and staggered conical strip inserts with three different twist ratios of 2.5, 3.5, and 4.5 in forward and backward flow patterns under a fully developed laminar flow regime of 0–50 lph through a horizontal test pipe section with a Using a mechanical dispersion approach to construct a shape-stable composite phase change material for thermal energy storage, Song et al. [19] enhanced the specific heat capacity and thermal conductivity of molten salt. This allowed for the material to have a higher thermal capacity. Nitrate (NaNO₃), which has a greater phase change latent heat, was selected to be coupled with a variety of nanoparticles (SiO₂, SiO₂+TiO₂) in order to enhance its specific heat capacity. Expanded graphite (EG) was used as a carrier matrix in order to improve its thermal conductivity. In this research, we discuss the synthesis of ZrO₂/SiC-H₂O

---

nanofluids as well as their characteristics for usage in applications involving energy storage. There are several studies on SiC doped different materials to employ in various biomedical, electronics and sensors applications[20-27].

2. MATERIALS AND METHODS

Zirconium oxide nanoparticles (also known as ZrO_2 NPs) and silicon carbide nanoparticles (also known as SiC NPs) were used in this study. Various concentrations of ZrO_2/SiC NPs were used during the synthesis of the ZrO_2/SiC-H_2O nanofluids. These concentrations include 0.3 gm/L, 0.6 gm/L, 0.9 gm/L, and 1.2 gm/L. The optical and electrical properties of ZrO_2/SiC-H_2O nanofluids were investigated in this research. Using a double beam spectrophotometer (Shimadzu, UV-18000A), the optical characteristics of ZrO_2/SiC-H_2O nanofluids were analyzed throughout a wavelength range of (200-1000) nm. In the process of storing thermal energy, it is necessary to do an analysis of the melting properties of ZrO_2/SiC-H_2O nanofluids while the system is being heated. The ZrO_2/SiC-H_2O nanofluids were utilized as the heat transfer fluid. The temperature of the heat transfer fluid may be changed from 40°C to 100°C using a stirrer, and a digital device was used to measure the temperature of the ZrO_2/SiC-H_2O nanofluids as they were being heated.

3. RESULTS AND DISCUSSION

Figures 1 and 2 show, at varying concentrations of ZrO_2/SiC NPs, the behavior of the absorbance and transmittance spectra of ZrO_2/SiC-H_2O nanofluids with photon wavelength. According to the figures, increasing the concentration of ZrO_2/SiC NPs from 0.3 gm/L to 1.2 gm/L at photon wavelengths (380nm) resulted in an increase in absorbance of about 83.7% and a decrease in transmittance of 81.2%. This behavior can be useful in solar collectors, heating systems, and cooling systems. The absorbance, which indicates greater nanofluid dispersion, will increase as ZrO_2/SiC NP concentrations rise [28].
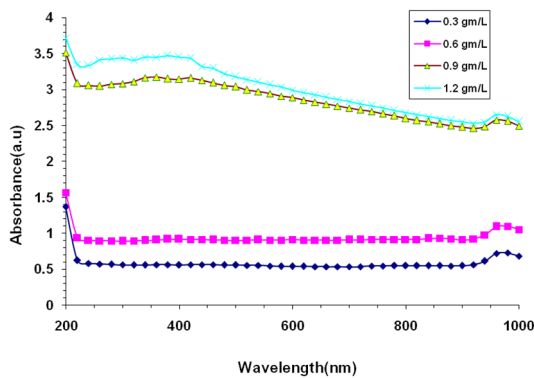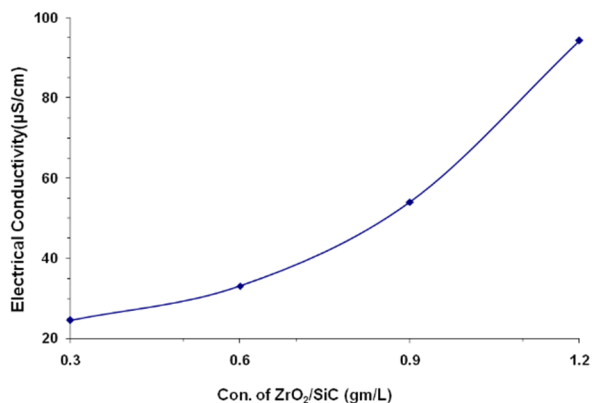

Figure 1. Behavior of absorbance of ZrO_2/SiC-H_2O nanofluids with photon wavelength for various concentrations of ZrO_2/SiC NPs
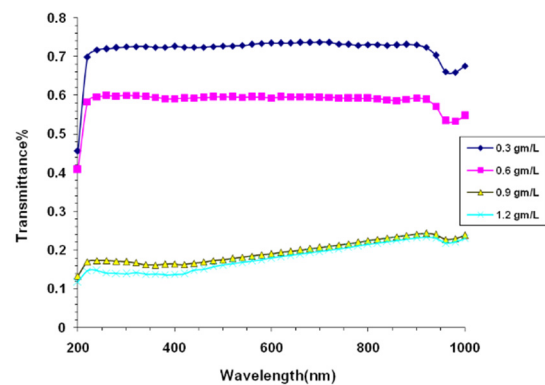

Figure 2. Behavior of transmittance of ZrO_2/SiC-H_2O nanofluids with photon wavelength for various concentrations of ZrO_2/SiC NPs

The relationship between the concentration of ZrO_2/SiC nanoparticles and the electrical conductivity (EC) of ZrO_2/SiC-H_2O nanofluids is shown in Figure 3. When the concentration of ZrO_2/SiC NPs reached 1.2 gm/L, an increase in electrical conductivity of ZrO_2/SiC-H_2O nanofluids occurred that was about 74% higher than before. The reason for this is because the increased electrical conductivity of nanofluids is due, in large part, to the surface charges of nanoparticles [29].

Figure 3. Variation of electrical conductivity (EC) of ZrO_2-H_2O nanofluids with concentrations of ZrO_2/SiC NPs
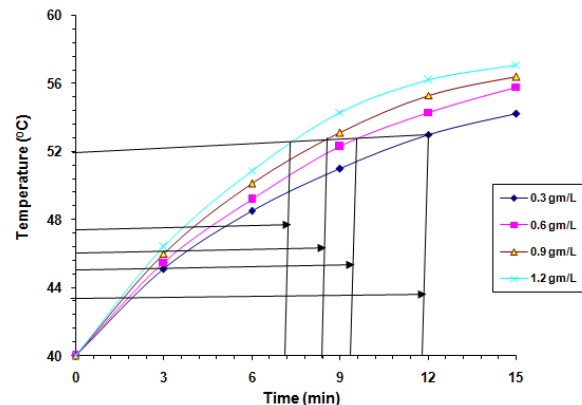
Figure 4. Melting curves of ZrO_2/SiC-H_2O nanofluids

The curves of melting for ZrO_2/SiC-H_2O nanofluids are shown in Figure 4. When there was a greater concentration of ZrO_2/SiC nanoparticles, the melting time was cut down significantly. Increases in thermal conductivity lead to increases in heat transmission, which in turn lead to reductions in melting times for ZrO_2/SiC-H_2O nanofluids that are used for energy storage [30-35]. The decrease in melting time reached 41.2% when the concentration of ZrO_2/SiC NPs rose from 0.3 gm/L to 1.2gm/L after 15 minutes. This is one of the reasons why ZrO_2/SiC-H_2O nanofluids may be beneficial in a variety of heating and cooling industries.

4. CONCLUSIONS

This study focuses on the creation and use of ZrO_2/SiC-H_2O nanofluids for energy storage. The conclusions that may be drawn from this are as follows:

1. With an increase in ZrO_2/SiC NP concentrations from 0.3 gm/L to 1.2 gm/L at photon wavelength (=380nm), the absorbance increased by about 83.7% and the transmittance decreased by 81.2%. 2. The increase in ZrO_2/SiC NP concentrations will increase the absorbance, which refers to the better nanofluid dispersion.

3. When the concentration of ZrO_2/SiC NPs reached 1.2 gm/L, the electrical conductivity of ZrO_2/SiC-H_2O nanofluids improved by nearly 74%.

4. As the concentration of ZrO_2/SiC nanoparticles increased, the melting time reduced.

5. When the concentration of ZrO_2/SiC NPs increases from 0.3 gm/L to 1.2 gm/L after 15 minutes, the decrease in melting time reaches 41.2%.

ORCID IDs
Ahmed Hashim, https://orcid.org/0000-0002-0778-1159; **Farhan Lafta Rashid**, https://orcid.org/0000-0002-7609-6585
Noor Al-Huda Al-Aaraji, https://orcid.org/0000-0002-5117-2983

REFERENCES
[1] V. Sridhara, and L.N. Satapathy, "Al₂O₃-based nanofluids: a review", Nanoscale Research Letters,**6**, 456 (2011). https://doi.org/10.1186/1556-276X-6-456
[2] S. Lee, U.-S. Choi, S. Li, and J.A. Eastan, "Measuring thermal conductivity of fluids containing oxide nanoparticles", ASME J. Heat Transfer,**121**, 280 (1999). https://doi.org/10.1115/1.2825978
[3] A. Hashim, F.L. Rashid, Z. Al-Ramadan, and M.H. Abdul-Allah, "Characterization of (PVA-BaSO4. 5 H2O) Composites", Diyala Journal for Pure Science, **8**, Part 1-3, 296-302 (2012). https://www.iasj.net/iasj/pdf/a5577c17b8b8e701
[4] A.M. Hashim, F.L. Rashid, and I.K. Fayyadh, "Preparation of Nanofluid (Al2O3-water) for Energy Storage", IOSR Journal of Applied Chemistry, **5**(3), 48-49 (2013). https://www.readcube.com/articles/10.9790%2F5736-0534849
[5] A.G. Hadi, F. Lafta, A. Hashim, H. Hakim, A.I.Q. Al-Zuheiry, S.R. Salman, and H. Ahmed, "Study the Effect of Barium Sulphate on Optical Properties of Polyvinyl Alcohol (PVA)", Universal Journal of Materials Science, **1**(2), 52-55 (2013). https://www.hrpub.org/download/201309/ujms.2013.010207.pdf
[6] Z.H. Obaid, F.L. Rashid, M.A. Habeeb, A. Hashim, and A. Hadi, "Synthesis of New Biomaterial Composite for Thermal Energy Storage and Release", Journal of Chemical and Pharmaceutical Sciences, **10**(1), 1-4 (2017). http://www.jchps.com/issues/Volume%2010_Issue%203/20171025_064723_1021016.pdf
[7] H.N. Obaid, M.A. Habeeb, F.L. Rashid, and A. Hashim, "Thermal energy storage by nanofluids", Journal of Engineering and Applied Sciences, **8**(5), 143-145 (2014). http://docsdrive.com/pdfs/medwelljournals/jeasci/2013/143-145.pdf
[8] F.L. Rashid, A. Hadi, A.A. Abid, and A. Hashim, "Solar energy storage and release application of water-phase change material (SnO2-TaC) and (SnO2–SiC) nanoparticles system", International Journal of Advances in Applied Sciences, **8**(2), 154-156 (2019). http://doi.org/10.11591/ijaas.v8.i2.pp154-156
[9] F.L. Rashid, and A. Hashim, "Recent Review on Nanofluid/ Nanocomposites for Solar Energy Storage", International Journal of Scientific Research and Engineering Development, **3**(4),780-789 (2020). http://www.ijsred.com/volume3/issue4/IJSRED-V3I4P94.pdf
[10] F.L. Rashid, and A. Hashim, "Development of Phase Change Materials/Nanoparticles for Thermal Energy Storage", International Journal of Scientific Research and Engineering Development, **3**(4), 790-799 (2020). http://www.ijsred.com/volume3/issue4/IJSRED-V3I4P95.pdf
[11] J.L.T. Chen, A.N. Oumer, and A.A. Azizuddin, "A review on thermo-physical properties of bio, non-bio and hybrid nanofluids", Journal of Mechanical Engineering and Sciences, **13**(4), 5875-5904 (2019). https://doi.org/10.15282/jmes.13.4.2019.12.04
[12] M. Ahmadi, H. Elmongy, T. Madrakian, and M. Abdel-Rehim, "Nanomaterials as sorbents for sample preparation in bioanalysis: A review", Analytica Chimica Acta, **958**, 1–21 (2017). https://doi.org/10.1016/j.aca.2016.11.062
[13] S. Izadi, T. Armaghani, R. Ghasemiasl, A.J. Chamkha, and M. Molana, "A comprehensive review on mixed convection of nanofluids in various shapes of enclosures", Powder Technology, **343**, 880–907 (2019). https://doi.org/10.1016/j.powtec.2018.11.006
[14] W.H. Azmi, S.N.M. Zainon, K.A. Hamid, and R. Mamat, "A review on thermo-physical properties and heat transfer applications of single and hybrid metal oxide nanofluids", Journal of Mechanical Engineering and Sciences, **13**, 5182–5211 (2019). https://doi.org/10.15282/jmes.13.2.2019.28.0425
[15] A.J. Chamkha, M. Molana, A. Rahnama, and F. Ghadami, "On the nanofluids applications in microchannels: A comprehensive review", Powder Technology, **332**, 287–322 (2018). https://doi.org/10.1016/j.powtec.2018.03.044
[16] M. Molana, "On the Nanofluids Application in the Automotive Radiator to Reach the Enhanced Thermal Performance: A Review", American Journal of Heat and Mass Transfer, **4**, 168–187 (2017).

[17] M.S. Rocha, E.L.L. Cabral, G. Sabundjian, H. Yoriyaz, A.C.S. Lima, A.B. Junior, A.C. Prado, et al, "Caracterization of Physical Properties of Ai$_2$O$_3$ and ZrO$_2$ Nanofluids for Heat Transfer Applications", in: *International Nuclear Atlantic Conference - INAC* (São Paulo, Brazil, 2015). http://repositorio.ipen.br/bitstream/handle/123456789/25147/21137.pdf?sequence=1&isAllowed=y

[18] M.I. Shajahan, J.J. Michael, M. Arulprakasajothi, S. Suresh, E.A. Nasr, and H.M.A. Hussein, "Effect of Conical Strip Inserts and ZrO$_2$/DI-Water Nanofluid on Heat Transfer Augmentation: An Experimental Study", Energies, **13**, 4554 (2020). https://doi.org/10.3390/en13174554

[19] W. Song, Y. Lu, Z. Fan, and Y. Wu, "Preparation and Thermophysical Properties of Sodium Nitrate/Nanoparticle/Expanded Graphite Composite Heat Storage Material", Frontiers in Energy Research, **10**, (2022). https://doi.org/10.3389/fenrg.2022.878747

[20] H. Ahmed, A. Hashim, and H.M. Abduljalil, "Determination of Optical Parameters of Films Of PVA/TiO$_2$/SiC and PVA/MgO/SiC Nanocomposites for Optoelectronics and UV-Detectors, Ukr. J. Phys. **65**(6), (2020). https://doi.org/10.15407/ujpe65.6.533

[21] A. Hashim, "Fabrication and characteristics of flexible, lightweight, and low-cost pressure sensors based on PVA/SiO$_2$/SiC nanostructures", J Mater Sci: Mater Electron **32**, 2796–2804 (2021). https://doi.org/10.1007/s10854-020-05032-9.

[22] A. Hashim, H. Abduljalil, and H. Ahmed, "Analysis of Optical, Electronic and Spectroscopic properties of (Biopolymer-SiC) Nanocomposites for Electronics Applications", Egypt. J. Chem. **62**, (2019). https://doi.org/10.21608/EJCHEM.2019.7154.1590

[23] H. Ahmed, and A. Hashim, "Structural, Optical and Electronic Properties of Silicon Carbide Doped PVA/NiO for Low-Cost Electronics Applications", Silicon, **13**, 1509 (2020). https://doi.org/10.1007/s12633-020-00543-w

[24] H. Ahmed, and A. Hashim, Geometry Optimization, Optical and Electronic Characteristics of Novel PVA/PEO/SiC Structure for Electronics Applications, Silicon, **13**, 2639 (2020). https://doi.org/10.1007/s12633-020-00620-0

[25] N.A.H. Al-Aaraji, A. Hashim, A. Hadi, and H.M. Abduljalil, "Effect of Silicon Carbide Nanoparticles Addition on Structural and Dielectric Characteristics of PVA/CuO Nanostructures for Electronics Devices", Silicon, **14**, 4699 (2022). https://doi.org/10.1007/s12633-021-01265-3

[26] A. Hashim, H.M. Abduljalil, and H. Ahmed, "Fabrication and Characterization of (PVA-TiO2)1-x/SiCx Nanocomposites for Biomedical Applications", Egypt. J. Chem. **63**(1), (2020). https://doi.org/10.21608/EJCHEM.2019.10712.1695

[27] H. Ahmed, A. Hashim, and H.M. Abduljalil, "Analysis of Structural, Electrical and Electronic Properties of (Polymer Nanocomposites/ Silicon Carbide) for Antibacterial Application", Egypt. J. Chem. **62**(4), 1167-1176, (2019). https://doi.org/10.21608/EJCHEM.2019.6241.1522

[28] A. Arifutzzaman, A.F. Ismail, I.I. Yaacob, M.Z. Alam, and A.A. Khan, "Stability investigation of water based exfoliated grapheneNanofluids", IOP Conf. Series: Materials Science and Engineering, **488**, (2019), https://doi.org/10.1088/1757-899X/488/1/012002

[29] M. Hadadian, E.K. Goharshadi, and A. Youssefi, "Electrical conductivity, thermal conductivity,and rheological properties of graphene oxide-basednanofluids", J.Nanopart. Res. **16**, (2014). https://doi.org/10.1007/s11051-014-2788-1

[30] A. Hadi, F.L. Rashid, H.Q. Hussein, and A. Hashim, "Novel of water with (CeO$_2$-WC) and (SiC-WC) nanoparticles systems for energy storage and release applications", IOP Conference Series: Materials Science and Engineering, **518**(3), (2019). https://doi.org/10.1088/1757-899X/518/3/032059

[31] F.L. Rashid, A. Hadi, N.H. Al-Garah, and A. Hashim, "Novel Phase Change Materials, MgO Nanoparticles, and Water Based Nanofluids for Thermal Energy Storage and Biomedical Applications", International Journal of Pharmaceutical and Phytopharmacological Research, **8**(1), (2018). https://eijppr.com/2KsaVdO

[32] N.H. Al-Garah, F.L. Rashid, A. Hadi, and A. Hashim, "Synthesis and Characterization of Novel (Organic–Inorganic) Nanofluids for Antibacterial, Antifungal and Heat Transfer Applications", Journal of Bionanoscience, **12**, (2018). https://doi.org/10.1166/jbns.2018.1538

[33] F.L. Rashid, S.M. Talib, A. Hadi, and A. Hashim, "Novel of thermal energy storage and release: water/(SnO$_2$-TaC) and water/(SnO$_2$–SiC) nanofluids for environmental applications", IOP Conf. Series: Materials Science and Engineering, **454**, 012113 (2018). https://doi.org/10.1088/1757-899X/454/1/012113

[34] A.S. Shareef, F.L. Rashid, A. Hadi, and A. Hashim, "Water-Polyethylene Glycol/(SiC-WC) and (CeO2-WC)Nanofluids for Saving Solar Energy", International Journal of Scientific & Technology Research, **8**(11), (2019) .https://www.ijstr.org/final-print/nov2019/Water-polyethylene-Glycol-sic-wc-And-ceo2-wcnanofluids-For-Saving-Solar-Energy-.pdf

[35] A. Hashim, and A. Hadi, "Synthesis and characterization of novel piezoelectric and energy storage nanocomposites: biodegradable materials–magnesium oxide nanoparticles", Ukrainian Journal of Physics, **62**(12), 1050-1056 (2017). https://doi.org/10.15407/ujpe62.12.1050

ОТРИМАННЯ ТА ВЛАСТИВОСТІ НАНОРІДИН ZrO$_2$/SiC-H$_2$O ДЛЯ ВИКОРИСТАННЯ У НАКОПИЧУВАЧАХ ЕНЕРГІЇ
Ахмед Хашим[a], Фархан Лафта Рашид[b], Нур Аль-Худа Аль-Аараджі[c], Бахаа Х. Рабі[a]
[a]Департамент фізики, освітній коледж чистих наук, Вавилонський університет, Вавилон, Ірак
[b]Університет Кербали, інженерний коледж, факультет нафтової інженерії, Ірак
[c]Департамент медичної фізики, коледж університету Аль-Мустакбал, Вавилон, Ірак

Більше половини споживаної енергії в цілому надходить у формі теплової енергії. Важливою технікою захисту навколишнього середовища для підвищення енергоефективності є вивчення того, як використовувати технологію накопичення теплової енергії (TES) для повного використання переривчастого та нестабільного тепла, такого як утилізація сонячного тепла та тепла промислових відходів. Відчутне накопичення тепла, зберігання прихованого тепла та термохімічне накопичення тепла – це всі види накопичення теплової енергії. У цій роботі описується створення нанофлюїдів ZrO$_2$/SiC-H$_2$O та їхні характеристики для використання в програмах зберігання енергії. Результати показують, що збільшення концентрації наночастинок ZrO$_2$/SiC з 0,3 г/л до 1,2 г/л при довжині хвилі фотона (=380 нм) збільшило поглинання приблизно на 83,7% і зменшило пропускну здатність на 81,2%. Крім того, коли концентрація ZrO$_2$/SiC наночастинок зростає, поглинання також зростає, що вказує на покращену дисперсію нанофлюїдів. Крім того, коли концентрація наночастинок ZrO2/SiC досягла 1,2 г/л, електропровідність нанофлюїдів ZrO$_2$/SiC-H$_2$O покращилася майже на 74%, а час плавлення скоротився зі збільшенням концентрації наночастинок ZrO$_2$/SiC.
Ключові слова: *накопичувач енергії; нанофлюїди; пропускання; поглинання; плавлення*

NANOFLUIDS OF PEG/MgO/SiC-H₂O AS EXCELLENT HEAT TRANSFER MEDIUM: SYNTHESIS, PROPERTIES AND APPLICATION†

Farhan Lafta Rashidᵃ, Ahmed Hashim*ᵇ, Noor Al-Huda Al-Aarajiᶜ, Aseel Hadiᵈ

ᵃUniversity of Kerbala, College of Engineering, Petroleum Engineering Department, Iraq
ᵇDepartment of Physics, College of Education for Pure Sciences, University of Babylon, Babylon, Iraq
ᶜDepartment of Medical Physics, Al-Mustaqbal University College, Babylon, Iraq
ᵈDepartment of Ceramic and Building Materials, College of Materials Engineering, University of Babylon, Iraq
*Corresponding Author e-mail: ahmed_taay@yahoo.com

Today, one of the most significant and widely used engineering fields is heat transfer science. Saving energy and increasing efficiency are crucial given the need for energy management. Numerous sectors, including the cooling of machinery in power plants, the car industry, electronic equipment, and heat exchangers, heavily rely on fluid heat transfer. Improved design and functionality of thermal systems are made possible by increased heat transfer rate by fluids. This study presents the production, characteristics, and potential uses of PEG/MgO/SiC-H₂O nanofluids as superior heat transfer media. Results indicate that when the quantity of MgO/SiC nanoparticles increased, the melting time reduced. Additionally, when the MgO/SiC NP concentration increased from 3 to 12 weight percent after 15 minutes, the reduction in melting time reached 65.5%. Additionally, when the concentration of MgO/SiC NPs was increased from 3 weight percent to 12 weight percent at photon wavelength (λ=400 nm), the electrical conductivity of PEG/MgO/SiC-H₂O nanofluids increased by about 30.6%. At the same time, the absorbance increased by about 66.4% and the transmittance decreased by 58.8%.

Keywords: *Heat transfer; applications; nanofluids; saving energy; energy management*
PACS: 64.75.Cd, 74.20.De, 78.66.Li, 78.66.Qn.

1. INTRODUCTION

Nanofluids have a lot of promise in a variety of disciplines, including solar applications where they can boost solar water heaters' heat-transfer coefficients or increase the capacity of thermal energy storage systems, and refrigeration where they can boost refrigeration systems' efficiency. Nanofluids have a lot of promise, but they aren't often used as refrigerants or heat-transfer fluids (HTFs). However, during the last ten years, the application of nanofluids in solar heat collectors has gained popularity [1-7]. One of the biggest obstacles to efficient heating or cooling is creating ideal operating conditions. These systems' primary function is to accelerate the pace of heat or cold transmission via the use of cutting-edge working fluids. However, when the use of transfer fluids is taken into account, a number of important operating and maintenance requirements must be satisfied. The two categories of criteria known as physicochemical and thermal properties define heat transfer fluids (HTFs), which are extensively employed in several industrial and consumer applications. The most crucial physicochemical variables are kinematic viscosity, flash point, and pour point. The flow in the system is determined by viscosity, and to guarantee that temperature gradients between the heat carrier and the heat transfer surface are sufficiently minimal, a turbulent flow that has a Reynolds number exceeding 2100 in linear channels with circular cross sections must be present [8–14].

Current developments in the research of nanofluids, including manufacturing techniques, the mechanism of stability evaluation, stability enhancement procedures, thermophysical characteristics, and characterization of nanofluids, were described by Ouabouch et al. in their article [15]. Additionally, the variables affecting thermophysical characteristics were investigated. The evolution of the correlations utilized to forecast the thermophysical characteristics of the dispersion was reported by Ali et al. [16]. Additionally, it evaluates how these sophisticated working fluids affect nuclear reactor systems, air conditioning and refrigeration systems, and parabolic trough solar collectors. The existing scientific knowledge gap is then presented to establish future research trajectories. The poor thermal conductivity of the CuO/water nanofluid, which was caused by the spherical form of the CuO nanoparticles, was addressed by Nfawa et al. [17] by adding a tiny quantity of magnesium oxide (MgO) nanoparticles to the nanofluid. The thermal conductivity of a novel CuO-MgO/water hybrid nanofluid has been investigated at various volume concentrations (0.125-1.25%) of 80 % CuO and 20% MgO nanoparticles suspended in water at various ranges of temperatures from 25 to 50°C. The production, stability, and thermal conductivity of the MWCNTs-SiC/Water-EG hybrid nanofluid were examined by Kakavandi and Akbari [18]. The nanoparticles were characterized using X-ray diffraction (XRD) and scanning electron microscopy (SEM) techniques. DLS test was used to track nanofluid stability. The DLS data showed that nanoparticles were present in the nanofluid. SiC and its nanocomposites are important in fields of sensors, biomedical and electronics [19-29]. The synthesis, characteristics, and uses of PEG/MgO/SiC-H₂O nanofluids as superior heat transfer medium is discussed in this work.

2. MATERIALS AND METHODS

The following materials were employed in this study: polyethylene glycol (PEG), magnesium oxide nanoparticles (MgO NPs), and silicon carbide nanoparticles (SiC NPs). In 50 ml of distilled water, 1 g of PEG was dissolved. The PEG/MgO/SiC-H_2O nanofluids were created using MgO/SiC NPs at concentrations of 3%, 6%, 9%, and 12%. PEG/MgO/SiC-H_2O nanofluids' optical and electrical properties were investigated. Using a double beam spectrophotometer (Shimadzu, UV-18000A) with a 200–1100 nm wavelength range, the optical characteristics of PEG/MgO/SiC-H_2O nanofluids were examined. The analysis of the PEG/MgO/SiC-H_2O nanofluids' melting properties throughout the heating process is part of the thermal energy storage. PEG/MgO/SiC-H_2O nanofluids, whose temperature can be adjusted from 35°C to 100°C with a stirrer, were utilized as the heat transfer fluid. A digital device was used to measure the temperature of the nanofluids as they heated.

3. RESULTS AND DISCUSSION

Figures 1 and 2 show, at different concentrations of MgO/SiC NPs, the behavior of the absorbance and transmittance spectra of PEG/MgO/SiC-H_2O nanofluids with photon wavelength. According to the figures, increasing the concentration of MgO/SiC NPs from 3 weight percent to 12 weight percent at photon wavelengths ($\lambda=400$nm) resulted in an increase in absorbance of approximately 66.4% and a decrease in transmittance of 58.8%. This behavior can be useful in solar collectors, heating and cooling systems. MgO/SiC NP concentration increases will result in higher absorbance, which indicates improved nanofluid dispersion [30].
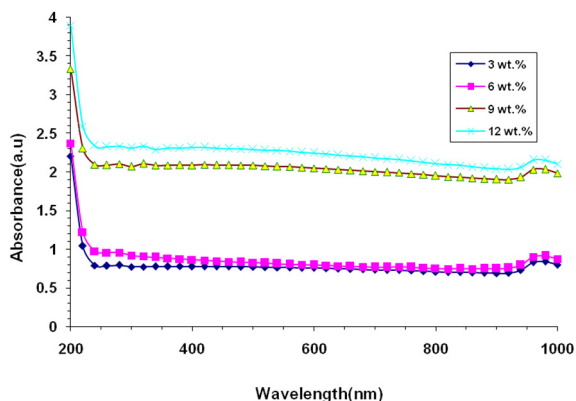
Figure 1. Behavior of absorbance spectra of PEG/MgO/SiC-H_2O nanofluids with photon wavelength for various concentrations of MgO/SiC NPs
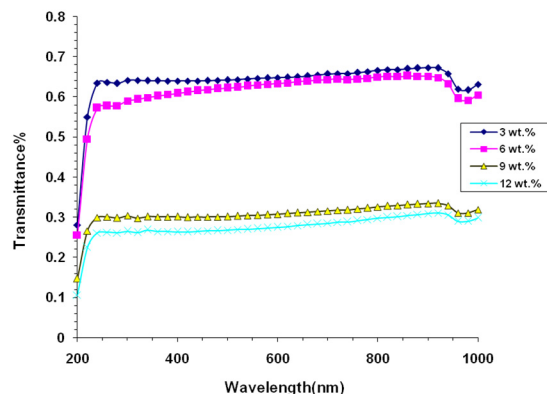
Figure 2. Behavior of transmittance spectra of PEG/MgO/SiC-H_2O nanofluids with photon wavelength for various concentrations of MgO/SiC NPs

The electrical conductivity (EC) of PEG/MgO/SiC-H_2O nanofluids varies with concentrations of MgO/SiC NPs, as shown in Fig. 3. When the concentration of MgO/SiC NPs rose to 12 weight percent, the electrical conductivity of PEG/MgO/SiC-H_2O nanofluids improved by roughly 30.6%. The rationale is that the electrical conductivity of the nanofluids depends significantly on the surface charges of nanoparticles [31].

The melting curves of PEG/MgO/SiC-H_2O nanofluids are shown in Fig. 4. As the concentration of MgO/SiC nanoparticles increased, the melting time decreased. PEG/MgO/SiC-H_2O nanofluids' decreased melting time for energy storage is connected to improved thermal conductivity, which increases heat transfer[32–39]. When the amount of MgO/SiC NPs increases from 3 weight percent to 12 weight percent within 15 minutes, the melting time is reduced by 65.5%, making the PEG/MgO/SiC-H_2O nanofluids beneficial in a variety of heating and cooling sectors.
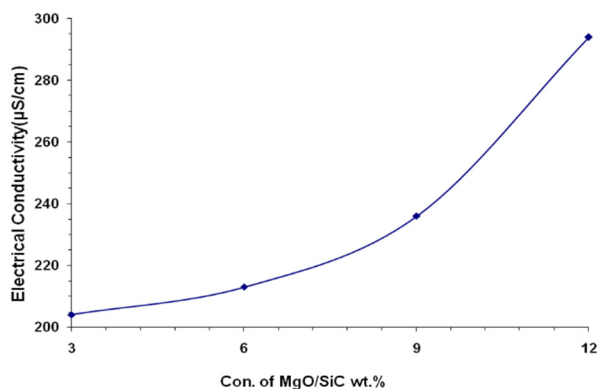
Figure 3. Variation of electrical conductivity (EC) of PEG/MgO/SiC-H_2O nanofluids with concentrations of MgO/SiC NPs
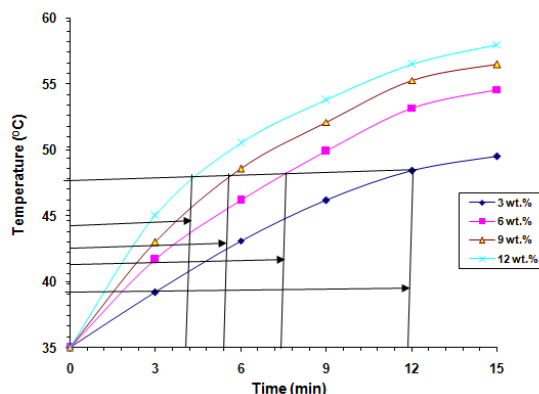
Figure 4. Melting curves of PEG/MgO/SiC-H_2O nanofluids

4.CONCLUSIONS

The category of HTFs that is now increasing and evolving the fastest is nanofluids. Their advantageous qualities include the variety of base fluids and integrated nanoparticles, which results in a composition that can be adjusted based on the need. From this research, the following findings might be made:

1. As the quantities of MgO/SiC nanoparticles increased, the melting time reduced.

2. When the MgO/SiC NP concentration increased from 3 weight percent to 12 weight percent after 15 minutes, the reduction in melting time reached 65.5%.

3. When the concentration of MgO/SiC NPs rose to 12 weight percent, the electrical conductivity of PEG/MgO/SiC-H$_2$O nanofluids improved by around 30.6%.

4. The concentration of MgO/SiC NPs was raised from 3 weight percent to 12 weight percent at photon wavelength (λ=400nm), resulting in an increase in absorbance of about 66.4% and a reduction in transmittance of 58.8%.

ORCID IDs

Farhan Lafta Rashid, https://orcid.org/0000-0002-7609-6585; **Ahmed Hashim,** https://orcid.org/0000-0002-0778-1159
Noor Al-Huda Al-Aaraji, https://orcid.org/0000-0002-5117-2983; **Aseel Hadi**, https://orcid.org/0000-0002-3351-2227

REFERENCES

[1] E.A.C. Panduro, F. Finotti, G. Largiller, and K.Y. Lervåg, "A review of the use of nanofluids as heat-transfer fluids in parabolic-trough collectors", Applied Thermal Engineering, **211**, 118346 (2022). https://doi.org/10.1016/j.applthermaleng.2022.118346

[2] S.U.S. Choi, J.A. Eastman, Enhancing Thermal Conductivity of Fluids with Nanoparticles, Technical Report ANL/MSD/CP-84938; CONF-951135-29, Argonne National Lab., IL (United States), 1995, https://www.osti.gov/biblio/196525

[3] R. Taylor, S. Coulombe, T. Otanicar, P. Phelan, A. Gunawan, W. Lv, G. Rosengarten, R. Prasher, and H. Tyagi, "Small particles, big impacts: A review of the diverse applications of nanofluids", J. Appl. Phys. **113**, 011301 (2013), http://dx.doi.org/10.1063/1.4754271

[4] F.L. Rashid, and A. Hashim, "Recent Review on Nanofluid/ Nanocomposites for Solar Energy Storage", International Journal of Scientific Research and Engineering Development, **3**(4), 780-789 (2020).

[5] F.L. Rashid, and A. Hashim, "Development of Phase Change Materials/Nanoparticles for Thermal Energy Storage", International Journal of Scientific Research and Engineering Development, **3**(4), 790-799 (2020).

[6] H.N. Azziz, A.S. Sharee, and F.L. Rashid, "Experimental Investigation of the Heat Transfer for the Effect of Nanoparticles with Different Base Fluid and Solar Collector Tilt Angle", Journal of Engineering and Applied Sciences, **13**(13), 10614 (2018).

[7] F.L. Rashid, A.K. Hussein, E.H. Malekshah, A. Abderrahmane, K. Guedri, and O. Younis, "Review of Heat Transfer Analysis in Different Cavity Geometries with and without Nanofluids", Nanomaterials, **12**, 2481 (2022). https://doi.org/10.3390/nano12142481

[8] N. Czaplicka, A. Grzegórska, J. Wajs, J. Sobczak, and A. Rogala, "Promising Nanoparticle-Based Heat Transfer Fluids – Environmental and Techno-Economic Analysis Compared to Conventional Fluids", Int. J. Mol. Sci. **22**, 9201 (2021). https://doi.org/10.3390/ijms22179201.

[9] L. Heller, *Literature Review on Heat Transfer Fluids and Thermal Energy Storage Systems in CSP Plants*, (STERG, Stellenbosch, South Africa, 2013).

[10] J. Gong, and K. Sumathy, *Active Solar Water Heating Systems*, (Elsevier Ltd., Amsterdam, The Netherlands, 2016). ISBN 9780081003022

[11] A.M. Hashim, F.L. Rashid, and I.K. Fayyadh, "Preparation of Nanofluid (Al$_2$O$_3$-water) for Energy Storage", IOSR Journal of Applied Chemistry, **5**(3), 48-49 (2013).

[12] Z.H. Obaid, F.L. Rashid, M.A. Habeeb, A. Hashim, and A. Hadi, "Synthesis of New Biomaterial Composite for Thermal Energy Storage and Release", Journal of Chemical and Pharmaceutical Sciences, **10**(3), 1125-1128 (2017). https://jchps.com/issues/Volume%2010_Issue%203/20171025_064723_1021016.pdf

[13] H.N. Obaid, M.A. Habeeb, F.L. Rashid, and A. Hashim, "Thermal energy storage by nanofluids", Journal of Engineering and Applied Sciences, **8**(5), 143-145 (2014).

[14] F.L. Rashid, A. Hadi, Al-Garah, H. Naheda, and A. Hashim, "Novel phase change materials, MgO nanoparticles, and water based nanofluids for thermal energy storage and biomedical applications", Int. J. Pharm. Phytopharmacol. Res, **8**(1), 46-56 (2018).

[15] O. Ouabouch, M. Kriraa, and M. Lamsaadi, "Stability, thermophsical properties of nanofluids, and applications in solar collectors: A review", AIMS Materials Science, **8**(4), 659–684 (2021). https://doi.org/10.3934/matersci.2021040

[16] N. Ali, A.M. Bahman, N.F. Aljuwayhel, S.A. Ebrahim, S. Mukherjee, and A. Alsayegh, "Carbon-Based Nanofluids and Their Advances towards Heat Transfer Applications – A Review, Nanomaterials, **11**, 1628 (2021). https://doi.org/10.3390/nano11061628

[17] S.R. Nfawa, A.R.A. Talib, A.A. Basri, and S.U. Masuri, "Novel use of MgO nanoparticle additive for enhancing the thermal conductivity of CuO/water nanofluid", Case Studies in Thermal Engineering, **27**, 101279 (2021). https://doi.org/10.1016/j.csite.2021.101279

[18] A. Kakavandi, and M. Akbari, "Experimental investigation of thermal conductivity of nanofluids containing of hybrid nanoparticles suspended in binary base fluids and propose a new correlation", International Journal of Heat and Mass Transfer, **124**, 742-751 (2018). https://doi.org/10.1016/j.ijheatmasstransfer.2018.03.103

[19] H. Ahmed, A. Hashim, H.M. Abduljalil, Determination of Optical Parameters of Films Of PVA/TiO2/SiC and PVA/MgO/SiC Nanocomposites for Optoelectronics and UV-Detectors, Ukr. J. Phys. **65**(6), (2020). https://doi.org/10.15407/ujpe65.6.533

[20] A. Hashim, "Fabrication and characteristics of flexible, lightweight, and low-cost pressure sensors based on PVA/SiO$_2$/SiC nanostructures", J. Mater. Sci: Mater. Electron. **32**, 2796–2804 (2021). https://doi.org/10.1007/s10854-020-05032-9

[21] A. Hashim, H. Abduljalil, and H. Ahmed, "Analysis of Optical, Electronic and Spectroscopic properties of (Biopolymer-SiC) Nanocomposites for Electronics Applications", Egypt. J. Chem. **62**, (2019). https://doi.org/10.21608/EJCHEM.2019.7154.1590

[22] H. Ahmed, and A. Hashim, "Structural, Optical and Electronic Properties of Silicon Carbide Doped PVA/NiO for Low Cost Electronics Applications", Silicon, **13**, 1509 (2021). https://doi.org/10.1007/s12633-020-00543-w

[23] H. Ahmed, and A. Hashim, "Geometry Optimization, Optical and Electronic Characteristics of Novel PVA/PEO/SiC Structure for Electronics Applications", Silicon, **13**, 2639 (2021). https://doi.org/10.1007/s12633-020-00620-0

[24] Al-Aaraji, N.AH., Hashim, A., Hadi, A. *et al.* Effect of Silicon Carbide Nanoparticles Addition on Structural and Dielectric Characteristics of PVA/CuO Nanostructures for Electronics Devices. *Silicon* (2021). https://doi.org/10.1007/s12633-021-01265-3.

[25] A. Hashim, H.M. Abduljalil, and H. Ahmed, "Fabrication and Characterization of (PVA-TiO$_2$)$_{1-x}$/ SiC$_x$ Nanocomposites for Biomedical Applications", Egypt. J. Chem. **63**(1), (2020). https://doi.org/10.21608/EJCHEM.2019.10712.1695

[26] Obaid, W.O., Hashim, A. Synthesis and Augmented Optical Properties of PC/SiC/TaC Hybrid Nanostructures for Potential and Photonics Fields. Silicon, **14**, 11199 (2022). https://doi.org/10.1007/s12633-022-01854-w

[27] H. Ahmed, and A. Hashim, "Tuning the Spectroscopic and Electronic Characteristics of ZnS/SiC Nanostructures Doped Organic Material for Optical and Nanoelectronics Fields", Silicon, (2022). https://doi.org/10.1007/s12633-022-02173-w

[28] A. Hashim, M.H. Abbas, N.AH. Al-Aaraji, et al. "Facile Fabrication and Developing the Structural, Optical and Electrical Properties of SiC/Y$_2$O$_3$ Nanostructures Doped PMMA for Optics and Potential Nanodevices", Silicon, (2022). https://doi.org/10.1007/s12633-022-02104-9

[29] A. Hashim, M.H. Abbas, N.A.H. Al-Aaraji, et al. "Controlling the Morphological, Optical and Dielectric Characteristics of PS/SiC/CeO$_2$ Nanostructures for Nanoelectronics and Optics Fields", J. Inorg. Organomet. Polym. (2022). https://doi.org/10.1007/s10904-022-02485-9

[30] A. Arifutzzaman, A.F. Ismail, I.I. Yaacob, M.Z. Alam, and A.A. Khan, "Stability investigation of water based exfoliated graphene Nanofluids", IOP Conf. Series: Materials Science and Engineering, **488**, (2019), https://doi.org/10.1088/1757-899X/488/1/012002.

[31] M. Hadadian, E.K. Goharshadi, and A. Youssefi, "Electrical conductivity, thermal conductivity, and rheological properties of graphene oxide-based nanofluids", J. Nanopart. Res. **16**, (2014), https://doi.org/10.1007/s11051-014-2788-1

[32] I.R. Agool, K.J. Kadhim, and A. Hashim, "Preparation of (polyvinyl alcohol–polyethylene glycol–polyvinyl pyrrolidinone–titanium oxide nanoparticles) nanocomposites: electrical properties for energy storage and release, International Journal of Plastics Technology", **20**(1), 121 (2016). https://doi.org/10.1007/s12588-016-9144-5

[33] A. Hashim, and A. Hadi, (2017). "Synthesis and Characterization of Novel Piezoelectric and Energy Storage Nanocomposites: Biodegradable Materials–Magnesium Oxide Nanoparticles", Ukrainian Journal of Physics, **62**(12), 1050, https://doi.org/10.15407/ujpe62.12.1050

[34] I.R. Agool, K.J. Kadhim, and A. Hashim, "Synthesis of (PVA-PEG-PVP-ZrO$_2$) Nanocomposites For Energy Release and Gamma Shielding Applications, International Journal of Plastics Technology", **21**(2), (2017). https://doi.org/10.1007/s12588-017-9196-1

[35] A. Hadi, A. Hashim, and D. Hassan, "Fabrication of new ceramics nanocomposites for solar energy storage and release", Bulletin of Electrical Engineering and Informatics, **9**(1), (2020), https://doi.org/10.11591/eei.v9i1.1323

[36] A. Hadi, F.L. Rashid, H.Q. Hussein, A. Hashim, "Novel of water with (CeO2-WC) and (SiC-WC) nanoparticles systems for energy storage and release applications", IOP Conference Series: Materials Science and Engineering, **518**(3), 5 (2019).https://doi.org/10.1088/1757-899X/518/3/032059

[37] N.H. Al-Garah, F.L. Rashid, A. Hadi, and A. Hashim, "Synthesis and Characterization of Novel (Organic–Inorganic) Nanofluids for Antibacterial, Antifungal and Heat Transfer Applications", Journal of Bionanoscience, **12**, (2018). https://doi.org/10.1166/jbns.2018.1538

[38] A.S. Shareef, F.L. Rashid, A. Hadi, and A. Hashim, "Water-Polyethylene Glycol/ (SiC-WC) and (CeO2-WC) Nanofluids for Saving Solar Energy", International Journal of Scientific & Technology Research, **8**(11), (2019).

[39] F.L. Rashid, S.M. Talib, A. Hadi, and A. Hashim, "Novel of thermal energy storage and release: water/(SnO2 -TaC) and water/(SnO2–SiC) nanofluids for environmental applications", IOP Conf. Series: Materials Science and Engineering, **454**, 012113 (2018). https://doi.org/10.1088/1757-899X/454/1/012113

**НАНОРІДИНИ PEG/MgO/SiC-H$_2$O ЯК ЧУДОВЕ ТЕПЛОПЕРЕДАЮЧЕ СЕРЕДОВИЩЕ:
СИНТЕЗ, ВЛАСТИВОСТІ ТА ЗАСТОСУВАННЯ**

Фархан Лафта Рашид[a], Ахмед Хашім[b], Нур Аль-Худа Аль-Аараджі[c], Асіль Хаді[d]
[a]Університет Кербали, інженерний коледж, факультет нафтової інженерії, Ірак
[b]Факультет фізики, Освітній коледж чистих наук, Вавилонський університет, Вавилон, Ірак
[c]Факультет медичної фізики, коледж університету Аль-Мустакбал, Вавилон, Ірак
[d]Департамент кераміки та будівельних матеріалів, Коледж інженерії матеріалів, Вавилонський університет, Ірак

Сьогодні однією з найбільш значущих і широко використовуваних галузей техніки є наука про теплообмін. З огляду на потребу в енергоменеджменті економія енергії та підвищення ефективності є надзвичайно важливими. Численні сектори, включаючи охолодження машин на електростанціях, автомобільну промисловість, електронне обладнання та теплообмінники, значною мірою покладаються на теплообмін рідиною. Покращений дизайн і функціональність теплових систем стали можливими завдяки підвищеній швидкості теплопередачі рідинами. У цьому дослідженні представлено виробництво, характеристики та потенційне використання нанофлюїдів PEG/MgO/SiC-H$_2$O як кращого теплообмінного середовища. Результати показують, що коли кількість наночастинок MgO/SiC збільшується, час плавлення зменшується. Крім того, коли концентрація MgO/SiC NP збільшилася з 3 до 12 масових відсотків через 15 хвилин, скорочення часу плавлення досягає 65,5%. Крім того, коли концентрація наночастинок MgO/SiC була збільшена з 3 вагових відсотків до 12 вагових відсотків на довжині хвилі λ=400 нм, електропровідність нанофлюїдів PEG/MgO/SiC H$_2$O зросла приблизно на 30,6 %. У той же час поглинання зросло приблизно на 66,4 %, а пропускна здатність зменшилася на 58,8 %.
Ключові слова: *теплообмін; застосування; нанофлюїди; енергозбереження; енергоменеджмент*

EXPLORING THE OPTICAL AND ELECTRICAL CHARACTERISTICS OF MgO/SiC-H₂O NANOFLUIDS FOR THERMAL ENERGY STORAGE[†]

Farhan Lafta Rashid[a], Ahmed Hashim[b]*, M.H. Abbas[c], Aseel Hadi[d]

[a]University of Kerbala, College of Engineering, Petroleum Engineering Department, Iraq
[b]Department of Physics, College of Education for Pure Sciences, University of Babylon, Babylon, Iraq
[c]Department of Medical Physics, Al-Mustaqbal University College, Babylon, Iraq
[d]Department of Ceramic and Building Materials, College of Materials Engineering, University of Babylon, Iraq
*Corresponding Author e-mail: ahmed_taay@yahoo.com

Heat is transferred to the storage medium during the charging phase of thermal energy storage (TES), and then released during the discharging phase. It may be used for industrial operations like metallurgical transformations or solar power facilities. Heat is stored in materials that alter temperature, phase, or chemical composition in sensible, latent, and thermochemical media, respectively. Optimal heat storage has a long history. This study investigates the optical and electrical properties of MgO/SiC-H₂O nanofluids for applications including thermal energy storage. Results indicate that when MgO/SiC NP concentrations were raised to 1.2 gm/L, absorbance rose by approximately 66.9% and transmittance by about 54%. Additionally, the increase in MgO/SiC NP concentration will raise absorbance, which indicates improved nanofluid dispersion. Additionally, when MgO/SiC nanoparticle concentrations approach 1.2 gm/L, the electrical conductivity of nanofluids increases by roughly 49.2%, and the melting time reduces as the concentration of MgO/SiC nanoparticles rises.

Keywords: *Optical characteristics; electrical characteristics; nanofluid; energy storage*
PACS: 47.35.Pq, 78.66.Li, 78.66.Sq, 78.67.Bf

1. INTRODUCTION

The enhanced thermal conductivity for a nanofluid containing copper in pump oil caused initial interest in nanofluids as potential heat transfer fluids to spike, but this interest was later dashed after numerous research groups tested a variety of available combinations of fluids and nanoparticles, primarily at room temperature. The bulk of the tests were done on water-based fluids, which are among nature's finest at heat transmission because they have a good balance of high thermal conductivity and low viscosity. The narrow temperature range of operation, high vapor pressure, and strong corrosiveness of water are some drawbacks [1–5]. By processing and creating materials with average crystallite sizes below 100 nm, or nanomaterials, nanotechnology opens up a new field of study. Quantum dots, carbon nanotubes, nanocomposites, and nanocrystalline materials are only a few examples of the variety of substances that fall under the umbrella term "nanomaterials" [6]. Chemical heat, latent heat, and sensible heat are the three components that make up the thermal energy storage. Storage of thermal energy at the temperature of the solid-to-liquid phase transition is the foundation of latent heat storage systems. This ability's essential function is to choose an exact (PCM) for a precise application based primarily on the temperature of that material's melting range (change of phase) (PCM). Because of the right characteristics of paraffin, such as stability, noncorrosiveness, and nontoxicity, it may be regarded as a great alternative for PCM use. The low heat conductivity of paraffin is a drawback to utilizing it as PCM. According to definitions given by experts [7-12], thermal energy storage is the temporary storing of thermal energy at any temperature (i.e., both low and high).

New kind of nanocomposites created by Hazim et al. [13] might be regarded promising materials for a variety of electrical and optical applications, including solar cells, sensors, electronics gates, transistors, lenses, lasers, etc. Different quantities of polymethylmethacrylate (PMMA), aluminum oxide (Al₂O₃) nanoparticles, and silver (Ag) nanoparticles were used to create the nanocomposites. An outline of the development of the usage of nanofluids in several applications was provided by Tawfik [14]. In accordance with this contribution, further research on the fundamentals and applications of nanofluids is urgently needed in order to comprehend the physical processes involved in employing nanofluids and to investigate many facets of their uses. Rasheed et al [15] thorough comparison of hybrid nanofluids and traditional forms of nanofluids provided a thorough grasp of the benefits of the latter. According to the findings that have been made public, hybrid nanofluids with improved thermal characteristics hold out hope for improved solar thermal PV/T system performance.

Verma and others [16] presented a clear and succinct review that concentrated on the mechanism and function of the optical characteristics of nanomaterials in enhancing absorptance or extinction coefficients from the solar spectrum. Polyvinyl alcohol (PVA), polyethylene oxide (PEO), and copper oxide (CuO) nanocomposites were created by Hashim et al. [17] and their structural and optical characteristics for use as humidity sensors were explored. Several studies on nanocomposites of SiC doped organic material to utilize in many applications such as biomedical, electronics and sensors [18-27]. In this research, MgO/SiC-H₂O nanofluids are prepared, and their optical and electrical characteristics are studied for applications in thermal energy storage.

2. MATERIALS AND METHODS

Silicon carbide and magnesium oxide nanoparticles (MgO NPs) were the materials employed in this study (SiC NPs). The nanofluids were made using MgO/SiC NPs at varied concentrations of 0.3 gm/L, 0.6 gm/L, 0.9 gm/L, and 1.2 gm/L. Researchers looked at the optical and electrical characteristics of MgO/SiC-H_2O nanofluids. Shimadzu's UV-18000A double beam spectrophotometer is used to test the optical characteristics of MgO/SiC-H_2O nanofluids from 200 to 1000 nm. Analyzing the MgO/SiC-H_2O nanofluids' melting properties throughout the heating process is part of the thermal energy storage. The MgO/SiC-H_2O nanofluids, whose temperature can be adjusted from 40°C to 100°C with a stirrer, were utilized as the heat transfer fluid. A digital device was used to monitor the temperature of the nanofluids while they were being heated.

3. RESULTS AND DISCUSSION

Figures 1 and 2 show, at various concentrations of MgO/SiC NPs, the absorbance and transmittance spectra of MgO/SiC-H_2O nanofluids with photon wavelength. By increasing the concentration of MgO/SiC NPs to 1.2gm/L, these figures showed that the absorbance rose by approximately 66.9% and the transmittance reduced by around 54%. The MgO/SiC-H_2O nanofluids have a greater absorption at UV spectrum, making them potentially useful in a variety of renewable energy areas, including solar collectors, energy storage, and heating and cooling systems. Increased absorbance, which corresponds to enhanced nanofluid dispersion, will be caused by an increase in MgO/SiC NP concentration [28].
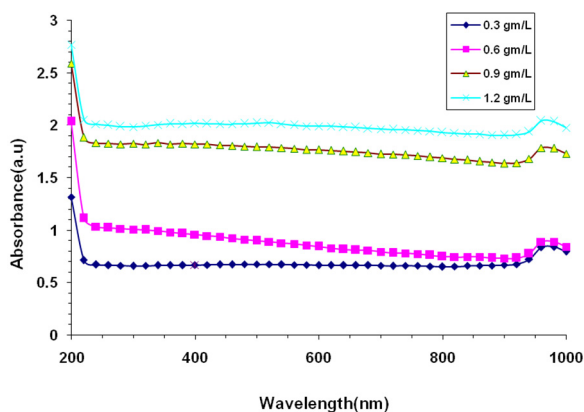
Figure 1. Absorbance spectra of MgO/SiC-H_2O nanofluids with photon wavelength for different concentrations of MgO/SiC NPs.
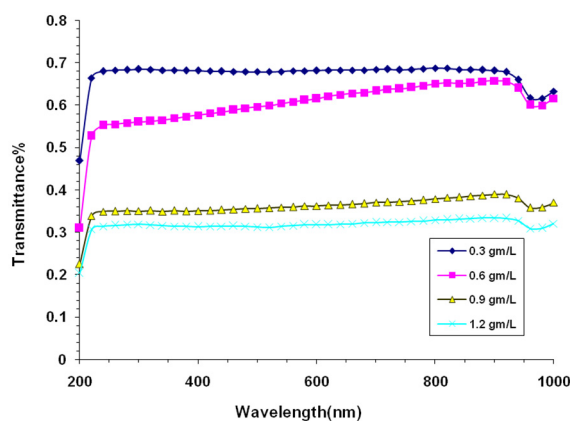
Figure 2. Transmittance spectra of MgO/SiC-H_2O nanofluids with photon wavelength for different concentrations of MgO/SiC NPs

The association between MgO/SiC NP concentrations and electrical conductivity of MgO/SiC-H_2O nanofluids is shown in Fig. 3. Due to an increase in the quantity of charge carriers[29,30], the electrical conductivity of nanofluids increases by roughly 49.2% when the concentration of MgO/SiC NPs reaches 1.2 gm/L.

The melting curves of the MgO/SiC-H_2O nanofluids are shown in Fig. 4. As the quantities of MgO/SiC nanoparticles increase, the melting time reduces. Due to improved thermal conductivity, MgO/SiC-H_2O nanofluids may melt more quickly in energy storage applications, increasing heat transmission [31–39]. When the concentration of MgO/SiC NPs increases from 0.3 gm/L to 1.2 gm/L within 15 min, the gain in melting time reaches 45%. As a result of this behavior, MgO/SiC-H_2O nanofluids may be thought of as a key for heating and cooling systems.
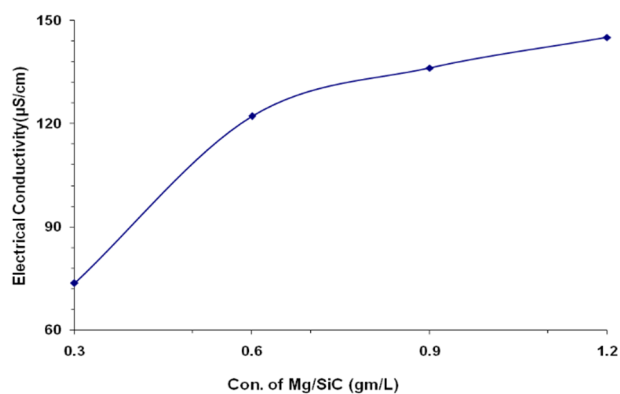
Figure 3. Behavior of electrical conductivity of MgO/SiC-H_2O nanofluids with concentrations of MgO/SiC NPs.
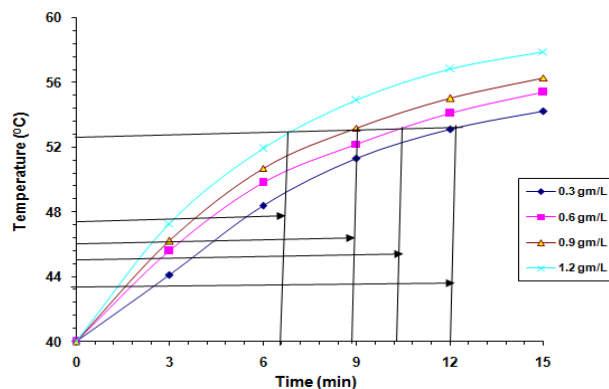
Figure 4. Melting curves of MgO/SiC-H_2O nanofluids

4. CONCLUSION

This study examines the optical and electrical properties of MgO/SiC-H$_2$O nanofluids for applications in thermal energy storage. This research allows us to reach the following conclusions:

1. When the concentration of MgO/SiC NPs was raised to 1.2 gm/L, the absorbance rose by approximately 66.9% and the transmittance by about 54%.

2. As the MgO/SiC NP concentration increases, the absorbance rises, indicating improved nanofluid dispersion.

3. When the concentration of MgO/SiC NPs increased to 1.2 gm/L, the electrical conductivity of nanofluids increased by roughly 49.2%.

4. As the concentration of MgO/SiC nanoparticles increases, the melting time reduces.

5. When the concentration of MgO/SiC NPs increases from 0.3 gm/L to 1.2 gm/L after 15 minutes, the gain in melting time reaches 45%.

ORCID IDs
Farhan Lafta Rashid, https://orcid.org/0000-0002-7609-6585; **Ahmed Hashim**, https://orcid.org/0000-0002-0778-1159
Aseel Hadi, https://orcid.org/0000-0002-3351-2227

REFERENCES

[1] E.V. Timofeeva, W. Yu, D.M. France, D. Singh, and J.L. Routbort, "Base fluid and temperature effects on the heat transfer characteristics of SiC in ethylene glycol/H$_2$O and H$_2$O nanofluids", Journal of Applied Physics, **109**, 014914 (2011). https://doi.org/10.1063/1.3524274

[2] J.A. Eastman, S.U.S. Choi, S.Li, L.J. Thompson, and S. Lee, "Enhanced thermal conductivity through the development of nanofluids", in: *Proceedings of the Symposium on Nanophase and Nanocomposite Materials II*, edited by S. Komarneni, J.C. Parker, and H.J. Wollenberger, Vol. 457, Materials Research Society Symposium Proceedings, (Warrendale, PA, 1997), pp. 3–11.

[3] S. Kabelac, and J. F. Kuhnke, "Heat transfer mechanisms in nanofluids Experiments and theory", in: *Proceedings of the 13th International Heat Transfer Conference*, edited by G. de Vahl Davis, and E. Leonardi, (Sydney, Australia, 2006), pp. 110–111.

[4] K. Elsaid, M.A. Abdelkareem, H.M. Maghrabie, E.T. Sayed, T. Wilberforce, A. Baroutaji, and A.G. Olabi, "Thermophysical properties of graphene-based nanofluids", International Journal of Thermofluids, **10**, 100073 (2021). https://doi.org/10.1016/j.ijft.2021.100073.

[5] H. Zhang, J. Baeyens, G. Cáceres, J. Degrève, Y. Lv, "Thermal energy storage: Recent developments and practical aspects", Progress in Energy and Combustion Science, **53**, 1-40 (2016). https://doi.org/10.1016/j.pecs.2015.10.003

[6] H.N. Obaid, M.A. Habeeb, F.L. Rashid, and A. Hashim, "Thermal Energy Storage by Nanofluids", Journal of Energy Technologies and Policy, **3**(5), (2013). https://www.iiste.org/Journals/index.php/JETP/article/download/5595/5707

[7] A. Hadi, A. Hashim, and D. Hassan, "Fabrication of new ceramics nanocomposites for solar energy storage and release", Bulletin of Electrical Engineering and Informatics, **9**(1), 83-86 (2020). https://beei.org/index.php/EEI/article/download/1323/1266

[8] H.K. Judran, A.G.T. Al-Hasnawi, F.N. Al-Zubaidi, W.A.K. Al-Maliki, F. Alobaid, and B. Epple, "A High Thermal Conductivity of MgO-H$_2$O Nanofluid Prepared by Two-Step Technique", Appl. Sci. **12**, 2655 (2022). https://doi.org/10.3390/app12052655.

[9] F.L. Rashid, A. Hadi, A.A. Abid, and A. Hashim, "Solar energy storage and release application of water - phase change material - (SnO$_2$-TaC) and (SnO$_2$–SiC) nanoparticles system", International Journal of Advances in Applied Sciences, **8**(2), 154-156 (2019). http://doi.org/10.11591/ijaas.v8.i2.pp154-156

[10] F.L. Rashid, and A. Hashim, "Recent Review on Nanofluid/ Nanocomposites for Solar Energy Storage", International Journal of Scientific Research and Engineering Development, **3**(4), 780-789 (2020). http://www.ijsred.com/volume3/issue4/IJSRED-V3I4P94.pdf

[11] A.M. Hashim, F.L. Rashid, and I.K. Fayyadh, "Preparation of Nanofluid (Al$_2$O$_3$-water) for Energy Storage",IOSR Journal of Applied Chemistry, **5**(3), 48-49 (2013). https://www.slideshare.net/IOSR/preparation-of-nanofluid-al2o3water-for-energy-storage

[12] Z.H. Obaid, F.L. Rashid, M.A. Habeeb, A. Hashim, and A. Hadi, "Synthesis of New Biomaterial Composite for Thermal Energy Storage and Release", Journal of Chemical and Pharmaceutical Sciences, **10**(3), 1125-1128 (2017).

[13] A. Hazim, A. Hashim, and H. M. Abduljalil, "Fabrication of Novel (PMMA-Al2O3/Ag) Nanocomposites and its Structural and Optical Properties for Lightweight and Low-Cost Electronics Applications", Egypt. J. Chem. **64**(1), 359-374 (2021).

[14] M.M. Tawfik, "Experimental Studies of Nanofluid Thermal Conductivity Enhancement and Applications: A Review", Renewable and Sustainable Energy Reviews, **75**, 1239-1253 (2017).

[15] T. Rasheed, T. Hussain, M.T. Anwar, J. Ali, K. Rizwan, M. Bilal, F.H. Alshammari, N. Alwadai, and A.S. Almuslem, "Hybrid Nanofluids as Renewable and Sustainable Colloidal Suspensions for Potential Photovoltaic/Thermal and Solar Energy Applications", Frontiers in Chemistry, **9**, (2021). https://doi.org/10.3389/fchem.2021.737033

[16] S.K. Verma, A.K. Tiwari, and M. Tripathi, "An evaluative observation on impact of optical properties of nanofluids in performance of photo-thermal concentrating systems", Solar Energy, **176**, 709 (2018). https://doi.org/10.1016/j.solener.2018.10.084

[17] A. Hashim, Y. Al-Khafaji, and A. Hadi, "Synthesis and Characterization of Flexible Resistive Humidity Sensors Based on PVA/PEO/CuO Nanocomposites", Transactions on Electrical and Electronic Materials, (2019). https://doi.org/10.1007/s42341-019-00145-3

[18] A. Hashim, H. Abduljalil, and H. Ahmed, "Analysis of Optical, Electronic and Spectroscopic properties of (Biopolymer-SiC) Nanocomposites for Electronics Applications", Egypt. J. Chem. **62**, (2019). https://doi.org/10.21608/EJCHEM.2019.7154.1590

[19] H. Ahmed, and A. Hashim, "Structural, Optical and Electronic Properties of Silicon Carbide Doped PVA/NiO for Low Cost Electronics Applications", Silicon, (2020). https://doi.org/10.1007/s12633-020-00543-w

[20] H. Ahmed, A. Hashim, H.M. Abduljalil, Determination of Optical Parameters of Films Of PVA/TiO$_2$/SiC and PVA/MgO/SiC Nanocomposites for Optoelectronics and UV-Detectors, Ukr. J. Phys. **65**(6), (2020). https://doi.org/10.15407/ujpe65.6.533

[21] A. Hashim, "Fabrication and characteristics of flexible, lightweight, and low-cost pressure sensors based on PVA/SiO$_2$/SiC nanostructures", J. Mater. Sci: Mater. Electron. **32**, 2796 (2021). https://doi.org/10.1007/s10854-020-05032-9

[22] H. Ahmed, and A. Hashim, "Geometry Optimization, Optical and Electronic Characteristics of Novel PVA/PEO/SiC Structure for Electronics Applications", Silicon, (2020). https://doi.org/10.1007/s12633-020-00620-0

[23] N.AH. Al-Aaraji, A. Hashim, and A. Hadi, et al. "Effect of Silicon Carbide Nanoparticles Addition on Structural and Dielectric Characteristics of PVA/CuO Nanostructures for Electronics Devices", Silicon, (2021). https://doi.org/10.1007/s12633-021-01265-3

[24] A. Hashim, H.M. Abduljalil, and H. Ahmed, "Fabrication and Characterization of (PVA-TiO$_2$)$_{1-x}$/SiC$_x$ Nanocomposites for Biomedical Applications", Egypt. J. Chem. **63**(1), (2020). https://doi.org/10.21608/EJCHEM.2019.10712.1695

[25] W.O. Obaid, and A. Hashim, "Synthesis and Augmented Optical Properties of PC/SiC/TaC Hybrid Nanostructures for Potential and Photonics Fields", Silicon, **14**, 11199 (2022). https://doi.org/10.1007/s12633-022-01854-w

[26] O.B. Fadil, and A. Hashim, "Fabrication and Tailored Optical Characteristics of CeO$_2$/SiO$_2$ Nanostructures Doped PMMA for Electronics and Optics Fields", Silicon, **14**, 9845 (2022). https://doi.org/10.1007/s12633-022-01728-1

[27] N.A.H. Al-Aaraji, A. Hashim, and A. Hadi, et al. "Synthesis and Enhanced Optical Characteristics of Silicon Carbide/Copper Oxide Nanostructures Doped Transparent Polymer for Optics and Photonics Nanodevices", Silicon, **14**, 10037 (2022). https://doi.org/10.1007/s12633-022-01730-7

[28] M. Mehrali, E. Sadeghinezhad, S.T. Latibari, S.N. Kazi, M. Mehrali, M.N.B.M. Zubir, and H.S.C. Metselaar, "Investigation of thermal conductivity and rheological properties of nanofluids contain in graphene nanoplatelets", Nanoscale Research Letters, **9**(15), (2014). https://doi.org/10.1186/1556-276X-9-15

[29] B. Bakthavatchalam, K. Habib, R. Saidur, N.A.A. Rashedi, "Investigation of Electrical Conductivity, OpticalProperty, and Stability of 2D MXene Nanofluid Containing Ionic Liquids", Appl. Sci. **10**, (2020). https://doi.org/10.3390/app10248943

[30] Z. Al-Ramadhan, A. Hashim, and A.J.K. Algidsawi, "The DC electrical properties of (PVC-Al$_2$O$_3$) composites", AIP Conference Proceedings, **1400**(1), (2011). https://doi.org/10.1063/1.3663109

[31] I.R. Agool, K.J. Kadhim, and A. Hashim, "Synthesis of (PVA-PEG-PVP-ZrO$_2$) Nanocomposites for Energy Release and Gamma Shielding Applications", International Journal of Plastics Technology, **21**(2), (2017). https://doi.org/10.1007/s12588-017-9196-1

[32] A. Hadi, A. Hashim, and D. Hassan, "Fabrication of new ceramics nanocomposites for solar energy storage and release", Bulletin of Electrical Engineering and Informatics, **9**(1), (2020), https://doi.org/10.11591/eei.v9i1.1323

[33] I.R. Agool, K.J. Kadhim, and A. Hashim, "Preparation of (polyvinyl alcohol–polyethylene glycol–polyvinyl pyrrolidinone–titanium oxide nanoparticles) nanocomposites: electrical properties for energy storage and release", International Journal of Plastics Technology, **20**(1), 121 (2016). https://doi.org/10.1007/s12588-016-9144-5

[34] A. Hashim, and A. Hadi, Synthesis and Characterization of Novel Piezoelectric and Energy Storage Nanocomposites: Biodegradable Materials–Magnesium Oxide Nanoparticles", Ukrainian Journal of Physics, **62**(12), 1050 (2017). https://doi.org/10.15407/ujpe62.12.1050

[35] N.H. Al-Garah, F.L. Rashid, A Hadi, and A. Hashim, "Synthesis and Characterization of Novel (Organic–Inorganic) Nanofluids for Antibacterial, Antifungal and Heat Transfer Applications", Journal of Bionanoscience, **12**, (2018). https://doi.org/10.1166/jbns.2018.1538

[36] F.L. Rashid, S.M. Talib, A. Hadi, and A. Hashim, "Novel of thermal energy storage and release: water/(SnO2-TaC) and water/(SnO2–SiC) nanofluids for environmental applications", IOP Conf. Series: Materials Science and Engineering, **454**, 012113 (2018). https://doi.org/10.1088/1757-899X/454/1/012113

[37] A.S. Shareef, F.L. Rashid, A. Hadi, and A. Hashim, "Water-Polyethylene Glycol/ (SiC-WC) and (CeO2-WC) Nanofluids for Saving Solar Energy", International Journal of Scientific & Technology Research, **8**(11), (2019) . https://www.researchgate.net/profile/Farhan-Lafta/publication/337315854_Water-Polyethylene_Glycol_Sic-Wc_And_Ceo2WcNanofluids_For_Saving_Solar_Energy/links/5dd14a87299bf1b74b49250d/Water-Polyethylene-Glycol-Sic-Wc-And-Ceo2WcNanofluids-For-Saving-Solar-Energy.pdf

[38] A. Hadi, F.L. Rashid, H.Q. Hussein, A. Hashim, "Novel of water with (CeO2-WC) and (SiC-WC) nanoparticles systems for energy storage and release applications", IOP Conference Series: Materials Science and Engineering, **518**(3), 5 (2019).https://doi.org/10.1088/1757-899X/518/3/032059

[39] F.L. Rashid, A. Hadi, N.H. Al-Garah, and A. Hashim, "Novel Phase Change Materials, MgO Nanoparticles, and Water Nanofluids for Thermal Energy Storage and Biomedical Applications", International Journal of Pharmaceutical and Phytopharmacological Research, **8**(1), 46 (2018) .https://eijppr.com/2KsaVdO

ДОСЛІДЖЕННЯ ОПТИЧНИХ ТА ЕЛЕКТРИЧНИХ ХАРАКТЕРИСТИК НАНОРІДИНИ MgO/SiC-H$_2$O ДЛЯ ЗБЕРІГАННЯ ТЕПЛОВОЇ ЕНЕРГІЇ
Фархан Лафта Рашид[a], Ахмед Хашим[b], М.Х. Аббас[c], Асіль Хаді[d]
[a]Університет Кербали, Інженерний коледж, Департамент нафтової інженерії, Ірак
[b]Факультет фізики, Освітній коледж чистих наук, Вавилонський університет, Вавилон, Ірак
[c]Кафедра медичної фізики, Університетський коледж Аль-Мустакбал, Вавилон, Ірак
[d]Кафедра кераміки та будівельних матеріалів, коледж інженерії матеріалів, Вавилонський університет, Ірак

Тепло передається накопичувальному середовищу під час фази зарядки накопичувача теплової енергії (TES), а потім виділяється під час фази розрядки. Його можна використовувати для промислових операцій, таких як металургійні перетворення або сонячні електростанції. Тепло зберігається в матеріалах, які змінюють температуру, фазу або хімічний склад відповідно у чутливому, латентному та термохімічному середовищах. Оптимальне зберігання тепла має довгу історію. У цьому дослідженні описано дослідження оптичних і електричних властивостей нанофлюїдів MgO/SiC-H$_2$O для застосувань, включаючи зберігання теплової енергії. Результати показують, що коли концентрації MgO/SiC NP були підвищені до 1,2 г/л, абсорбція зросла приблизно на 66,9 %, а пропускна здатність приблизно на 54 %. Крім того, збільшення концентрації наночастинок MgO/SiC збільшить поглинання, що вказує на покращену дисперсію нанофлюїдів. Також, коли концентрації наночастинок MgO/SiC наближаються до 1,2 г/л, електропровідність нанофлюїдів збільшується приблизно на 49,2 %, а час плавлення скорочується зі збільшенням концентрації наночастинок MgO/SiC.
Ключові слова: *оптичні характеристики; електричні характеристики; нанорідина; накопичення енергії*

PREPARATION OF NANOFLUIDS FROM INORGANIC NANOSTRUCTURES DOPED PEG: CHARACTERISTICS AND ENERGY STORAGE APPLICATIONS†

Ahmed Hashim[a]*, Farhan Lafta Rashid[b], M.H. Abbas[c], Bahaa H. Rabee[a]

*a*Department of Physics, College of Education for Pure Sciences, University of Babylon, Babylon, Iraq
*b*University of Kerbala, College of Engineering, Petroleum Engineering Department, Iraq
*c*Department of Medical Physics, Al-Mustaqbal University College, Babylon, Iraq
Corresponding Author e-mail: ahmed_taay@yahoo.com

Polymeric nanocomposites have drawn a lot of interest when it comes to innovative materials because of their enhanced optical, electrical, and magnetic properties. These materials have a high rising modulus, are flame resistant, and may also halt oxidation and agglomeration. These improvements in properties are related to interactions between nanoparticles and polymers. The addition of nanoparticles to polymers prolongs their life, changes their surface via passivation defect levels, and provides low cost, simple device manufacture, as well as adjustable electrical and optical properties. This study examines the properties and potential uses of nanofluids made from inorganic nanostructures doped with PEG. The results demonstrate that when the concentration of ZrO_2/SiC NPs increased to 12wt%, the electrical conductivity of nanofluids increased by roughly 43.6%. Additionally, when the concentration of ZrO_2/SiC nanoparticles increases, the melting time reduces. Additionally, when the concentration of ZrO_2/SiC NPs increases from 3 weight percent to 12 weight percent within 15 minutes, the growth of melting time reaches 51.2%, and the absorbance increases by approximately 80.3% while transmittance decreases by about 82.5%.

Keywords: *nanocomposites; inorganic nanostructures; PEG; energy storage*
PACS: 68.03.Kn, 78.66.Li, 78.66.Nk, 82.35.Np.

1. INTRODUCTION

The past few years have witnessed a huge increase in interest in nanotechnology since miniaturization and nanomaterials are often predicted to be the key to a sustainable future. In this regard, a significant portion of the scientific community is currently concentrating on a very difficult and pertinent research area, which is the synthesis of novel nanostructured hybrid materials capable of absorbing the photonic energy from sunlight with the intention of converting it into electrical or chemical energy. Whereas, substantial study on the use of solar energy has been sparked by rising worries about energy and environmental issues. Among these, several methods for employing semiconductor photocatalysts to degrade organic dyes and/or produce photocatalytic hydrogen for fuel cells are investigated [1-4]. While electrical features are designed to know conveyance of the fee widespread presence in these compounds, optical qualities are intended to be anti-reflective, getting polarization characters and greater reflection. The dopant addition will customize the polymer matrix-based polymers' electrical and optical characteristics. Additionally, the outstanding qualities of inorganic compounds, such as thermal resistance, heat strength, and high strength, can be combined with the advantages of polymer fabrics, such as nice moldability, high power, and durability, to create composite materials, which require high strength and chemical resistance. The electrical, magnetic, mechanical, optical, and thermal properties of nanofillers can be enhanced by incorporating organic and inorganic materials into their structures. Nanofillers can be used in a wide range of applications, such as the production of tissue, filters, catalysis, scaffolds, wound dressing, and sensors [5–11].

Phase change materials (PCMs) based on poly(ethylene glycol) 400 gmol1 and nano-enhanced by either carbon black (CB), a raw graphite/diamond nano mixture (G/D-r), a purified graphite/diamond nano mixture (G/D-p), or nano-Diamond nano powders with purity grades of 87% or 97% were presented by Cabaleiro et al (nD87 and nD97, respectively). In order to create PEG/MgCaCO3 as a ss-PCM, MgO-CaCO3 matrices were first constructed and examined by Zahir et al. [13]. PEG-5MgCaCO3 (P-5-MCC), PEG-10MgCaCO3 (P-10-MCC), and PEG-15MgCaCO3 samples were detected in the samples (P-15-MCC). A technique for the manufacture of gelatin-stabilized copper oxide nanoparticles was created by Gvozdenko et al. [14]. The process of synthesis used direct chemical precipitation. For the manufacture of copper oxide, copper sulfate, chloride, and acetate were employed as precursors. As a stabilizer, gelatin was utilized. It was discovered that only when copper acetate was utilized as a precursor would monophase copper oxide II develop. The addition of SiCto polymers has many applications in various approaches like electronics sensors and biomedical [15-21]. This study examines the properties and potential uses of nanofluids made from inorganic nanostructures doped with PEG.

2. MATERIALS AND METHODS

This study made use of polyethylene glycol (PEG), zirconium oxide nanoparticles (ZrO_2 NPs), and silicon carbide nanoparticles as its raw materials (SiC NPs). After dissolving 1 gram of PEG in 50 milliliters of distilled water, we were

able to create the PEG-H2O fluid. The various concentrations of ZrO_2/SiC NPs that were used in the fabrication of the nanofluids are 3%, 6%, 9%, and 12%. $PEG/ZrO_2/SiC-H_2O$ nanofluids had their optical and electrical characteristics investigated as part of this study. The double beam spectrophotometer (Shimadzu, UV-18000A) with a wavelength range of (200-1000) nm is used to analyze the optical characteristics of the $PEG/ZrO_2/SiC-H_2O$ nanofluids. The technique of assessing the melting features of $PEG/ZrO_2/SiC-H_2O$ nanofluids during the heating process is included in the thermal energy storage. The $PEG/ZrO_2/SiC-H_2O$ nanofluids were used as the heat transfer fluid. The temperature of the heat transfer fluid can be varied from 35 degrees Celsius to 100 degrees Celsius using a stirrer, and a digital device was used to measure the temperature of the $PEG/ZrO_2/SiC-H_2O$ nanofluids while they were being heated.

3. RESULTS AND DISCUSSION

For various concentrations of ZrO_2/SiC NPs, the absorbance and transmittance spectra of $PEG/ZrO_2/SiC-H_2O$ nanofluids are shown in Figs. 1 and 2, respectively. These graphs showed that when ZrO_2/SiC NP concentrations climbed from 3 weight percent to 12 weight percent, absorbance increased by around 80.3% and transmittance reduced by about 82.5%. The $PEG/ZrO_2/SiC-H_2O$ nanofluids exhibit increased UV absorption, making them potential nanofluids for use in a variety of renewable areas, including solar collectors, energy storage, and heating and cooling systems. The absorbance, which alludes to greater nanofluid dispersion, will grow when ZrO_2/SiC NP concentration rises [22].
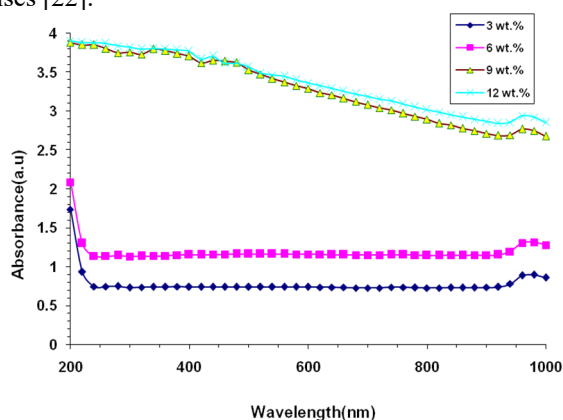
Figure 1. Absorbance and transmittance spectra of $PEG/ZrO_2/SiC-H_2O$ nanofluids with photon wavelength for different concentrations of ZrO_2/SiC NPs
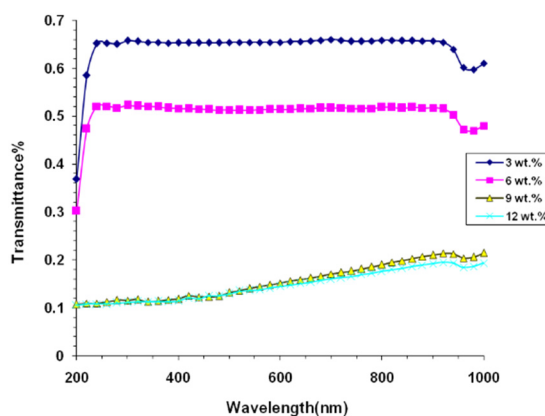
Figure 2. Transmittance spectra of $PEG/ZrO_2/SiC-H_2O$ nanofluids with photon wavelength for different concentrations of ZrO_2/SiC NPs

The association between the concentrations of ZrO_2/SiC NPs and the electrical conductivity of $PEG/ZrO_2/SiC-H_2O$ nanofluids is shown in Fig. 3. When ZrO_2/SiC NP concentrations approach 12 weight percent, the electrical conductivity of nanofluids increases by roughly 43.6%, which is caused by an increase in the number of charge carriers[23]. The melting curves of $PEG/ZrO_2/SiC-H_2O$ nanofluids are shown in Fig. 4. As the concentration of ZrO_2/SiC nanoparticles increases, the melting time reduces. $PEG/ZrO_2/SiC-H_2O$ nanofluids' reduced melting time for energy storage applications is owing to improved thermal conductivity, which increases heat transfer[24–32]. When the concentration of ZrO_2/SiC NPs increases from 3 weight percent to 12 weight percent within 15 minutes, the increment in melting time reaches 51.2%. As a result of this behavior, $PEG/ZrO_2/SiC-H_2O$ nanofluids may be thought of as a key for heating and cooling systems.
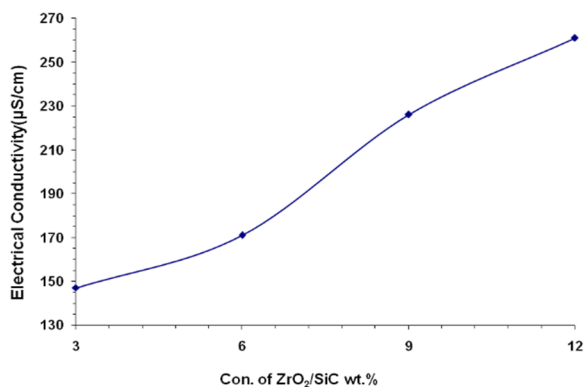
Figure 3. Variation of electrical conductivity of $PEG/ZrO_2/SiC-H_2O$ nanofluids and concentrations of ZrO_2/SiC NPs
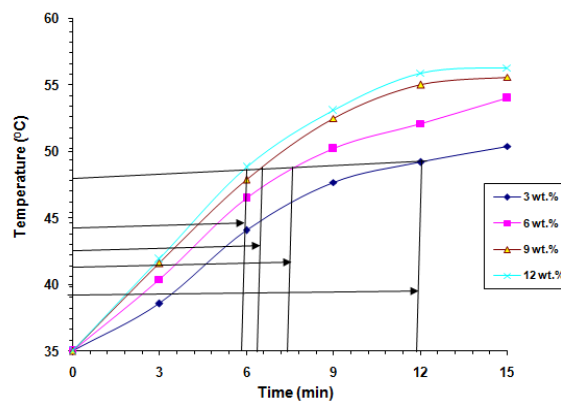
Figure 4. Melting curves of $PEG/ZrO_2/SiC-H_2O$ nanofluids

4.CONCLUSIONS

Because of its simpler construction process and ability to easily control the properties of polymer electrolytes by altering the blended polymer composition, polymeric blends may have a more beneficial impact. The following list of potential consequences follows:

1.When the concentration of ZrO_2/SiC NPs increased to 12 weight percent, the electrical conductivity of nanofluids increased by around 43.6%.

2. As the concentration of ZrO_2/SiC nanoparticles increases, the melting time reduces.

3. When the concentration of ZrO_2/SiC NPs increases from 3 weight percent to 12 weight percent within 15 minutes, the increment in melting time reaches 51.2%.

4. As the concentration of ZrO_2/SiC NPs rose from 3 weight percent to 12 weight percent, the absorbance increased by approximately 80.3% and the transmittance dropped by about 82.5%.

5. The increase in ZrO_2/SiC NP concentration will result in a higher absorbance, which indicates improved nanofluid dispersion.

ORCID IDs

Ahmed Hashim, https://orcid.org/0000-0002-0778-1159; **Farhan Lafta Rashid**, https://orcid.org/0000-0002-7609-6585
Bahaa H. Rabee, https://orcid.org/0000-0001-9780-1311

REFERENCES

[1] N. Hayder, M.A. Habeeb, and A. Hashim, "Structural, Optical and Dielectric Properties of (PS-In$_2$O$_3$/ZnCoFe$_2$O$_4$) Nanocomposites", Egypt. J. Chem. **62**(2), 577-592 (2019). https://doi.org/10.21608/ejchem.2019.14646.1887

[2] A. Babapoor, A.R. Haghighi, S.M. Jokar, and M.A. Mezjin, "The Performance Enhancement of Paraffin as a PCM During the Solidification Process: Utilization of Graphene and Metal Oxide Nanoparticles", Iran. J. Chem. Chem. Eng. 41(1), (2022). https://doi.org/10.30492/ijcce.2020.127799.4135

[3] A.M. Hashim, F.L. Rashid, and I.K. Fayyadh, "Preparation of Nanofluid (Al2O3-water) for Energy Storage", IOSR Journal of Applied Chemistry, **5**(3), 48-49 (2013). https://www.slideshare.net/IOSR/preparation-of-nanofluid-al2o3water-for-energy-storage

[4] Z.H. Obaid, F.L. Rashid, M.A. Habeeb, A. Hashim, and A. Hadi, "Synthesis of New Biomaterial Composite for Thermal Energy Storage and Release", Journal of Chemical and Pharmaceutical Sciences, **10**(3), 1125-1128 (2017).

[5] Batool Mohammed, Hind Ahmed, Ahmed Hashim, Improving the Optical Properties of PVA/PEG Blend Doped with BaTiO3 NPs, Journal of Physics: Conference Series 1963 (2021) 012005. https://doi.org/10.1088/1742-6596/1963/1/012005

[6] G.M. Nasr, A.S.A. El-Haleem, A. Klingner, A.M. Alnozahy, and M.H. Mourad, "The DC Electrical Properties of Polyvinyl Alcohol/Multi-Walled Carbon Nanotube Composites", Journal of Multidisciplinary Engineering Science and Technology, **2**(5), (2015).https://www.jmest.org/wp-content/uploads/JMESTN42350633.pdf

[7] C. Tyagi, and A. Sharma, "Linear and Nonlinear optical study of pure PVA and CdSe doped PVA nanocomposite", AIP Conference Proceedings, **1728**, 020151 (2016). https://doi.org/10.1063/1.4946202

[8] H.N. Obaid, M.A. Habeeb, F.L. Rashid, A. Hashim, "Thermal energy storage by nanofluids", Journal of Engineering and Applied Sciences, **8**(5), 143-145 (2014). https://doi.org/10.36478/jeasci.2013.143.145

[9] F.L. Rashid, A. Hadi, A.A. Abid, and A. Hashim, "Solar energy storage and release application of water - phase change material - (SnO$_2$-TaC) and (SnO$_2$–SiC) nanoparticles system", International Journal of Advances in Applied Sciences (IJAAS), **8**(2), 154-156 (2019). https://doi.org/10.11591/ijaas.v8.i2.pp154-156

[10] F.L. Rashid, and A. Hashim, "Recent Review on Nanofluid/ Nanocomposites for Solar Energy Storage", International Journal of Scientific Research and Engineering Development, **3**(4), 780-789 (2020). http://www.ijsred.com/volume3/issue4/IJSRED-V3I4P94.pdf

[11] F.L. Rashid, and A. Hashim, "Development of Phase Change Materials/Nanoparticles for Thermal Energy Storage", International Journal of Scientific Research and Engineering Development, **3**(4), 790-799 (2020). http://www.ijsred.com/volume3/issue4/IJSRED-V3I4P95.pdf

[12] D. Cabaleiro, S. Hamze, J. Fal, M.A. Marcos, P. Estellé, and G. Zyła, "Thermal and Physical Characterization of PEG Phase Change Materials Enhanced by Carbon-Based Nanoparticles", Nanomaterials, **10**, 1168 (2020). https://doi.org/10.3390/nano10061168

[13] Md.H. Zahir, M.M. Rahman, S.K.S. Basamad, K.O. Mohaisen, K. Irshad, M.M. Rahman, Md.A. Aziz, A. Ali, and M.M. Hossain, "Preparation of a Sustainable Shape-Stabilized Phase Change Material for Thermal Energy Storage Based on Mg^{2+}-Doped CaCO3/PEG Composites", Nanomaterials, **11**, 1639 (2021). https://doi.org/10.3390/nano11071639

[14] A.A. Gvozdenko, S.A. Siddiqui, A.V. Blinov, A.B. Golik, A.A. Nagdalian, D.G. Maglakelidze, E.N. Statsenko, et al., "Synthesis of CuO nanoparticles stabilized with gelatin for potential use in food packaging applications", Scientifc Reports, 12, 12843 (2022). https://doi.org/10.1038/s41598-022-16878-w

[15] Al-Aaraji, N.AH., Hashim, A., Hadi, A. *et al.* Effect of Silicon Carbide Nanoparticles Addition on Structural and Dielectric Characteristics of PVA/CuO Nanostructures for Electronics Devices. *Silicon* (2021). https://doi.org/10.1007/s12633-021-01265-3

[16] A. Hashim, H.M. Abduljalil, and H. Ahmed, "Fabrication and Characterization of (PVA-TiO2)$_{1-x}$/SiC$_x$ Nanocomposites for Biomedical Applications", Egypt. J. Chem., **63**(1), (2020).https://doi.org/10.21608/EJCHEM.2019.10712.1695

[17] A. Hashim, H. Abduljalil, and H. Ahmed, "Analysis of Optical, Electronic and Spectroscopic properties of (Biopolymer-SiC) Nanocomposites for Electronics Applications", Egypt. J. Chem. **62**, (2019).https://doi.org/10.21608/EJCHEM.2019.7154.1590

[18] H. Ahmed, and A. Hashim, "Structural, Optical and Electronic Properties of Silicon Carbide Doped PVA/NiO for Low Cost Electronics Applications", Silicon, (2020).https://doi.org/10.1007/s12633-020-00543-w

[19] H. Ahmed, A. Hashim, and H.M. Abduljalil, "Determination of Optical Parameters of Films Of PVA/TiO2/SiC and PVA/MgO/SiC Nanocomposites for Optoelectronics and UV-Detectors", Ukr. J. Phys. **65**(6), (2020). https://doi.org/10.15407/ujpe65.6.533

[20] A. Hashim, "Fabrication and characteristics of flexible, lightweight, and low-cost pressure sensors based on PVA/SiO$_2$/SiC nanostructures", J. Mater. Sci: Mater. Electron.**32,** 2796–2804 (2021). https://doi.org/10.1007/s10854-020-05032-9

[21] H. Ahmed, and A. Hashim, "Geometry Optimization, Optical and Electronic Characteristics of Novel PVA/PEO/SiC Structure for Electronics Applications", Silicon, (2020).https://doi.org/10.1007/s12633-020-00620-0

[22] M. Mehrali, E. Sadeghinezhad, S.T. Latibari, S.N. Kazi, M. Mehrali, M.N.B.M. Zubir, H. Simon, and C. Metselaar, "Investigation of thermal conductivity andrheological properties of nanofluids containinggraphene nanoplatelets", Nanoscale Research Letters, **9**(15), (2014). https://doi.org/10.1186/1556-276X-9-15

[23] B. Bakthavatchalam, K. Habib, R. Saidur, N. Aslfattahiand, and A. Rashedi, "Investigation of Electrical Conductivity, Optical Property, and Stability of 2D MXene Nanofluid Containing Ionic Liquids", Appl. Sci., **10**, (2020). https://doi.org/10.3390/app10248943

[24] A. Hadi, A. Hashim, and D. Hassan, "Fabrication of new ceramics nanocomposites for solar energy storage and release, Bulletin of Electrical Engineering and Informatics", **9**(1), (2020), https://doi.org/10.11591/eei.v9i1.1323

[25] I.R. Agool, K.J. Kadhim, and A. Hashim, "Preparation of (polyvinyl alcohol–polyethylene glycol–polyvinyl pyrrolidinone–titanium oxide nanoparticles) nanocomposites: electrical properties for energy storage and release", International Journal of Plastics Technology, **20**(1), https://doi.org/10.1007/s12588-016-9144-5

[26] A.Hashim,and A. Hadi, "Synthesis and Characterization of Novel Piezoelectric and Energy Storage Nanocomposites: Biodegradable Materials–Magnesium Oxide Nanoparticles", Ukrainian Journal of Physics, **62**(12),1050-1056, (2017).https://doi.org/10.15407/ujpe62.12.1050

[27] I.R. Agool, K.J. Kadhim, and A. Hashim, "Synthesis of (PVA-PEG-PVP-ZrO$_2$) Nanocomposites For Energy Release and Gamma Shielding Applications, International Journal of Plastics Technology", **21**(2), (2017).https://doi.org/10.1007/s12588-017-9196-1

[28] N.H. Al-Garah, F.L. Rashid, A. Hadi, and A. Hashim, "Synthesis and Characterization of Novel (Organic–Inorganic) Nanofluids for Antibacterial, Antifungal and Heat Transfer Applications", Journal of Bionanoscience, **12**, 1538 (2018). https://doi.org/10.1166/jbns.2018

[29] F.L. Rashid, A. Hadi, N.H. Al-Garah, and A. Hashim, "Novel Phase Change Materials, MgO Nanoparticles, and Water Based Nanofluids for Thermal Energy Storage and Biomedical Applications", International Journal of Pharmaceutical and Phytopharmacological Research, **8**(1), (2018).https://eijppr.com/2KsaVdO

[30] F.L. Rashid, S.M. Talib, A. Hadi, and A. Hashim, "Novel of thermal energy storage and release: water/(SnO$_2$-TaC) and water/(SnO2–SiC) nanofluids for environmental applications", IOP Conf. Series: Materials Science and Engineering, **454**, 012113 (2018). https://doi.org/10.1088/1757-899X/454/1/012113

[31] A.S. Shareef, F.L. Rashid, A. Hadim, and A. Hashim, "Water-Polyethylene Glycol/ (SiC-WC) and (CeO$_2$-WC) Nanofluids For Saving Solar Energy", International Journal of Scientific & Technology Research, **8**(11), (2019).https://www.researchgate.net/profile/Farhan-Lafta/publication/337315854_Water-Polyethylene_Glycol_Sic-Wc_And_Ceo2WcNanofluids_For_Saving_Solar_Energy/links/5dd14a87299bf1b74b49250d/Water-Polyethylene-Glycol-Sic-Wc-And-Ceo2WcNanofluids-For-Saving-Solar-Energy.pdf

[32] A. Hadi, F. L. Rashid, H. Q. Hussein, A. Hashim, Novel of water with (CeO2-WC) and (SiC-WC) nanoparticles systems for energy storage and release applications, IOP Conference Series: Materials Science and Engineering, **518**(3), 5 (2019).https://doi.org/10.1088/1757-899X/518/3/032059

ПРИГОТУВАННЯ НАНОРІДИН З НЕОРГАНІЧНИХ НАНОСТРУКТУРЛЕГОВАНИХ ПЕГ: ХАРАКТЕРИСТИКИ ТА ЗАСТОСУВАННЯ ДЛЯ ЗБЕРІГАННЯ ЕНЕРГІЇ

Ахмед Хашим[a], Фархан Лафта Рашид[b], М.Х. Аббас[c], Бахаа Х. Рабі[a]
[a]Факультет фізики, Освітній коледж чистих наук, Вавилонський університет, Вавилон, Ірак
[b]Університет Кербали, інженерний коледж, факультет нафтової інженерії, Ірак
[c]Кафедра медичної фізики, коледж університету Аль-Мустакбал, Вавилон, Ірак

Полімерні нанокомпозити викликають великий інтерес, коли мова заходить про інноваційні матеріали через їхні покращені оптичні, електричні та магнітні властивості. Ці матеріали мають високий модуль зростання, вогнестійкі, а також можуть зупинити окислення та агломерацію. Ці покращення властивостей пов'язані із взаємодією між наночастинками та полімерами. Додавання наночастинок до полімерів подовжує їх життя, змінює їхню поверхню через рівні дефектів пасивації та забезпечує низьку вартість, просте виготовлення пристроїв, а також регульовані електричні та оптичні властивості. У цьому дослідженні розглядаються властивості та потенційне використання нанофлюїдів, виготовлених з неорганічних наноструктур, легованих PEG. Результати демонструють, що коли концентрація наночастинок ZrO$_2$/SiC зросла до 12 мас.%, електропровідність нанофлюїдів зросла приблизно на 43,6 %. Крім того, коли концентрація наночастинок ZrO2/SiC збільшується, час плавлення скорочується. Крім того, коли концентрація наночастинок ZrO$_2$/SiC збільшується з 3 вагових відсотків до 12 вагових відсотків протягом 15 хвилин, збільшення часу плавлення досягає 51,2 %, а поглинання збільшується приблизно на 80,3 %, тоді як пропускна здатність зменшується приблизно на 82,5 %.
Ключові слова: *нанокомпозити; неорганічні наноструктури; ПЕГ; зберігання енергії*

INFLUENCE OF DEPOSITION VOLTAGE ON STRONTIUM SULPHIDE DOPED SILVER FOR OPTOELECTRONIC APPLICATION†

Shaka O. Samuel[a,d], M. Lagbegha-ebi Frank[b], E.P. Ogherohwo[c], Arthur Ekpekpo[d], J.T. Zhimwang[e], Imosobomeh L. Ikhioya[f]*

[a]*Department of Science Laboratory Technology, Delta State University, Abraka, Delta State, Nigeria*
[b]*International Institute of Tourism and Hospitality, Yenagoa, Bayelsa State, Nigeria*
[c]*Federal University of Petroleum Resources, Effurun, Delta State, Nigeria*
[d]*Department of Physics, Delta State University, Abraka, Delta State, Nigeria*
[e]*Federal University of Lokoja, Nigeria*
[f]*Department of Physics and Astronomy, University of Nigeria, Nsukka, 410001, Enugu State, Nigeria*
*Corresponding Author e-mail: imosobomeh.ikhioya@unn.edu.ng
Received December 19, 2022; revised January 17, 2023; accepted January 20, 2023

In the research electrochemical deposition technique was use in deposition of undoped SrS and doped SrS with silver were 0.01 mol of thioacetamide (C_2H_5NS), 0.1 mol of strontium chloride hexahydrate ($SrCl_2·6H_2O$), and 0.01 mol of silver nitrate ($AgNO_3$) were utilized as the cationic, anionic, and dopant concentrations. The XRD spectra of the SrS and SrS doped silver showed prominent crystalline peaks at angles of 26.69°, 37.97°, 51.39°, and 65.56° for SrS and 26.42°, 33.42°, 37.98°, and 51.32° for SrS/Ag, respectively, with corresponding diffraction planes (111), (112), (200), and (211). However, the diffraction pattern shows that the peak intensity increases as the deposition voltage increases. The undoped SrS material morphology has a clove-like substance with precipitate; the large nano grain on the substrate's surface exhibits photon absorption but shows no traces of pinholes. When doped SrS is deposited at various precursor voltages, it forms uniform surfaces devoid of pinholes. The cell also penetrates the substrate being used for the deposition, as seen by the elemental makeup of the films. It was observed that SrS/Ag at 10V and 12V had little precipitate on the surfaces; this is because a carbon electrode was utilized, which tends to react with electrolyte at low voltages but does not do so at 14 V. The films show that when the deposition voltage increased, the electrical resistivity decreased from $1.42×10^9$ to $1.37×10^9$ $\Omega·m$ and the thickness decreased from 125.02 to 123.025 nm. This further led to an increase in conductivity from $7.04×10^8$ to $7.29×10^8$ S/m. It was discovered that the absorbance decreases as the electromagnetic radiation's wavelength grows and the deposition voltage rises. According to research done on the deposited material, its energy bandgap lies between 1.55 and 2.51 eV.
Keywords: *Undoped SrS; bandgap energy; XRD; SEM; EDX*
PACS: 42.55.Rz, 42.70.Qs, 87.64.Dz**,** 78.70.Dm, 83.85.Hf

1. INTRODUCTION

The current century has seen a fast increase in the need for non-stop, renewable energy sources and energy storage technologies [1]. Growing interest in solar cells and photovoltaic devices, which can replace and, if possible, outperform the inefficient systems of energy storage devices currently in vogue, is a result of the pressing demand for effective energy storage devices [2]. As a result, nano scientists and engineers have been working diligently over the years to create some trustworthy wide-bandgap metal chalcogenide that will lower the risk of exposure to harmful elements while also reducing the overall shortfall of energy consumption [3]. Transition metals have gained significant interest in the search for materials with strong potentials for electrochemical energy storage devices [4–7], as evidenced by the sharp rise in the number of studies on these metals in recent years [8]. Their stronger redox chemical valences for use in photovoltaic solar cells are one important factor that could have caused this. Due to their numerous existing applications, the SrS metal has been viewed as the most appealing over time. A substance with intriguing physical, chemical, and optoelectronic applications is strontium sulphide semiconductor. Materials made of strontium sulphide are used in anti-reflection coatings, temperature controllers in satellites, microelectronic devices, photoconductors, magnetic sensors, gas sensors, solar cells, interference filters, superconducting films, infrared (IR) detectors, polarizers, decorating, and anti-corrosive coatings [8–11].

In each of these applications, a semiconductor-based optoelectronic device is an essential part of the system. One of the key advantages of semiconductor devices is their compact design. A typical edge-emitting laser, for instance, measures roughly 500×250×100 m³. A single wafer can be used to manufacture thousands of these devices. As a result, these coherent radiation sources are incredibly tiny even when packaged [15]. Gas lasers, for example, cannot be compared to semiconductor lasers in terms of size, modulation rates, application variety, or power consumption. Furthermore, semiconductor devices can be specifically tailored to meet the requirements of a given application by simply altering the composition of the several layers that make up the structure [16]. Out of all the purposes mentioned above, the usage of semiconductor devices in telecommunications has the biggest impact on how people live today. The extensive research and development that went into developing semiconductor devices for light emission and detection is what gave rise to these capabilities [17].

Optical communications led to improvements in optoelectronics, such as the development of avalanche photodiodes, vertical-cavity surface-emitting lasers, semiconductor optical amplifiers, and optical modulators. Carrier-photon interactions are researched in the context of designing efficient and high-performance emitters and detectors. We suggested talking about how different metal dopants, the concentration of precursors, the temperature of precursors, and the voltage of the deposition with a time constant can change the semiconductor band structure to improve device attributes. Optoelectronic devices are widely used in a variety of applications nowadays and are widely available. Some of the parts of these devices include photo-detectors, optical amplifiers, and optical modulators, in addition to sources like light-emitting diodes (LEDs) and laser diodes. With the aid of these tools, photons may be produced, modulated, detected, and switched just like electrons in an electrical circuit [18].

Wide-gap semiconductors are necessary for modern optoelectronics because of their higher conductivity and transparency, according to Masaya et al. in (2021) [19]. The development of high-performance transparent electronic devices is significantly constrained by the major technological drawbacks of p-type transparent conducting materials, despite the fact that n-type TCMs have had tremendous success. In the current study, we hypothesize that the hybrid functional approach can produce transparent ambipolar conducting in SrS. A newly developed and incredibly effective electroluminescent phosphor material, Sey-Shing, (2019) SrS/Cu, was produced [20]. The EL characteristics of SrS/Cu can be varied by altering the co-dopant material. True blue is displayed by SrS/Cu devices that have been co-doped with Ag, but cyan is displayed by SrS/Cu thin film EL devices that have only been singly doped, with varying between 0.27 and 0.32 SrS/Cu, Ag has a significantly higher luminous efficiency than existing blue EL phosphors like (SrCa)Ga2S4/Ce and blue filtered SrS/Ce, ranging from 0.15 to 0.24 lm/W, when the hue is matched. It is projected that the color and brightness performance of the following generation of color TFEL displays will improve once SrS/Cu, Ag is put into production. The SrS/Ce phosphor was produced through solid-state diffusion, according to Vijay et al. in 2020 [21]. Powder X-ray diffraction, transmission electron microscopy, thermogravimetric analysis, and photoluminescence spectra were used to assess the product's properties. Photoluminescence spectra were also used to check the product's optical properties. Thermoluminescence and electron spin resonance investigations have also been conducted on the SrS/Ce phosphor. The broad TL glow curve exhibits three unique peaks, two of which are strong peaks at 137 and 275°C and one of which is a shoulder at 362°C. There are two defect centers visible at ambient temperature. One of them has an isotropic g-value of 2.0039, indicating that it belongs to a F+ center. There may be a connection between the F+ center and the 137°C TL peak.

Numerous research teams have reported their success in growing thin films using a range of techniques, including spray pyrolysis, solvothermal synthesis, ion beam assisted coating, chemical bath deposition, DC magnetron sputtering, spray pyrolysis, vacuum evaporation, thermal evaporation, SILAR, molecular beam epitaxy, and electrodeposition. In the current experiment, SrS and SrS/Ag material was deposited at room temperature using the electrodeposition approach since it offers comparative advantages over other methods in terms of economy, convenience, and ability to deposit vast regions of films [15-21]. It is extensively used to deposit different metal chalcogenides and is regularly employed with electrically conductive materials such conductive polymers, alloys, and metals. On the surface of the substrate, homogeneous deposits are produced by managing the rate at which precipitates emerge from the solution. Simple growth control in terms of thickness, rate of deposition, and film quality is additionally made possible by modifying the pH, temperature, deposition voltage and concentration of the solution bath. Dopants attempt to change the electrical, optical, and electronic properties of semiconducting materials [12-14].

Silver was used as a dopant to increase the conductivity of the material by reducing the energy needed for electrons to go from the valence band to the conduction band. The investigation's findings present materials that are suitable for usage in optoelectronic and solar cell applications.

2. EXPERIMENTAL DETAIL

Chemicals that have been evaluated analytically are purchased and used without further purification. FTO conductive glass served as the substrate. The substrates underwent acetone and methanol immersion, distilled water washing, and a 30-minute treatment with an ultrasonic bath in acetone. After being cleansed in distilled water, they were baked to dry. Thioacetamide (C_2H_5NS), 0.1 mol of strontium chloride hexahydrate ($SrCl2.6H2O$), and 0.01 mol of silver nitrate ($AgNO3$) were utilized as the cationic, anionic, and dopant concentrations. The films were deposited using the electrochemical deposition process. The electrochemical apparatus had a bath that included distilled water, 20 ml of each cationic and anionic precursor, and a 100 ml beaker. The cathode and anode materials were fluorine-doped tin oxide and carbon, and direct current voltage was generated by the power supply. The chamber has three electrode configurations: a working electrode, an electrode made of silver-silver chloride (Ag/AgCl), which serves as the reference electrode, and platinum mesh as the positive electrode. For all depositions, the fluorine-doped tin oxide substrate was positioned perpendicular to the chamber, including the counter and reference electrodes. For 10 seconds, the synthesis was conducted at a potentiostat setting of 200 mV against SCE. As a result, the synthesized films were cleaned and dried. The target materials, which consist of equal amounts (20 ml) of strontium chloride, thioacetamide, and 10 ml of silver nitrate solutions, were metered into the beakers during the deposition process. After the syntheses, the films were heated and annealed for 30 minutes to remove concentrated tensions under a variable voltage supply of 10V to 14V. By adding 10 ml of 0.01 mol of silver nitrate to the electrochemical bath, the silver nitrate dopant was introduced. The samples were collected at pH levels of 7.0 and room temperature. Scanning electron microscopy, DW-XRD 2700A X-ray diffractometer

with Cu-Kα line (λ = 1.54184 Å) in 2θ range from 10° - 80°, a four-point probe (Model T345), and a UV-1800 visible spectrophotometer was used to characterize the prepared SrS and SrS/Ag films for their surface morphological, structural, elemental, electrical, and optical properties.

3.   RESULTS AND DISCUSSION

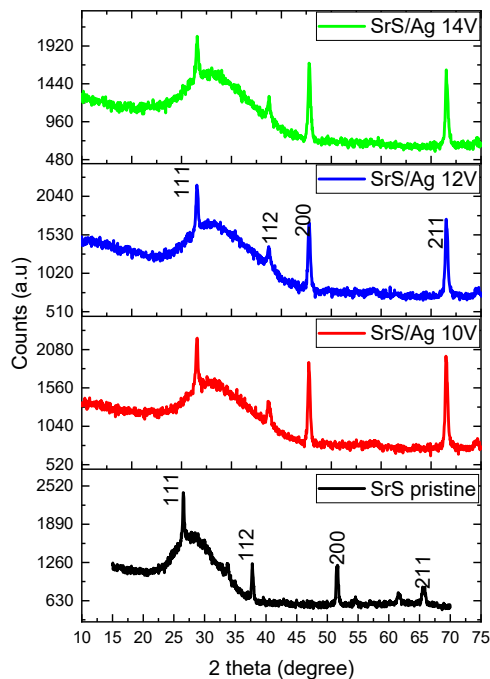## 3.1. XRD study of SrS and SrS doped silver at various deposition voltages for optoelectronic application

Figure 1. XRD spectrum

The XRD spectra of the SrS and SrS doped silver thin films in Figure 1 showed prominent crystalline peaks at angles of 26.69°, 37.97°, 51.39°, and 65.56° for SrS and 26.42°, 33.42°, 37.98°, and 51.32° for SrS/Ag, respectively, with corresponding diffraction planes (111), (112), (200), and (211).

However, the diffraction pattern shows that the peak intensity increases as the deposition voltage increases. Cell shrinkage may result from interstitial cation or solvent molecule removal, a rise in the precursor molecules' deposition voltage, or both. The crystallite of SrS and SrS doped silver thin films was identified using Debye Scherrer's formula;

$$D = \frac{K\lambda}{\beta cos(\theta)} \qquad (1)$$

Where θ is Bragg's angle, β is FWHM, λ is the X-ray wavelength, K = 0.94, and D is the crystallite size.

Important factors like crystallite size and d-spacing are summarized in Table 1. As the deposition voltage rises, the size of SrS and SrS-doped silver crystallites also rises. Due to the restriction of crystallite motion at the interface between the dopant and host crystallite brought on by stress generation, the doped SrS has a smaller value of crystallite size than the undoped SrS.

Table 1. Structural parameters of SrS and SrS/Ag

Sample	2θ (degree)	d (spacing) Å	Lattice constant ()	(β) FWHM	(hkl)	Grain Size(D) nm	Dislocation density, σ lines/m²
SrS pristine	26.6971	3.3360	5.7781	0.1851	111	7.6958	5.1445
	37.9741	2.3672	4.7345	0.1851	112	7.9188	4.9700
	51.3944	1.7762	3.5524	0.1851	200	8.3100	4.8648
	65.5611	1.4225	3.1809	0.1851	211	8.9066	4.3940
SrS/Ag 10V	26.4226	3.3700	5.8371	0.3840	111	3.7089	2.2143
	33.5574	2.6680	5.3361	0.3840	112	3.7713	2.1417
	37.9823	2.3667	4.7335	0.3840	200	3.8186	2.0890
	51.3258	1.7784	3.9767	0.3840	211	4.0060	1.8982
SrS/Ag 12V	26.4226	3.3700	5.8371	0.4136	111	3.4433	2.2148
	33.5574	2.6680	5.3361	0.4136	112	3.5013	2.1421
	37.9823	2.3667	4.7335	0.4136	200	3.5452	2.0894
	51.3258	1.7784	3.9767	0.4136	211	3.7191	1.8986
SrS/Ag 14V	26.4226	3.3700	5.8371	0.3616	111	3.9384	1.9639
	33.5574	2.6680	5.3361	0.3616	112	4.0046	1.8994
	37.9823	2.3667	4.7335	0.3616	200	4.0549	1.8527
	51.3258	1.7784	3.9767	0.3616	211	4.2538	1.6835

3.2. Surface morphology of SrS and SrS doped silver at various deposition voltages for optoelectronic application

The surface morphology of undoped and doped SrS materials is shown in Figure 2. The undoped SrS material morphology can be seen in the micrograph as clove-like substance with precipitate; the large nano grain on the substrate's surface exhibits photon absorption but shows no traces of pinholes.

When doped SrS is deposited at various precursor voltages, it forms uniform surfaces devoid of pinholes. The cell also penetrates the substrate being used for the deposition, as seen by the elemental makeup of the films. It was observed that SrS/Ag at 10V and 12V had little precipitate on the surfaces; this is because a carbon electrode was utilized, which tends to react with electrolyte at low voltages but does not do so at 14 V. In contrast to other nanoparticles, the SrS/Ag at 14 V is devoid of precipitation, and the nanoparticle is clearer. The material that was deposited will make a good candidate for photovoltaic and other applications due to its surface shape. The elemental composition of SrS that has not been doped

and SrS that has been doped with silver is shown in Figure 3 and Table 2. The spectrum clearly demonstrates that Sr, S, and Ag were present on the substrate, and the presence of other elements on the spectrum is due to the use of the FTO substrate, which contains additional elements, as the substrate for the deposition.
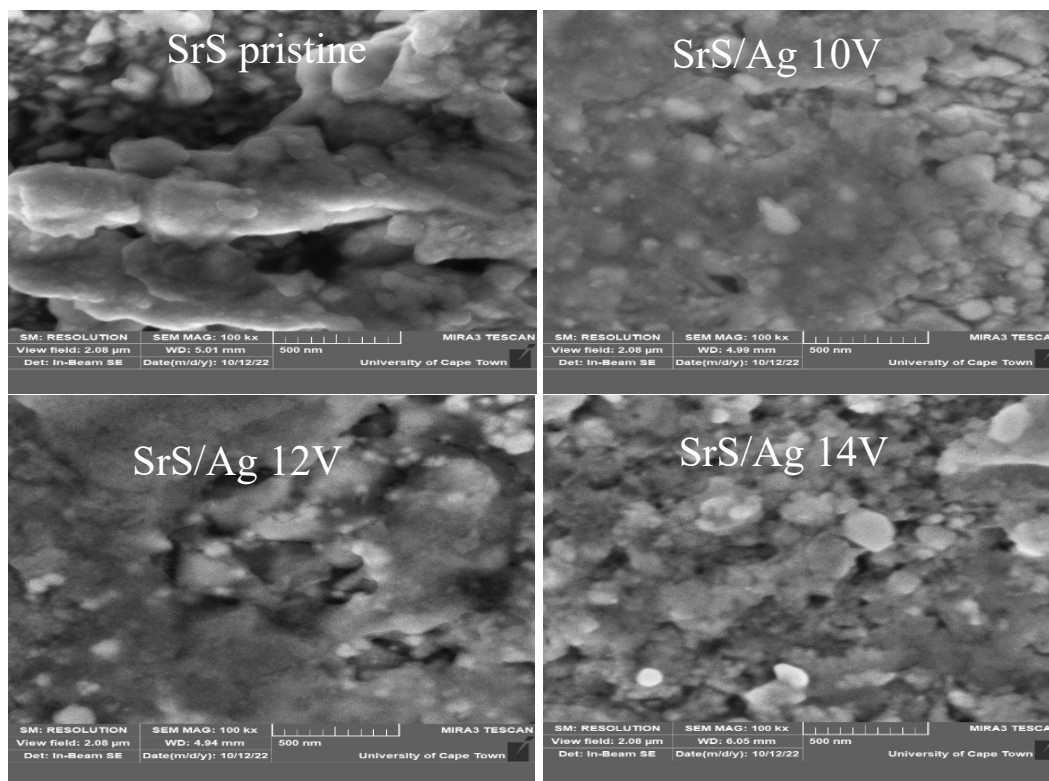
Figure 2. SEM micrograph of SRS/Ag
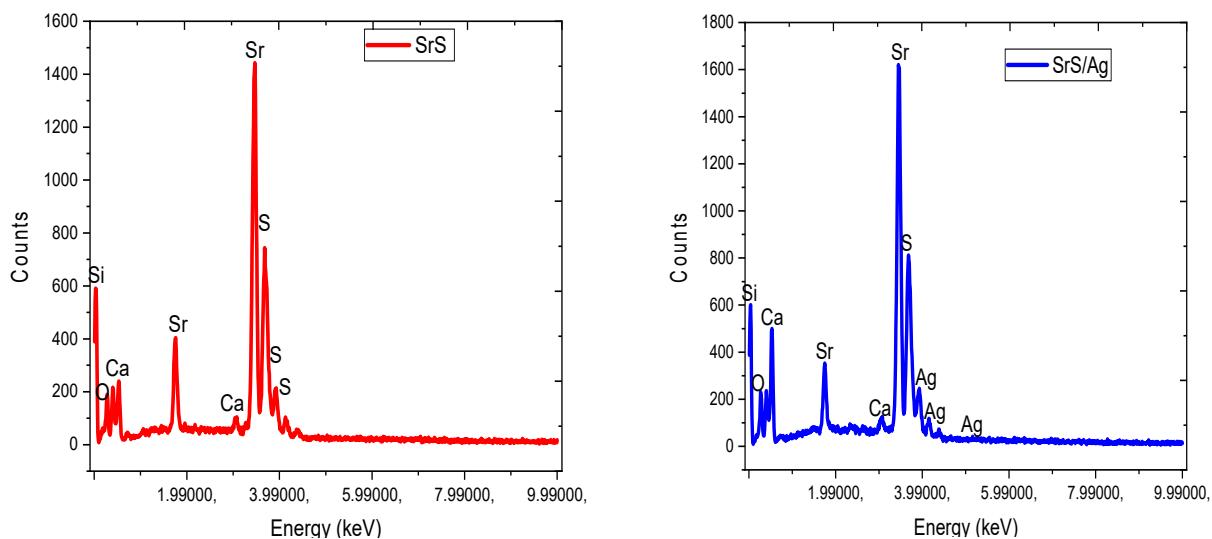
Figure 3. SrS and SrS/Ag EDX plots

Table 2. EDX spectra atomic weight percentages of the constituent elements.

Strontium Sulphide		Strontium Sulphide doped Silver	
Component	**Atomic Weight (%)**	**Component**	**Atomic Weight (%)**
Strontium	54.07	Strontium	58.30
Sulphide	24.01	Sulphide	19.08
Silicon	12.01	Silicon	10.0
Calcium	6.99	Calcium	3.60
Oxygen	3.01	Oxygen	2.00
-	-	Silver	7.02

3.3. Electrical study of SrS and SrS/Ag for optoelectronic application

The electrical analysis of silver-doped and undoped SrS is shown in Figure 3 and Table 3. The films show that when the deposition voltage increased, the electrical resistivity decreased from 1.42×10^9 to 1.37×10^9 $\Omega \cdot m$ and the thickness decreased from 125.02 to 123.025 nm. This further led to an increase in conductivity from 7.04×10^8 to 7.29×10^8 S/m. Low resistance and high conductivity of the material will be useful for optoelectronic applications. As sheet thickness is reduced, resistivity declines and conductivity increase, as seen in Figure 4 (a). Synthesized films are a preferable option for photovoltaic and solar cell applications. Plots of resistivity and conductivity versus deposition voltage are shown. Figure 4 (b) shows that resistivity increases while conductivity decreases.

Table 3. Electrical properties of SrS and SrS doped silver at various deposition voltages for optoelectronic application

Films	Thickness, t (nm)	Resistivity, ($\Omega \cdot m$)	Conductivity, (S/m)
SrS	125.02	1.32×10^9	7.57×10^8
SrS/Ag 10V	124.10	1.42×10^9	7.04×10^8
SrS/Ag 12V	123.11	1.39×10^9	7.19×10^8
SrS/Ag 14V	123.05	1.37×10^9	7.29×10^8
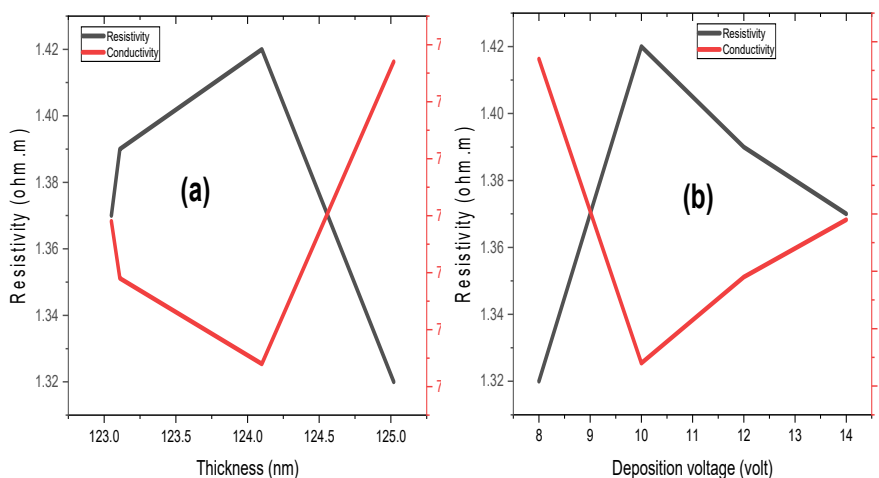
Figure 4. (a) resistivity and conductivity Vs thickness (b) resistivity and conductivity Vs deposition voltage

3.4. Optical study of SrS and SrS/Ag material deposited at the different voltages for optoelectronic application

Plots of the absorbance, transmittance, and reflectance of silver-doped SrS and undoped SrS are shown in Figure 5 for various deposition voltages between 10 and 14 volts. It is extremely obvious from Figure 5(a) that as light passes through the film and into the cells, the light is absorbed, making the material suitable for optoelectronic application. The SrS that was not doped had the maximum absorbance because it absorbed lighter than others. It was discovered that the absorbance decreases as the electromagnetic radiation's wavelength grows and the deposition voltage rises. Figure 5(b) shows that the undoped SrS has the lowest transmittance in the spectra while the doped SrS with silver deposited at 14 V has the highest transmittance in the spectra as the transmittance increases with increase in the deposition voltage and a corresponding increase in the wavelength of electromagnetic radiation. The reflectance of the material placed at various voltages is shown in Figure 5(c). Deposition voltage has a significant impact on SrS films because it causes a drop in the reflectance of SrS that has been doped with silver. A better material for optoelectronic applications is that which was deposited using 12V since it has the maximum reflectance.
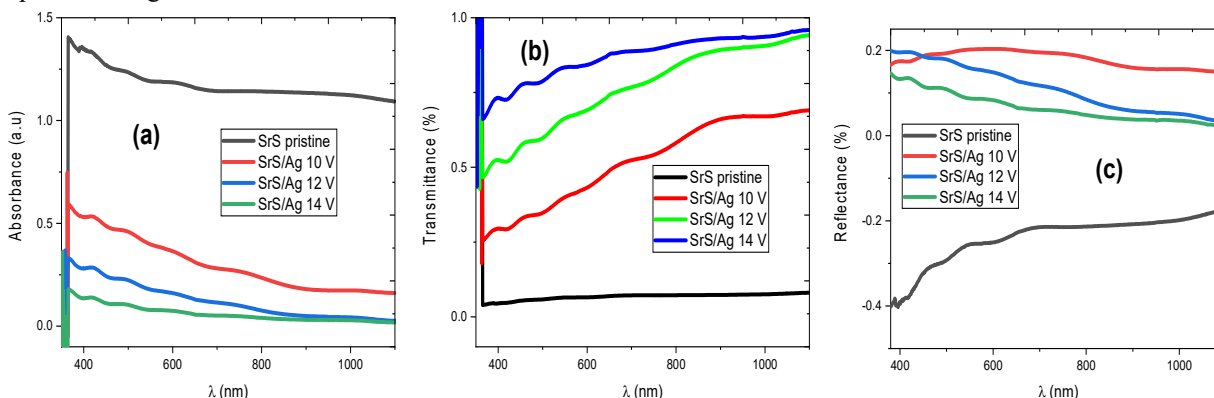
Figure 5. (a) absorbance, (b) transmittance, and (c) reflectance Vs wavelength

The plot of (hv)2 as a function of hv as shown in Figure 6 was used to determine the energy bandgap for undoped SrS and doped SrS deposited at various deposition voltages. According to research done on the deposited material, its energy bandgap lies between 1.55 and 2.51 eV. Due to the influence of the silver dopant on SrS, which was simulated as a substitutional dopant in its lattice location, it was determined that the bandgap energy for doped decreased from 2.10 to 2.51 eV. This doped material will be a promising material for optoelectronic and other applications because of the energy bandgap it displays.
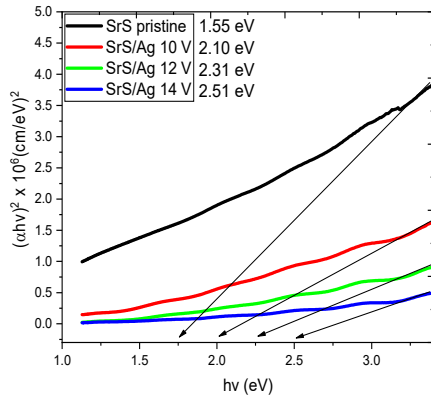
Figure 6. absorption coefficient square Vs photon energy

Plots of refractive index for undoped and doped SrS deposited at various deposition voltages are shown in Figure 7 (a). There was a rise in the refractive index of both doped and undoped material, as seen in the refractive index Vs hv spectra. It was observed from the spectra that an increase in the deposition voltage caused a reduction in the material's refractive index, and a decrease in the deposition voltage determined the usual scattering behavior of the films. For all of the produced films in Figure 7 (b), the coefficient of extinction increases as the photon energy increases. When compared to the films created at 12V and 14V, the undoped and doped SrS deposited with 10V certified high coefficient of extinction values. This rise in coefficient absorption can be coupled with a decline in transmission and an increase in the extinction value for the material with lower deposition voltage. The graph of the optical conductivity of doped and undoped SrS is shown in Figure 7 (c). Due to the high absorbance value of the synthesized material, which will eventually function as a superior material for optoelectronic applications, all the films recorded a moderate optical conductivity.
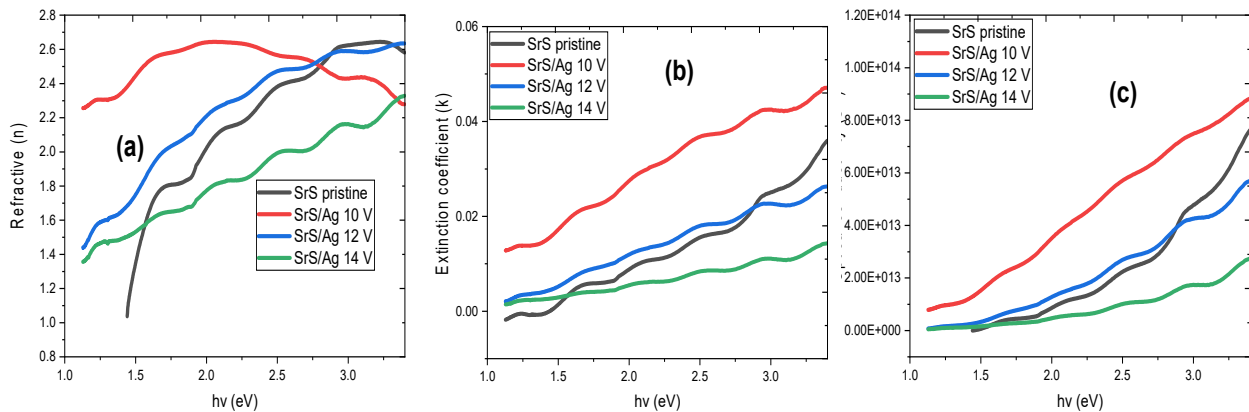
Figure 7. (a) refractive index, (b) extinction coefficient, (c) optical conductivity Vs photon energy

The doped and undoped SrS deposited at various deposition voltages are shown in Figure 8.
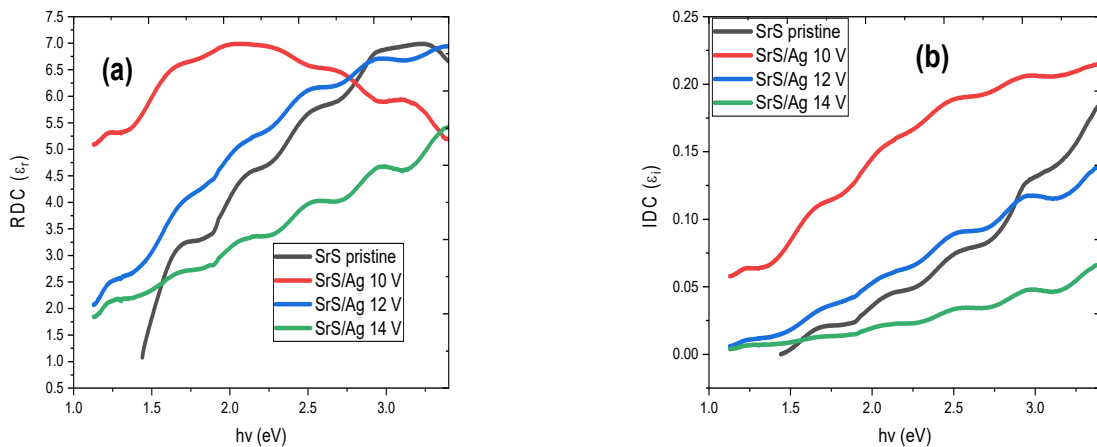
Figure 8. (a) real and (b) imaginary dielectric constant Vs photon energy

The dielectric loss demonstrates the loss of electrical energy in the form of thermal energy, whereas the dielectric constant shows how well dielectric materials store electrical energy (see Figure 8). Permittivity develops into a complex variable with real and made-up components in many modern fields. The real part (r) determines the level of polarization,

whereas the imaginary part (i) is related to dielectric losses. R's value rises as polarization does. The frequency has an effect on the dielectric constant. As frequency rises, the value declines because polarization mechanisms can no longer keep up with the fast-changing field. The amount of energy that has been used or consumed is represented by the imaginary component, which is always positive. As photon radiation increased, the actual portion of the material deposited rose dramatically, as shown in the spectra. The material is a strong candidate for optoelectronic applications since the real and imaginary properties of dielectric materials were improved by a deposition voltage.

4. CONCLUSIONS

We have successfully deposited undoped SrS and doped SrS with silver via electrochemical deposition technique. The XRD spectra of the SrS and SrS doped silver showed prominent crystalline peaks at angles of 26.69°, 37.97°, 51.39°, and 65.56° for SrS and 26.42°, 33.42°, 37.98°, and 51.32° for SrS/Ag, respectively, with corresponding diffraction planes (111), (112), (200), and (211). However, the diffraction pattern shows that the peak intensity increases as the deposition voltage increases. As the deposition voltage rises, the size of SrS and SrS-doped silver crystallites also rises. Due to the restriction of crystallite motion at the interface between the dopant and host crystallite brought on by stress generation, the doped SrS has a smaller value of crystallite size than the undoped SrS. The undoped SrS material morphology can be seen in the micrograph as clove-like substance with precipitate; the large nano grain on the substrate's surface exhibits photon absorption but shows no traces of pinholes. When doped SrS is deposited at various precursor voltages, it forms uniform surfaces devoid of pinholes. The cell also penetrates the substrate being used for the deposition, as seen by the elemental makeup of the films. It was observed that SrS/Ag at 10V and 12 V had little precipitate on the surfaces; this is because a carbon electrode was utilized, which tends to react with electrolyte at low voltages but does not do so at 14 V. The films show that when the deposition voltage increased, the electrical resistivity decreased from 1.42×10^9 to 1.37×10^9 Ω·m and the thickness decreased from 125.02 to 123.025 nm. This further led to an increase in conductivity from 7.04×10^8 to 7.29×10^8 S/m. It was discovered that the absorbance decreases as the electromagnetic radiation's wavelength grows and the deposition voltage rises. The undoped SrS has the lowest transmittance in the spectra while the doped SrS with silver deposited at 14V has the highest transmittance in the spectra as the transmittance increases with increase in the deposition voltage and a corresponding increase in the wavelength of electromagnetic radiation. According to research done on the deposited material, its energy bandgap lies between 1.55 and 2.51 eV. Due to the influence of the silver dopant on SrS, which was simulated as a substitutional dopant in its lattice location, it was determined that the bandgap energy for doped decreased from 2.10 to 2.51 eV.

ORCID IDs

Imosobomeh L. Ikhioya, https://orcid.org/0000-0002-5959-4427

REFERENCE
[1]   A. Chaves, J.G. Azadani, H. Alsalman, D.R. da Costa, R. Frisenda, A.J. Chaves, S.H. Song, et al., "Bandgap engineering of two-dimensional semiconductor materials", npj 2D Mater. Appl. **4**, 29 (2020). https://doi.org/10.1038/s41699-020-00162-4
[2]   M. Seifrid, G.N.M. Reddy, B.F. Chmelka, and G.C. Bazan, "Insight into the structures and dynamics of organic semiconductors through solid-state NMR spectroscopy", Nat. Rev. Mater. **5**, 910–930 (2020). https://doi.org/10.1038/s41578-020-00232-5
[3]   J. Shi, J. Zhang, L. Yang, M. Qu, D.-C. Qi, and K.H.L. Zhang, "Wide Bandgap Oxide Semiconductors: from Materials Physics to Optoelectronic Devices", Advanced materials, **33**, 2006230 (2021). https://doi.org/10.1002/adma.202006230
[4]   P.E. Agbo, and P.A. Nwofe, "Comprehensive studies on the optical properties of ZnO-core shell thin films", J. Nanotechnol. Adv. Mater. **3**(2), 63–97 (2015). https://www.naturalspublishing.com/files/published/7l62lvt2v9965a.pdf
[5]   S. Gedi, V.R.M. Reddy, C. Park, J. Chan-Wook, and R.K.T. Reddy, "Comprehensive optical studies on SnS layers synthesized by chemical bath deposition", Optical Materials, **42**, 468–475 (2015). https://doi.org/10.1016/j.optmat.2015.01.043
[6]   M.H. Suhail, and R.A. Ahmed, "Structural, optical and electrical properties of doped copper ZnS thin films prepared by chemical spray pyrolysis technique", Advances in Applied Science Research, **5**(5), 139-147 (2014). https://www.primescholars.com/articles/avo-analysis-of-3d-seismic-data-at-gfield-norway.pdf
[7]   W.D. Callister, and D.G. Rethwisch, *Materials science and engineering*, vol. 5, (John Wiley & Sons, NY, 2011).
[8]   D. Zhao, S. Sathasivam, J. Li, and C.J. Carmalt, "Transparent and Conductive Molybdenum-Doped ZnO Thin Films via Chemical Vapor Deposition", ACS Applied Electronic Materials, **2**(1), 120-125 (2020). https://doi.org/10.1021/acsaelm.9b00647
[9]   I.L. Ikhioya, and A.J. Ekpunobi, "Electrical and Structural Properties of ZnSe Thin Films by Electrodeposition Technique", Journal of the Nigerian Association of Mathematical Physics, **29**, 325-330 (2015). https://www.researchgate.net/profile/Imosobomeh-Ikhioya/publication/323316123_of_NAMP_Electrical_and_Structural_Properties_of_ZnSe_Thin_Films_by_Electrodeposition_Technique/links/5a8d63c10f7e9b27c5b4adbc/of-NAMP-Electrical-and-Structural-Properties-of-ZnSe-Thin-Films-by-Electrodeposition-Technique.pdf
[10] I.I. Lucky, D.N. Okoli, and A.J. Ekpunobi, "Effect Of Temperature On SnZnSe Semiconductor Thin Films For Photovoltaic Application", SSRG International Journal of Applied Physics, **6**(2), 55-67 (2019). https://doi.org/10.14445/23500301/IJAP-V6I2P109
[11] I.I. Lucky, E.M. Chigozirim, O.D.O, and A.C. Rita, "The Influence of Precursor Temperature on The Properties of Erbium-Doped Zirconium Telluride Thin Film Material Via Electrochemical Deposition", SSRG International Journal of Applied Physics, **7**(1), 102-109 (2020). https://doi.org/10.14445/23500301/IJAP-V7I1P115
[12] I.L. Ikhioya, A.C. Nkele, E.M. Chigozirim, S.O. Aisida, M. Maaza, and F.I. Ezema, "Effects of Erbium on the Properties of Electrochemically-Deposited Zirconium Telluride Thin Films," Nanoarchitectonics, **2**(1), 18-26 (2021). https://doi.org/10.37256/nat.212021503

[13] I.L. Ikhioya, A.C. Nkele, C.F. Okoro, C. Obasi, G.M. Whyte, M. Maaza, and F.I. Ezema, "Effect of temperature on the morphological, structural and optical properties of electrodeposited Yb-doped ZrSe₂ thin films", Optik, **220**, 165180 (2020). https://doi.org/10.1016/j.ijleo.2020.165180

[14] I.L. Ikhioya, A.C. Nkele, S.N. Ezema, M. Maaza, and F. Ezema, "A study on the effects of varying concentrations on the properties of ytterbium-doped cobalt selenide thin films", Optical Materials, **101**, 109731 (2020). https://doi.org/10.1016/j.optmat.2020.109731

[15] X.-Z. Li, Y.-Y. Gu, H.-Q. Cheng, and X.-M. Meng, "Van der Waals Epitaxial Two-dimensional CdSₓSe₍₁₋ₓ₎ Semiconductor Alloys with Tunable-composition and Application to Flexible Optoelectronics", Nanoscale, **9**(36), 13786–13793 (2017). https://doi.org/10.1039/c7nr04968d

[16] S.H. Lee, S.B. Kim, Y.-J. Moon, S.M. Kim, H.J. Jung, M.S. Seo, K.M. Lee et al., "High-responsivity Deep Ultraviolet-selective Photodetectors Using Ultrathin Gallium Oxide Films", ACS Photonics, **4**(11), 2937-2943 (2017). https://doi.org/10.1021/acsphotonics.7b01054

[17] J. Yang, W. Yu, Z. Pan, Q. Yu, Q. Yin, L. Guo, Y. Zhao, et al, "Ultra-broadband Flexible Photodetector Based on Topological Crystalline Insulator SnTe with High Responsivity", Small, **14**(37), 1802598 (2018). https://doi.org/10.1002/smll.201802598

[18] V.E. Zaikova, N.V. Melnikova, A.V. Tebenkov, A.A. Mirzorakhimov, O.P. Shchetnikov, A.N. Babushkin, and G.V. Sukhanova, "Electrical Properties of Polycrystalline Materials from the System Cu-As-Ge-Se under High Pressure Condition", Journal of Physics: Conf. Series, **917**, 082009 (2017). https://doi.org/10.1088/1742-6596/917/8/082009

[19] M. Hamada, K. Matsuura, T. Hamada, I. Muneta, K. Kakushima, K. Tsutsui, and H. Wakabayashi, "ZrS₂ Symmetrical-ambipolar FETs with Near-midgap TiN Film for both Top-gate Electrode and Schottky-barrier Contact", Jpn. J. Appl. Phys. **60**, SBBH05 (2021). https://doi.org/10.35848/1347-4065/abd6d7

[20] S. Sey-Shing, "A New Blue Emitting TFEL Phosphor: SrS: Cu", Displays, **19**(4), 145-149 (2019). https://doi.org/10.1016/S0141-9382(98)00044-4

[21] S. Vijay, T. K. Gundu, J. M. Rao, and Z. Jun-Jie, "Synthesis and characterization of Ce-Doped SrS Phosphors", Radiation Effects and Defects in Solids, **160**(7), 265-274 (2005). https://doi.org/10.1080/10420150500375534

ВПЛИВ НАПРУГИ ОСАДЖЕННЯ НА ЛЕГОВАНИЙ СРІБЛОМ СУЛЬФІД СТРОНЦІЮ ДЛЯ ОПТОЕЛЕКТРОННОГО ЗАСТОСУВАННЯ

Шака О. Самуель^{a,d}, М. Лагбегха-ебі Франк^b, Е.П. Огерохво^c, Артур Екпекпо^d, Дж.Т. Джимванг^e, Імособоме Л. Іхіоя^f
^aВідділ наукових лабораторних технологій, Університет штату Дельта, Абрака, штат Дельта, Нігерія
^bМіжнародний інститут туризму та гостинності, Йєнагоа, штат Байелса, Нігерія
^cФедеральний університет нафтових ресурсів, Еффурун, штат Дельта, Нігерія
^dКафедра фізики, Університет штату Дельта, Абрака, штат Дельта, Нігерія
^eФедеральний університет Локоджі, Нігерія
^fДепартамент фізики та астрономії, Університет Нігерії, Нсукка, 410001, штат Енугу, Нігерія

У дослідницькій методиці електрохімічного осадження використовували нелегований SrS і легований SrS сріблом: 0,01 моль тіоацетаміду (C₂H₅NS), 0,1 моль гексагідрату хлориду стронцію (SrCl₂,6H₂O) і 0,01 моль нітрату срібла (AgNO₃) концентрації катіонів, аніонів і допантів. Рентгенівські спектри срібла, легованого SrS та SrS, показали помітні кристалічні піки під кутами 26,69°, 37,97°, 51,39° та 65,56° для SrS та 26,42°, 33,42°, 37,98° та 51,32° для SrS/Ag відповідно , з відповідними площинами дифракції (111), (112), (200) і (211). Однак дифракційна картина показує, що пікова інтенсивність зростає зі збільшенням напруги осадження. Морфологія нелегованого матеріалу SrS має гвоздикоподібну речовину з осадом; велике нанозерно на поверхні підкладки демонструє поглинання фотонів, але не має слідів точкових отворів. Коли легований SrS осаджується при різних початкових напругах, він утворює однорідні поверхні без точкових отворів. Клітина також проникає в субстрат, який використовується для осадження, як видно з елементного складу плівок. Було помічено, що SrS/Ag при 10 В і 12 В мало осаду на поверхнях; це пояснюється тим, що використовувався вугільний електрод, який має тенденцію реагувати з електролітом при низькій напрузі, але не реагує при 14 В. Плівки показують, що коли напруга осадження зросла, питомий електричний опір зменшився з 1,42×10⁹ до 1,37×10⁹ Ом·м, а товщина зменшилася з 125,02 до 123,025 нм. Це додатково призвело до збільшення провідності з 7,04×10⁸ до 7,29×10⁸ См/м. Було виявлено, що поглинання зменшується зі збільшенням довжини хвилі електромагнітного випромінювання та підвищенням напруги осадження. Згідно з дослідженнями, проведеними на осадженому матеріалі, його ширина забороненої зони становить від 1,55 до 2,51 еВ.

Ключові слова: *нелегований SrS; заборонена зона; XRD; SEM; EDX*

COMPUTATIONAL INVESTIGATION OF IR AND UV-VIS SPECTRA OF 2-ISOPROPYL-5-METHYL-1,4-BENZOQUINONE USING DFT AND HF METHODS†

Salah M.A. Ridha[a]*, **Zahraa Talib Ghaleb**[b], **Abdulhadi Mirdan Ghaleb**[a]

aDepartment of Physics, College of Science, University of Kirkuk, Kirkuk, Iraq
bDepartment of Chemistry, College of Science, University of Kirkuk, Kirkuk, Iraq
*Corresponding Author e-mail: salahyagmuroglu@uokirkuk.edu.iq*
Received December 16, 2022; revised December 28, 2022; accepted January 5, 2023

A theoretical study on the thymoquinone compound has been performed through two theoretical methods, DFT/B3LYP and HF with 6-31G, 6-31G(d,p) and 6-31++G(d,p) basis sets using Gaussian 09 program. Some theoretical properties, like vibrational and electronic properties especially UV-Vis and FT-IR spectra, of the title compound were analyzed and then compared with available experimental data. The calculated harmonic vibrational frequencies have been scaled with standard scaling factors 0.9 and 0.965 for HF and DFT/B3LYP, respectively and then compared with available experimental FT-IR spectrum. Furthermore, the statistical analysis was investigated to evaluate the performance of both the HF and DFT methods, including root mean square error (RMSE), mean absolute error (MAE) and mean percentage error (MPE). According to the assigned vibrational modes of the title compound, it could be concluded that the DFT/B3LYP method with 6-31++G(d,p) basis set had the best agreement with experimental data. UV-Vis absorption spectra, excitation energies, maximum absorption wavelength, electronic transitions and oscillator strengths of the title compound were calculated by time dependent density functional theory (TD-DFT) method using the same basis set and compared with available experimental data. The results showed the best performer was HF method with 6-31G basis set.
Keywords: *Thymoquinone; DFT; HF; UV-Vis; FT-IR; TD-DFT*
PACS: 87.10.-e, 31.15.A-, 31.15.aj, 31.15.E-, 31.15.ee, 31.15.eg

Nigella sativa L. (Ranunculaceae), better known as black seed or black cumin, is cultivated in many countries of the world in East Africa, the Middle East, Mediterranean countries, South Asia, etc. [1]. 2-isopropyl-5-methyl-1,4-benzoquinone called as thymoquinone is an organic compound with the formula $C_{10}H_{12}O_2$ and its geometric structure with the labeling of atoms are given in Figure 1.
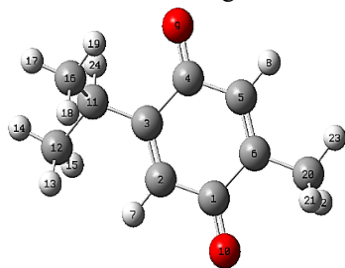
Figure 1. Molecular structure of Thymoquinone compound along with numbering of atoms

It is a derivative of benzoquinone by placement of an isopropyl and methyl groups on carbon 2 and carbon 5, respectively. Thymoquinone (TQ) is an important component of Nigella sativa seed and commercial seed oils, TQ is the main active constituent of black seed oil [2]. Thymoquinone, the main component of black cumin seeds, has been identified from ethanol extract [3]. As first suggested and extracted by El-Dakhakhny in 1965 [4]. Black cumin seeds along with the active ingredient thymoquinone are mainly used for medicinal purposes [5]. With this together, this medicinal plant is effective against cancer of the kidneys, lungs, prostate and liver in the blood system [6]. Also, Nigella sativa gives powerful benefits to many inflammatory cancers such as the liver [7]. N. Sativa oil is considered one of the beneficial oils for human health, thanks to the antioxidant, anti-inflammatory, anti-bacterial activities of these oils, and its active effect on the immune system [8-12].Nigella sativa (black cumin) seeds are also used in traditional medicine to treat a wide range of diseases including diarrhea and asthma [13].Various other studies revealed that the pharmacological activity of Nigella sativa is mainly due to its oil constituent, that are rich in thymoquinone and about 30–48 % of the total content[14].

The main goal of this work was to validate the chemical model that best describes the electronic and spectroscopic properties of TQ molecule. Hence, both Density Functional Theory (DFT) and Hartree-Fock (HF) methods with several basis sets were selected to calculate the electronic and spectroscopic properties, which were compared with experimental results. Furthermore, we checked the relative performance of DFT/B3LYP and HF methods for comparison, at the different 6-31G, 6-31G(d,p), and 6-31++(d,p) levels through statistical study for thymoquinone molecule.

COMPUTATIONAL DETAILS

In this work, all the calculations for Thymoquinone (TQ) molecule were carried at Hartree-Fock (HF) [15] and Density Functional Theory (DFT) using Becke's three-parameter hybrid method [16] with the Lee, Yang, and Parr correlation functional [17] (B3LYP) level with the several basis sets (6-31G, 6-31G(d, p), 6-31++G(d, p)) using the Gaussian 09 W package [18] program for simulation of FTIR and UV-Vis spectra of the title molecule. Gauss-View 5.0 [19] molecular visualization program, a graphical interface was used to assign the vibrational modes for motions observed against fundamental frequencies. The geometrical optimizations, followed by a frequency calculation

for the Thymoquinone molecule has been done, using the same basis sets at different level theories and no imaginary wavenumbers were obtained, so the structure is at the minimum energy state. In order to improve the computed values to be in agreement with the observed experimental values, it was necessary to scale down the calculated harmonic frequencies. Hence, the vibrational frequencies calculated at HF and DFT/B3LYP methods were scaled by 0.90 and 0.965 [20], respectively. The theoretical vibrational wave numbers were also plotted with the results obtained by different levels frequency calculations and compared with the experimental IR spectrum.

Simulated Ultraviolet- Visible (UV-Vis) absorption spectra, electronic transition, vertical excitation energies and oscillator strengths for the optimized (TQ) molecule were computed at different levels in each method by the Time Dependent - Density Functional Theory (TD-DFT) using the same basis sets, then compared with the experimental UV-Vis spectrum.

RESULTS AND DISCUSSION
Vibrational Frequencies

Vibration frequencies calculated by HF and DFT/B3LYP with the several basis sets (6-31G, 6-311G(d,p), 6-31++G(d, p)) for the title compound are listed in Table 1. The calculated spectra by DFT/B3LYP method are in a better agreement than HF method with the experimental one. A general better performance of DFT/B3LYP versus HF at 6-31++G(d, p) basis set can be quantitatively characterized by using the calculated mean percentage error (MPE), mean absolute error (MAE), and root mean square error (RMSE) between the calculated and observed vibrational frequencies are presented in Table 2, also histograms of the errors are shown in Figures 2 and 3. It is not surprising that the HF frequencies are in poor agreement with the experimental vibrational modes compared to the other theoretical DFT/B3LYP method. This expectation is due to the neglect of electron correlation in HF calculations. After scaling, the HF calculations are in much better agreement, showing a noticeable decrease in the RMSE, MAE and MPE of around 146-151 cm^{-1}, 137-145 cm^{-1} and 9-11 cm^{-1}, respectively. Also, as shown in Table 2, the effect scaling factor on the errors in the HF frequencies where the agreement for un-scaled frequencies is strongly skewed toward overestimation. In contrast to HF method, the errors for DFT/B3LYP are shown in Table 2, show that the calculated vibrational frequencies are closer to the experimental ones than the HF method at all basis sets used in this study. As we noted the DFT/B3LYP method at 6-31++ G(d, p) basis set is the most successful procedure for predicting vibrational frequencies in agreement with experimental fundamentals. All methods show an improved errors from scaled IR data. The effect of scaling factor and basis sets on the errors is evident from Figures 2-3, where the histograms for DFT/B3LYP and HF methods show a noticeable improvement using scaling factor and high levels of basis sets.

The (IR) infrared spectrum of the title compound (TQ) has been previously reported [21]. The spectra obtained from scaled HF and DFT/B3LYP methods at different basis sets are shown in Figure 4. After we were applied the scale factor for HF and DFT/B3LYP methods, we observed a good agreement between the experimental and the calculated values. These results indicate that the DFT/B3LYP calculation at 6-31++G(d, p) basis set approximate the observed vibrational modes much better than the HF results. Therefore, the theoretical calculations will be discussed with the experimental results based on the DFT/B3LYP method at the basis set 6-31++ G(d,p). The small deviation between experimental and calculated vibrational modes can be come from the theoretical calculations belong to gaseous phase and experimental results belong to solid phase.

The characteristic strong band due to carbonyl group stretching of a cyclohexadiene was observed near 1655cm^{-1} and the respective calculated band is assigned at 1659 cm^{-1}, which is supported by previous studies with values of (1648 cm^{-1}) and (1661cm^{-1}) for thymoquinone and 1,4 benzoquinone, respectively [21,22]. In the methyl groups, three observed bands occur at 2878, 2928, and 2970 cm^{-1}; bands 2878 and 2928 cm^{-1} attributed to symmetric stretching and the band at 2970 cm^{-1} arises from asymmetric stretching, and the value previously reported [21] was 2969 cm^{-1} while computations predicts these modes at 2930, 2933, and 3001 cm^{-1}. Also, two types of bending vibrations can be observed in the methyl groups, one of them is a symmetric bending vibration that includes in phase bending and the other anti-symmetric bending vibration which includes out-of-phase bending of C-H bonds. The symmetrical bending vibration (δ_sCH3) occurs near 1360 cm^{-1} (calculated 1360 cm^{-1}), the anti-symmetrical bending vibrations (δ_{as}CH3) near 1437 cm^{-1}(calculated 1431 cm^{-1}) and 1461 cm^{-1}(calculate 1463 cm^{-1}) and the values previously reported [23] were 1375 cm^{-1} and 1450 cm^{-1} for the anti-symmetrical and symmetrical bending vibrations, respectively.

The weak band observed at wavenumber 3050 cm^{-1} was attributed to C-H stretching vibration in the vinyl C-H (C=C-H groups) and respective calculated band at 3080 cm^{-1} which had previously been reported [22] at 3058 cm^{-1}.The out-of-plane bending bands of the vinyl(two C-H groups) are observed at 808 cm^{-1} and 871 cm^{-1} (calculated 846 and 907 cm^{-1}), 783 and 832 cm^{-1} for γ-Trepinene [24]. These two bands are partially mixed with the rocking motion of the methyl groups linked to the ring. In the spectral range region (1300-1000 cm^{-1}), the bands observed at 1024 cm^{-1} which is due to the stretching C3$_{ring}$ – C(CH3)$_2$ bond (calculated 999 cm^{-1}), 1104 cm^{-1}, 1180 cm^{-1} and 1247 cm^{-1} (in plane bending of the vinyl C-H (C = C-H groups); calculated 1110, 1197 and 1218 cm^{-1}, respectively) and 1304 cm^{-1} for the (C-C)$_{ring}$ stretching band (calculated 1325 cm^{-1}). The recognition of C=C stretching band is an exceptionally troublesome task, since the strong C=O stretching band in title compound is present in this frequency range. The C=C stretching band in 1,4-cyclohexadiene has been observed at wavenumber 1640 cm^{-1}which contains no methyl and isopropyl substituents, while in γ-Trepinene [24] at 1670 cm^{-1} which contains no oxygen atoms substituent; however, the medium band observed at 1615 cm^{-1} belong to C=C stretching band while the calculated value appeared at 1604 cm^{-1}.

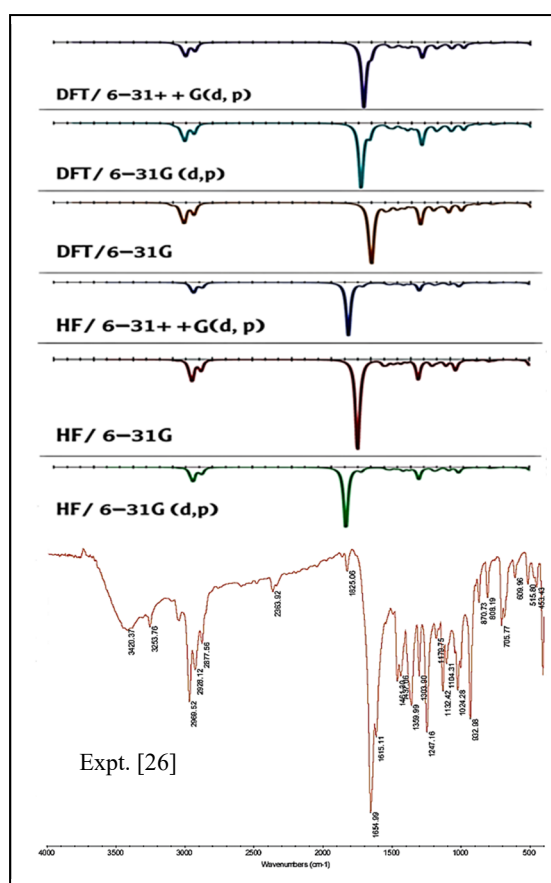**Table 1.** Experimental and calculated IR spectral data of the title compound together with their assignments

No.	Observed frequency* IR(cm⁻¹)	Calculated frequency (cm⁻¹) with DFT/B3LYP/6-31G			Calculated frequency (cm⁻¹) with DFT/B3LYP/6-31G (d,p)			Calculated frequency (cm⁻¹) with DFT/B3LYP/6-31++ g(d,p)			Calculated frequency (cm⁻¹) with HF/6-31G			Calculated frequency (cm⁻¹) with HF/ 6-31G (d,p)			Calculated frequency (cm⁻¹) with HF/ 6-31++ g(d,p)			Vibrational
		Un-scaled (cm⁻¹)	scaled (cm⁻¹)	IR Intensity	Un-scaled (cm⁻¹)	scaled (cm⁻¹)	IR Intensity	Un-scaled (cm⁻¹)	Scaled (cm⁻¹)	IR Intensity	Un-scaled (cm⁻¹)	scaled (cm⁻¹)	IR Intensity	Un-scaled (cm⁻¹)	scaled (cm⁻¹)	IR Intensity	Un-scaled (cm⁻¹)	scaled (cm⁻¹)	IR Intensity	
1		55.77	54	1.53	55.08	53	2.23	52.22	50	2.28	55.01	50	3.57	53.53	48	4.12	15.30	14	3.95	ρ(C16C11C12)
2		70.65	68	4.61	69.88	67	2.99	67.44	65	4.13	73.14	66	4.75	73.71	67	2.62	70.86	64	3.51	γ(all structure)
3		129.72	125	5.04	123.73	119	4.38	121.34	117	4.26	138.7	125	6.07	132.52	120	5.23	130.0	117	4.70	γ(all structure)
4		131.35	127	0.14	129.79	125	0.03	138.53	134	0.19	148.2	134	0.18	153.03	138	0.03	155.2	140	0.06	ρ(C20H3)
5		178.76	173	0.52	176.17	170	0.39	174.47	168	0.50	191.4	173	0.48	188.40	170	0.36	186.9	169	0.45	β(C11C16C12)
6		195.32	189	0.31	186.26	180	0.36	185.68	179	0.37	207.5	187	0.44	198.72	179	0.48	199.0	180	0.42	ρ(C20H3), γ(O=C4C5ring)
7		237.17	229	0.12	236.52	228	0.09	232.83	225	0.11	250.8	227	0.20	251.40	227.	0.15	248.8	225	0.20	ρ(C12H3; C16H3)
8		257.91	249	0.18	252.76	244	0.08	248.34	240	0.09	281.3	254	0.42	271.93	246	0.16	267.6	242	0.13	ρ(C12H3), γ(O=C1C2ring)
9		266.93	258	0.04	268.72	259	0.02	265.13	256	0.04	291.58	263	0.01	298.07	269	0.01	295.50	267	0.02	ρ(C12H3; C16H3)
10		294.89	285	0.20	288.22	278	0.10	286.75	277	0.14	315.25	285	0.39	307.52	278	0.19	305.86	276	0.19	β(C6ring-C20H3)
11		303.15	293	3.38	296.32	286	2.67	295.52	285	2.31	324.776	293	3.66	316.86	286	2.82	315.92	285	2.66	β(C16C11C12), β(C6ring-C20H3)
12		400.45	386	4.49	384.69	371	0.37	384.18	371	0.91	436.52	394	9.16	415.45	375	0.40	413.25	373	0.73	γ(ring),ρ(C20H3), β(C12C11C16)
13		407.11	393	20.54	403.22	389	0.12	403.88	390	8.27	442.24	399	26.59	435.16	393	5.62	434.26	392	5.77	β(C=O)ring, β(C12C11C16)
14	409.7 m	415.08	401	0.42	405.31	391	22.45	404.92	391	13.33	450.18	407	1.18	439.74	397	25.56	438.68	396	24.19	β(C=O)ring, β(C12C11C16)
15	453.43 w	462.84	447	1.77	452.77	437	2.87	453.19	437	2.47	501.67	453	3.42	488.61	441	5.60	487.70	440	5.01	γ(CCC)ring, γ(C11H)
16		489.26	472	0.46	479.71	463	0.66	479.31	463	0.60	526.09	475	0.69	513.56	464	0.86	512.25	463	0.81	γ(CCC)ring,γ(CH)ring, ω(C12H3;C11H;C16H3)
17	515.8 w	535.93	517	1.20	522.82	505	1.68	522.56	504	1.55	577.84	522	2.27	563.62	509	3.10	562.60	508	2.80	γ(CCC)ring,γ(CH)ring, ω(C12H3;C11H;C16H3)
18		626.74	605	0.97	617.15	596	0.74	616.52	595	0.63	672.24	607	1.37	660.32	596	0.97	659.44	595	0.80	β(C5C6ring-C20H3), β(CCring-O), β(CH)ring
19	609.96 w	682.53	659	2.59	672.65	649	2.08	671.80	648	1.75	734.81	664	4.23	723.40	653	2.72	722.02	652	2.29	β(C=C-C)ring, ω(C12H3; C20H3)
20		703.43	679	2.67	693.24	669	2.66	691.33	667	2.50	750.85	678	3.79	740.15	668	3.60	738.25	667	3.36	Breath(ring)
21	705.77 m	722.76	697	5.43	712.80	688	5.67	711.14	686	4.84	781.82	706	11.56	772.11	697	10.53	768.92	694	8.75	γ(ring), ρ(C12H3;C16H3;C20H3)
22		796.61	769	0.36	792.42	765	0.28	788.96	761	0.21	865.26	781	0.82	862.81	779	0.52	854.20	771	0.56	γ(ring), γ(CH)ring
23		825.49	797	8.33	814.33	786	5.91	814.13	786	5.47	885.45	780	6.84	874.00	789	3.68	872.61	788	3.36	β(CH)ring, ω(C12H3;C16H3;C20H3)
24	808.19 w	887.26	856	5.07	879.97	849	4.03	876.87	846	3.69	947.32	855	2.84	941.81	850	2.50	940.15	849	2.15	ϑ(C-C)ring γ(CH)ring,ρ(C12H3;C16H3)
25		916.77	885	1.63	893.30	862	1.04	889.53	858	1.52	1010.92	913	3.90	977.23	882	1.67	970.47	876	2.64	γ(CH)ring
26		954.44	921	33.46	936.34	904	13.25	935.23	902	11.32	1041.81	941	2.90	1011.55	913	0.91	1010.03	912	0.82	γ(CH)ring, ω(C16H3)
27	870.73 w	965.17	931	8.56	940.28	907	22.17	939.46	907	29.17	1062.20	959	61.39	1036.32	936	58.13	1033.74	933	61.17	γ(CH)ring, ρ(C12H3; C16H3)
28		995.23	960	0.02	975.14	941	0.15	971.09	937	0.10	1064.53	961	4.31	1044.49	943	0.89	1042.12	941	0.70	$\boldsymbol{\rho}$(C12H3; C16H3)
29	932.98 m	1050.61	1014	5.43	1022.07	986	14.45	1021.23	985	17.13	1125.07	1016	3.82	1105.44	998	1.04	1104.18	997	0.78	$\boldsymbol{\omega}$(C20H3)

No.	Exp*	1	2	3	4	5	6	7	8	9	10	11	12	13	14	15	16	17	18	Assignment
30	1024.28 m	1055.63	1019	42.03	1038.46	1002	30.55	1035.65	999	28.57	1142.88	1032	33.13	1117.64	1009	31.54	1115.83	1008	31.75	ϑ(C3ring−C11),ω(C12H3;C16H3;C20H3)
31		1097.02	1059	5.97	1062.02	1025	2.96	1059.52	1022	2.40	1201.34	1085	5.37	1162.28	1049	1.50	1159.72	1047	1.11	ρ(C20H3)
32		1132.43	1093	9.40	1115.10	1076	6.08	1110.46	1072	7.51	1221.39	1103	9.22	1203.23	1087	5.93	1200.78	1084	6.26	ω(C12H3), γ(C11H)
33		1153.93	1114	4.55	1131.45	1092	10.68	1126.71	1087	6.45	1248.55	1127	16.66	1223.07	1104	18.56	1220.65	1102	15.30	ω(C12H3;C16H3),β(C11H)
34	1104..31 w	1173.96	1133	31.85	1152.90	1113	32.13	1150.47	1110	36.33	1265.43	1143	22.80	1244.25	1124	25.07	1242.42	1122	26.61	β(CH) ring,ω(C12H3;C20H3)
35	1132.42 m	1228.64	1186	1.81	1207.06	1165	2.71	1202.13	1160	4.60	1330.19	1201	1.64	1308.14	1181	2.44	1305.09	1178	3.36	β(C11H), ω(C16H3; C12H3)
36	1179.75 w	1270.72	1226	22.62	1238.48	1195	3.53	1240.59	1197	4.07	1374.35	1241	123.42	1346.54	1216	0.57	1348.22	1217	0.64	β(CH)ring
37	1247.16 m	1276.93	1232	90.15	1265.70	1221	112.89	1262.43	1218	106.36	1379.13	1245	0.22	1369.76	1237	126.03	1366.05	1234	120.21	β(CH)ring,ϑ(C-C)ring
38		1352.14	1305	7.50	1329.27	1283	16.85	1323.66	1277	7.53	1469.08	1327	9.62	1449.65	1309	18.81	1446.51	1306	15.03	β(C11H), β(CH)ring
39		1353.15	1306	3.99	1332.78	1286	1.70	1327.13	1281	8.61	1472.55	1330	0.83	1457.42	1316	3.52	1452.84	1312	4.02	β(C11H)
40	1303.9 w	1399.63	1351	18.91	1376.64	1328	29.29	1372.77	1325	28.07	1519.14	1372	19.75	1501.04	1355	33.07	1498.03	1353	31.66	ϑ(C-C)ring, ω(C20H2), β(CH)ring
41		1422.64	1373	4.66	1399.18	1350	1.17	1394.42	1346	1.39	1551.12	1401	2.85	1529.84	1381	1.42	1525.56	1378	1.89	δ_s(C16H3; C12H3), ϑ(C-C)ring, β(C11H)
42	1359.99 m	1444.55	1394	11.09	1414.43	1365	9.02	1409.26	1360	10.90	1568.77	1417	10.65	1545.73	1396	5.07	1541.82	1392	5.34	δ_s(C16H3;C12H3)
43		1462.93	1412	5.25	1426.77	1377	5.36	1421.41	1372	8.66	1587.83	1434	6.82	1558.18	1407	3.97	1553.63	1403	5.44	δ_s(C16H3;C12H3)
44		1464.14	1413	15.78	1430.24	1380	3.29	1423.35	1373	4.69	1589.78	1436	8.06	1560.83	1409	3.67	1556.51	1406	3.97	δ_s(C20H3)
45		1515.02	1462	10.20	1481.25	1429	7.17	1472.23	1421	8.97	1631.53	1473	9.84	1600.15	1445	6.40	1593.96	1439	7.90	δ_{as}(C20H3)
46	1437.06 w	1523.52	1470	8.16	1490.41	1438	9.42	1482.96	1431	10.49	1639.39	1480	9.67	1608.92	1453	9.21	1605.27	1450	9.92	δ_{as}(C20H3)
47		1534.05	1480	3.91	1503.20	1451	2.13	1493.22	1441	1.69	1647.82	1488	1.72	1618.28	1461	1.10	1611.84	1455	0.98	δ_{as}(C16H3;C12H3)
48		1537.13	1483	5.75	1505.91	1453	4.61	1496.81	1444	5.05	1651.35	1491	6.42	1922.26	1736	4.12	1616.32	1460	4.32	δ_{as}(C16H3;C12H3)
49		1551.84	1497	9.35	1520.45	1467	7.05	1511.43	1459	10.48	1666.23	1505	12.12	1636.35	1478	7.89	1630.57	1472	10.67	δ_{as}(C16H3;C12H3)
50	1461.3 w	1555.05	1501	13.62	1526.83	1473	7.34	1516.18	1463	10.93	1669.37	1507	10.73	1643.05	1484	5.63	1636.22	1478	6.87	δ_{as}(C16H3;C12H3)
51	1615.11 m	1633.83	1571	1.74	1673.18	1615	64.58	1662.52	1604	76.18	1835.44	1657	2.81	1851.63	1672	36.66	1838.57	1660	41.93	ϑ(C=C) ring
52	1654.99 s	1657.04	1599	266.75	1707.52	1648	2.84	1693.27	1634	4.40	1855.23	1675	28.04	1878.72	1697	3.73	1865.03	1684	4.30	ϑ(Cring = O), ϑ(C=C) ring
53		1675.36	1617	80.40	1739.90	1679	238.52	1719.58	1659	445.30	1882.82	1700	555.63	1980.18	1788	638.24	1959.37	1769	764.7	ϑ(Cring = O)
54		1723.85	1663	0.68	1745.11	1684	111.43	1726.59	1666	13.32	1934.68	1747	1.46	2001.16	1807	13.83	1982.53	1790	4.46	β(CCC)ring, ϑ(C=O)ring
55	2877.56 w	3042.57	2936	19.50	3042.26	2936	17.49	3036.23	2930	22.41	3189.13	2880	26.64	3182.75	2874	26.46	3179.12	2871	29.15	ϑ_s(C12-H3)
56	2928.12 w	3047.03	2940	32.42	3046.31	2940	23.13	3039.74	2933	28.34	3194.14	2884	30.72	3188.32	2879	30.59	3184.86	2876	32.75	ϑ(C11-H),ϑ_s(C16-H3),ϑ_s(C12-H2)
57		3054.48	2948	10.52	3054.02	2947	8.38	3049.07	2942	9.72	3206.67	2896	14.77	3201.14	2891	17.77	3199.53	2889	19.03	ϑ_s(C16-H3)
58		3055.14	2948	7.92	3056.24	2949	7.28	3054.12	2947	4.00	3222.93	2910	1.34	3223.43	2911	1.70	3219.28	2907	1.75	ϑ(C11-H)
59		3113.92	3005	11.09	3110.21	3001	8.55	3103.05	2994	5.96	3256.16	2940	2.42	3246.79	2932	3.30	3241.23	2927	4.23	ϑ_{as}(C12-H3), ϑ_{as}(C16-H2)
60		3114.54	3006	8.90	3112.39	3003	6.57	3106.51	2998	5.33	3266.33	2949	41.57	3258.25	2942	54.20	3252.94	2937	38.66	ϑ_{as}(C20-H2)
61	2969.52 m	3122.66	3013	38.17	3117.24	3008	41.29	3109.43	3001	44.90	3268.12	2951	65.44	3259.63	2943	63.28	3254.32	2939	79.44	ϑ_{as}(C12-H3),ϑ_{as}(C16-H2), ϑ(C11-H)
62		3127.05	3018	41.21	3112.59	3004	31.50	3114.67	3006	32.96	3273.19	2956	10.79	3267.07	2950	13.80	3264.51	2948	11.77	ϑ_{as}(C16-H3)
63		3148.53	3038	16.69	3144.03	3034	15.06	3132.72	3023	16.20	3289.41	2970	20.89	3281.61	2963	24.21	3274.25	2957	25.09	ϑ_{as}(C12-H3)
64		3151.46	3041	12.83	3146.74	3037	11.17	3139.93	3030	11.97	3294.13	2975	14.07	3286.32	2968	16.17	3282.73	2964	16.23	ϑ_{as}(C20-H3)
65	3050 w	3215.83	3103	6.86	3193.91	3082	6.57	3191.81	3080	6.00	3390.34	3061	3.87	3368.54	3042	4.52	3366.85	3040	4.21	ϑ(CH)ring
66		3229.97	3117	2.95	3207.18	3095	2.89	3206.22	3094	2.36	3409.27	3079	2.06	3387.62	3059	2.17	3387.62	3059	1.87	ϑ(CH)ring

ϑ: stretching, ϑ_s: symmetric stretching, ϑ_{as}: asymmetric stretching, δ_s: symmetric bend, δ_{as}: anti-symmetric bend, β: in plane bending, ω: wagging, ρ: rocking, γ: out of plane bending, w: weak, m: medium; s: strong.
*Experimental from reference [25]

Table 2. Mean percentage error (MPE), mean absolute error (MAE) and root mean square error (RMSE) from experimental fundamentals with different basis sets

Method	Basis Set	MPE %		MAE		RMSE	
		Un-scaled	Scaled	Un-scaled	Scaled	Un-scaled	Scaled
HF	$6-31G$	14.04	3.32	181.61	37.09	198.22	47
	$6-31G(d,p)$	12.81	3.05	171.08	34.25	191.42	44.61
	$6-31++G(d,p)$	12.53	2.95	167.3	29.59	187	41.22
DFT/B3LYP	$6-31G$	5.71	3	75.46	35.25	89.66	40.86
	$6-31G(d,p)$	4.56	2.29	64.8	23.73	78.98	28.25
	$6-31++G(d,p)$	4.28	2.18	60.45	21.64	74.65	26.28
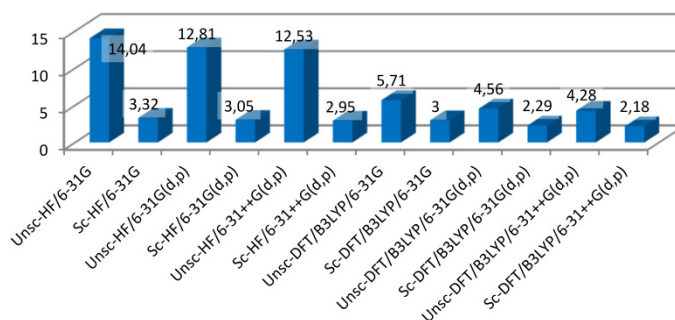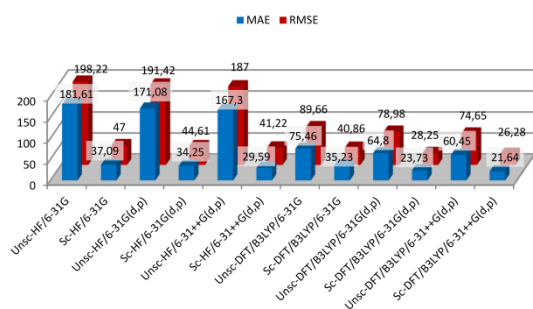
Figure 2. Histogram of RMSE and MAE of the title compound for the un-scaled and scaled HF and DFT/B3LYP methods, at various basis sets

Figure 3. Histogram of MPE of the title compound for the un-scaled and scaled HF and DFT/B3LYP method, at various basis sets

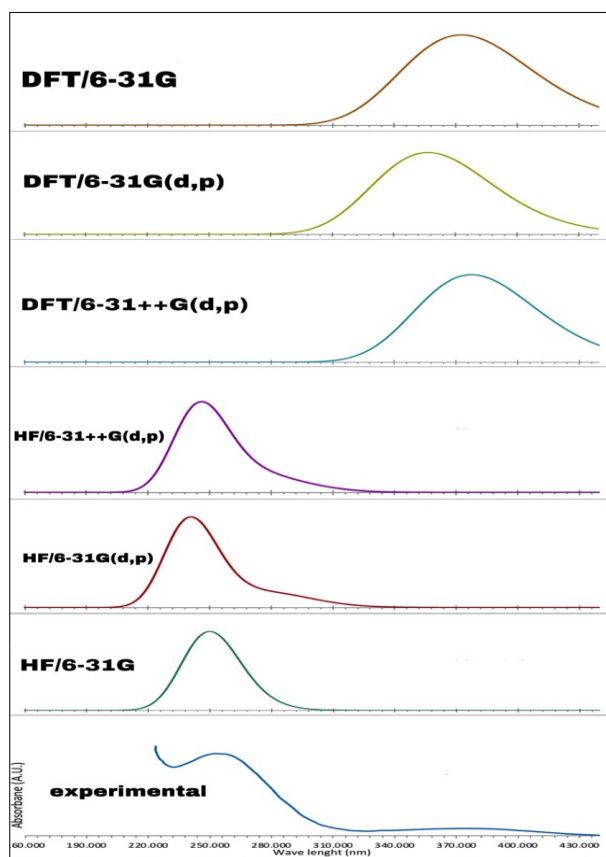**Figure 4.** Experimental (from ref [25]) and calculated (scaled) IR spectra of the title compound

UV-Visible absorption spectra

The UV-Visible absorption spectra analysis of Thymoquinone compound have been studied by theoretical calculations under the same optimization conditions that were previously mentioned in this article. The calculated results

including the maximum absorption wavelengths (λ_max), oscillator strengths (f), molecular orbitals undergoing transitions, vertical excitation energy, the major contributions, and the experimental wavelength are shown in the Table 3 and the UV-Visible spectra of the title compound as obtained from TD-DFT method at several basis sets with experimental spectrum are shown in Figure 5. According the results obtained in the UV-Visible theoretical spectra, the theoretical model that appear the best agreement, is HF method with 6-31G basis set that estimates the λ_max about 249 nm in relation to the 254 nm experimental maximum absorption wave length reported by M.S. Iqbal, et al. [14]. It is seen from Table 4, calculations performed at HF/6-31G method in best agreement with the experimental result compared to the DFT/B3LYP method and other basis sets. The electronic transition is represented as a result of the contribution of the highest occupied molecular orbital to the lowest unoccupied molecular orbital (HOMO→LUMO) with the absorption wavelength, which implies the transfer of electron density as ($\pi \rightarrow \pi^*$) transition with 91% donating.This electronic absorption is mainly described at the maximum absorption wavelength249 nm by electronic excitation from HOMO to LUMO and corresponds to the transition from the ground state to the first excited state. The maximum absorption peak (λ_max) optimized by HF/6-31G level reduces the error to 5 nmю While for the rest of the basis sets, especially for the DFT method, the difference is large. These outcomes demonstrate it is not necessary that the same computational method for all calculations, for example, IR and UV-Vis spectra, agree with the experimental results.

Table 3. The experimental and calculated maximum absorption wavelength (λ_max) excitation energies and oscillator strengths of the title compound.

Basis sets	The calculated with TD-DFT/-HF in gas phase					The calculated with TD-DFT/B3LYP in gas phase				
	wavelength λ_max(nm)	Energy (ev)	Osc. Strenght	Major Contribution	Transition	wavelength λ_max(nm)	Energy (ev)	Osc. Strenght	Major Contribution	Transition
6-31G	249.39	4.9608	0.0008	HOMO->LUMO 90.9%	$\pi \rightarrow \pi^*$	372.74	3.3263	0.0004	HOMO-2->LUMO 97.3%	$\pi \rightarrow \pi^*$
6-31G(d,p)	240.82	5.1483	0.0007	HOMO->LUMO 93.5%	$\pi \rightarrow \pi^*$	356.6	3.4768	0.0004	HOMO -2-> LUMO 97.8%	$\pi \rightarrow \pi^*$
6-31G++(d,p)	245.83	5.0434	0.0007	HOMO->LUMO 92.6%	$\pi \rightarrow \pi^*$	357.53	3.4678	0.0005	HOMO -2-> LUMO 96.9%	$\pi \rightarrow \pi^*$
Experimental**	254 nm									

Figure 5. Experimental (from reference [14]) and calculated UV-Vis spectra of the title compound

CONCLUSION

In this study, the FT-IR and UV-Vis spectra of the compound thymoquinone (TQ) have been calculated by two chemical models DFT/B3LYP and HF using 6-31G, 6-31G(d,p) and 6-31++G(d,p) basis sets and compared with

experimental results. Also, the present study aims to explore the performances two chemical models regarding statistical analysis of IR vibrational frequencies for the title compound, using root mean square error (RMSE), mean absolute error (MAE) and mean percentage error (MPE) calculations to give numerical estimates of these performances. The performed statistical analysis between computed and experimental vibrational frequencies showed the best performance of DFT/B3LYP method, especially with large basis sets. The DFT/B3LYP method with 6-31++G(d,p) basis set for predicting vibrational frequencies was the most successful procedure. Furthermore, it was found the theoretical scaled vibrational frequencies by DFT/B3LYP method with 6-31++G(d,p) basis set showed good agreement with the experimental data. Although DFT/B3LYP performs well for vibrational frequencies, it is less efficient for UV-Visible spectrum, where the best results were obtained for the maximum absorption wavelength through the HF method with the basis set 6-31G. These outcomes demonstrate it is not necessary that the same computational method for all calculations, for example, IR, UV-Visand NMR spectra, agree with the experimental results.

ORCID IDs

Salah M.A. Ridha, https://orcid.org/0000-0003-0569-3849; **Zahraa Talib Ghaleb**, https://orcid.org/0000-0003-0569-3849
Abdulhadi Mirdan Ghaleb, https://orcid.org/0000-0002-2202-8827

REFERENCES

[1] B.H. Ali, and G. Blunden, "Pharmacological and toxicological properties of Nigella sativa", Phytother. Res. **17**, 299-305 (2003). https://doi.org/10.1002/ptr.1309

[2] Z. Erisgin, M. Atasever, K. Cetinkaya, S.A. Dizakar, S. Omeroglu, and H. Sahin, "Protective effects of, Nigella sativa oil against carboplatin-induced liver damage in rats", Biomedicine & Pharmacotherapy, **110**, 742-747 (2019). https://doi.org/10.1016/j.biopha.2018.12.037

[3] P.K. Perera, D.T. Karunaratne, and N. Kalka, *Antiinflammatory Actions and Potential Usage for Arthritic Conditions, Bioactive Food as Dietary Interventions for Arthritis and Related Inflammatory Diseases*, (2nd edition), (Academic Press, 2019), pp. 323-341. https://doi.org/10.1016/B978-0-12-813820-5.00019-2

[4] M. El-Dakhakhny, "Studies on the Egyptian Nigella sativa L. IV. Some pharmacological properties of the seeds' active principle in comparison to its dihydro compound and its polymer", Arzneimittel-forsch, **15**(10), 1227–1229 (1965).

[5] M.E. Abd El-Hack, M. Alagawany, M.R. Farag, R. Tiwari, K. Karthik, and K. Dhama, "Nutritional, Healthical and Therapeutic Efficacy of Black Cumin (Nigella sativa) in Animals, Poultry and Humans", International Journal of Pharmacology, **12**, 232-248 (2016). https://doi.org/10.3923/ijp.2016.232.248

[6] H. Mollazadeh, A.R. Afshari, and H. Hosseinzadeh, "Review on the Potential Therapeutic Roles of Nigella sativa in the Treatment of Patients with Cancer: Involvement of Apoptosis: Black cumin and cancer", J. Pharmacopuncture, **20**(3), 158-172 (2017). https://doi.org/10.3831%2FKPI.2017.20.019

[7] M.A. Randhawa, M. Al-Ghamdi, M. Al-Ghamdi, "Anticancer Activity of Nigella sativa (Black Seed) - A Review", The American Journal of Chinese Medicine, **39**(6), 1075 (2011). https://doi.org/10.1142/S0192415X1100941X

[8] D.R. Worthen, O.A. Ghosheh, P.A. Crooks, "The in vitro anti-tumor activity of some crude and purified components of blackseed, Nigella sativa L", Anticancer Res. **18**, 1527-1532 (1998).

[9] M. Burits, F. Bucar, "Antioxidant activity of Nigella sativa essential oil", Phytotherapy Research, **14**, 323-328 (2000). https://doi.org/10.1002/1099-1573(200008)14:5%3C323::AID-PTR621%3E3.0.CO;2-Q

[10] P.J. Houghton, R. Zarka, B. de la Heras, J.R.S. Hoult, "Fixed oil of Nigella sativa and derived thymoquinone inhibit eicosanoid generation in leukocytes and membrane lipid peroxidation", Planta Medica, **61**, 33-36 (1995). https://doi.org/10.1055/s-2006-957994

[11] N.M. Morsi, "Antimicrobial effect of crude extracts of Nigella sativa on multiple antibiotics-resistant bacteria", Acta Microbiologica Polonica, **49**, 63-74 (2000).

[12] M.L. Salem, and M.S. Hossain, "In vivo acute depletion of CD8(+) T cells before murine cytomegalovirus infection upregulated innate antiviral activity of natural killer cells", International Journal of Immunopharmacology, **22**, 707-718 (2000). https://doi.org/10.1016/S0192-0561(00)00033-3

[13] A.H. Gilani, N. Aziz, I.M. Khurram, K.S. Chaudhary, A. Iqbal, "Bron-chodilator."Spasmolytic and Calcium Antagonist Activities of Nigella sativa seeds (Kalonji): a traditional herbal product with Multiple Me-dicinal Uses", J. Pak. Med. Assoc. **51**, 115-119 (2001). https://ecommons.aku.edu/pakistan_fhs_mc_bbs/422

[14] M.S. Iqbal, A. Jafri, Md. Arshadb, and M.I. Ansari, "Stress response due to sodium azide treatment inside Nigella sativa L. plant and its effect on antioxidative property", Biocatalysis and Agricultural Biotechnology, **19**, 101171 (2019). https://doi.org/10.1016/j.bcab.2019.101171

[15] C. Moller, and M.S. Plesset,"Note on an Approximation Treatment for Many-Electron Systems", Phys. Rev. **46**, 618–622 (1934). https://doi.org/10.1103/PhysRev.46.618

[16] A.D. Becke, "Density-Functional Exchange-Energy Approximation with Correct Asymptotic-Behavior", Phys. Rev. A, **38**(6), 3098–3100 (1988). https://doi.org/10.1103/PhysRevA.38.3098

[17] C.T. Lee, W.T. Yang, and R.G. Parr, "Development of the Colle-Salvetti Correlation-Energy Formula into a Functional of the Electron-Density", Phys. Rev. B, **37**(2), 785–789 (1988). https://doi.org/10.1103/PhysRevB.37.785

[18] M.J. Frisch, G.W. Trucks, H.B. Schlegel, G.E. Scuseria, M.A. Robb, J.R. Cheeseman, J.A. Montgomery, et al, *Gaussian 03, Revision C.02*, (Gaussian, Inc, Wallingford CT, 2004).

[19] R. Denning, T. Keith, J. Millam, K. Eppinnett, W. Hovell, and R.G. Gilliland, *Version 3.09*, (Semichem. Inc., Shawnee Mission, KS, 2003).

[20] M.A. Palafox, "DFT computations on vibrational spectra: Scaling procedures to improve the wavenumbers", Physical Sciences Reviews, **3**(6), 20170184 (2018). https://doi.org/10.1515/psr-2017-0184

[21] *Integrated Spectral Data Base System for Organic Compounds*, (Ibaraki, Japan, National Institute of Advanced In-dustrial Science and Technology, 2003).

[22] Y. Yamakita, and M. Tasumi, "Vibrational analyses of p-benzoquinodimethane and p-benzoquinone based on ab initio Hartree-Fock and second-order Moller-Plessetcalculations", J. Phys. Chem. **99**, 8524-8534(1995). https://doi.org/10.1021/j100021a013

[23] R. Gupta, "Study of spectral and NLO properties of 2-methyl-5-(Propan-2-yl) phenol by DFT", IJSRED, **4**(3), 689-705 (2021). http://www.ijsred.com/volume4/issue3/IJSRED-V4I3P94.pdf

[24] K.M. Marzec, I. Reva, R. Fausto, and L.M. Proniewicz, "Comparative Matrix Isolation Infrared Specroscopy Study of 1,3- and 1,4- DieneMonoterpenes (α- Phellandrene and γ-Terpinene)", J. Phys. Chem. A, **115**, 4342-4353 (2011). https://doi.org/10.1021/jp2013122

[25] R. Abu-Dahab, F. Odeh, S.I. Ismail, H. Azzam, and A. Al Bawab, "Preparation, characterization and antiproliferative activity of thymoquinone-β-cyclodextrin self-assembling nanoparticles", Pharmazie, **68**, 939–944 (2013). https://doi.org/10.1691/ph.2013.3033

ОБЧИСЛЮВАЛЬНЕ ДОСЛІДЖЕННЯ IR ТА UV-VIS СПЕКТРІВ 2-ІЗОПРОПІЛ-5-МЕТИ L-1,4-БЕНЗОХІНОНУ ЗА ДОПОМОГОЮ МЕТОДІВ DFT ТА HF

Салах М.А. Рідха[a], Захра Таліб Галеб[b], Абдулхаді Мірдан Галеб[a]

[a]Департамент фізики наукового коледжу, Кіркукського університету, Кіркук, Ірак
[b]Департамент хімії наукового коледжу Кіркукського університету, Кіркук, Ірак

Проведено теоретичне дослідження сполуки тимохінону за допомогою двох теоретичних методів, DFT/B3LYP і HF з базовими наборами 6-31G, 6-31G(d,p) і 6-31++G(d,p) з використанням програми Гауссіан 09. Деякі теоретичні властивості, такі як вібраційні та електронні властивості, особливо UV-vis та IR-спектри, були проаналізовані, а потім порівняні з доступними експериментальними даними. Розраховані частоти гармонійних коливань були масштабовані зі стандартними коефіцієнтами масштабування 0,9 і 0,965 для HF і DFT/B3LYP відповідно, а потім порівняні з наявним експериментальним спектром FT-IR. Крім того, було досліджено статистичний аналіз для оцінки ефективності методів HF і DFT, включаючи середньоквадратичну помилку (RMSE), середню абсолютну помилку (MAE) і середню помилку у відсотках (MPE). Відповідно до призначених вібраційних режимів сполуки, можна зробити висновок, що метод DFT/B3LYP з базовим набором 6-31++G(d,p) мав найкращу узгодженість з експериментальними даними. Спектри поглинання в УФ-видимому діапазоні, енергії збудження, максимальну довжину хвилі поглинання, електронні переходи та сили осциляторів зазначеної в заголовку сполуки розраховували методом залежної від часу теорії функціоналу щільності (TD-DFT) з використанням того самого базового набору та порівнювали з наявними експериментальними даними. Результати показали, що найкращим результатом був ВЧ-метод із базовим набором 6-31G.

Ключові слова: *тимохінон; DFT; HF; UV-Vis; FT-IR; TD-DFT*